Targeting of lamivudine into the HIV reservoir in mesenteric and peripheral lymph nodes

Abigail Wong

School of Pharmacy

University of Nottingham

Nottingham

United Kingdom

Thesis submitted to The University of Nottingham for the degree of Doctor in Philosophy

Acknowledgements

First and foremost, I would like to thank my primary supervisor, Dr. Pavel Gershkovich, for all his knowledge, patience and support during my PhD. None of this would have been possible without his guidance and motivation. I would also like to thank my secondary supervisors, Dr. Maria Marlow and Dr. Michael J. Stocks, for all their help and support with microneedle fabrication and medicinal chemistry, respectively.

I would also like to thank my husband, Timothy Firmston-Williams, for giving long distance a chance. We were only dating for 5 months when I left to study abroad for 3 years and look at us now! We're happily married! I'd also like to thank my parents, Vincent Wong and Katie Chow, who let me off the hook for my prior student loans so that I could pursue my next degree and passion halfway across the world.

Thank you to all the staff at the Biodiscovery Institute, Boots Science Building and Bio Support Unit for all their help and training.

I would also like to thank all my colleagues for all their help and support and for all their collaboration. Special thanks to my labmate, Dr. Yenju Chu, for being an honorary supervisor. I am eternally grateful for all the help and support when I was new and lost (and when I was no longer new, but still lost). Thanks to Dr. Chaolong Qin for all the early-stage help developing the HPLC-UV method and to Dr. Wanshan Feng for all the late-stage help with all the animal work. Thanks to everyone in the Gershkovich Lab: Dr. Carlos Sanders-Velez, Dr. Alice Brookes, Dr. Adelaide Jewell, Liuhang Ji, Haojie Chen, Graziamarina Sinatra, Branislav Vukovic, Fady Mina, Yufei Zhu, Yunfei Zhong, Junting Wang and Ali Ali. A million thanks to Dr. Fiona Smith for

all her help with the microneedle patches and Dr. Eleonora Comeo for helping with medicinal chemistry. Additional thanks to all the undergraduate, MSc and PhD students who played a part in my project: Suhani Lakhani, Sadia Rahman, Adam Jeffries and Sham Nawshirawan.

Abigail Wong

List of publications originating from this thesis

A. Wong, Y. Chu, H. Chen, W. Feng, L. Ji, C. Qin, M. J. Stocks, M. Marlow, and P. Gershkovich. Distribution of lamivudine into lymph node HIV reservoir, *Int. J. Pharm. 648 (2023)*.

Table of Contents

Abstract

Efficient delivery of antiretroviral agents to lymph nodes is important in order to decrease the size of the HIV reservoir within the lymphatic system. Lymph nodes are a major site for HIV replication and are implicated in harbouring latent reservoirs. Lamivudine (3TC) is a nucleoside reverse transcriptase inhibitor (NRTI) used in first-line therapy for the treatment of HIV. Due to its hydrophilicity, 3TC, is not expected to associate with chylomicrons and therefore is predicted to have negligible direct uptake into intestinal lymphatics following oral administration with lipids. Negligible amounts of 3TC are also expected to be transported into peripheral lymphatics following subcutaneous (SC) administration due to faster flow rate in blood capillaries compared to lymph capillaries. The aim of this project was to develop a strategy to deliver 3TC to the HIV reservoir in multiple lymph nodes throughout the body using both oral and SC or transdermal administrations.

First, a high performance liquid chromatography with ultraviolet detector (HPLC-UV) bioanalytical method for the detection of 3TC in rat plasma was developed and partially validated. The developed method had a limit of quantification (LOQ) of 15 ng/mL. The calibration curve showed linearity from 15 to 10,000 ng/mL, which was sufficient for the purposes of this study. In addition, this method was designed to be easily modifiable to simultaneously quantify highly lipophilic prodrugs.

Next, 3TC was assessed for association with natural and artificial chylomicrons and solubility in sesame oil. As 3TC association with chylomicrons was undetectable, fatty acid ester prodrugs of 3TC were designed using a previously

described *in silico* model with the goal of increased chylomicron association. These prodrugs were then synthesized and assessed for conversion to 3TC in incubated rat plasma and fasted state simulated intestinal fluid (FaSSIF). In addition, the prodrugs (3TC-stearate and 3TC-oleate) were evaluated for association with artificial chylomicrons and solubility in sesame oil. Although both prodrugs had increased association with chylomicrons compared to 3TC, following these assessments, it was determined that neither of the synthesized prodrugs would be good candidates for oral *in vivo* studies due to low solubility in sesame oil (3TC-stearate) or low stability in FaSSIF (3TC-oleate).

Next, pharmacokinetic studies were performed for 3TC in male Sprague-Dawley rats. The biodistributions of 3TC following oral lipid-based, oral lipid-free, SC and intravenous (IV) administrations were assessed using time points determined from the pharmacokinetic studies. In oral administration studies, mesenteric lymph nodes (MLNs) were found to have significantly higher concentrations of 3TC compared to other peripheral lymph nodes with mean tissue:serum ratios for MLNs ranging from 1.4 to 2.9. An analysis of collected mesenteric lymph fluid showed that 3TC is primarily found in the “fluid only” compartment (free of cells and chylomicrons). There were low-to-undetectable concentrations of 3TC in lymph fluid cells and chylomicrons. In SC administration studies, right-side inguinal and popliteal lymph nodes that drain the site of injection were found to have significantly higher concentrations of 3TC than left-side non-draining nodes. The tissue:serum ratios were as high as 3.2 on the right-side inguinal node. In IV administration studies, lymph nodes had tissue:serum ratios ranging from 0.9 to 1.4.

Because SC administration biodistribution studies showed high concentrations of 3TC in lymph nodes that drain the site of injection, we then formulated dissolvable 3TC-loaded microneedle (MN) patches. These patches were rigid and were able to be inserted into Parafilm M® and pig skin to appropriate depths. Franz cell diffusion studies showed that the microneedle patches successfully delivered 14.5% of the total 3TC in the patch across a matrix of porcine skin into the receptor fluid of phosphate buffered saline (PBS) with an additional 13% of total 3TC being found in the skin. In conjunction with our SC administration biodistribution studies, the *in vitro* data show that dissolvable 3TC-loaded microneedle patches may be a patient-friendly way to deliver 3TC to peripheral lymph nodes.

Using a combined oral and subcutaneous or transdermal administration approach could be a holistic way to deliver 3TC to numerous lymph nodes throughout the body. By doing so, antiretrovirals can be delivered to tissues that harbour HIV latent reservoirs, which could help to improve the prognosis people living with HIV and work synergistically with possible HIV-curative strategies.

Abbreviations

3TC – Lamivudine

3TC-MP – Lamivudine monophosphate

3TC-TP – Lamivudine triphosphate

ACN – Acetonitrile

AIDS – Acquired immunodeficiency syndrome

ART – Antiretroviral therapy

ARV – Antiretroviral drug

AUC – Area under the curve

$AUC_{0\text{-}inf}$ – Area under the curve from time zero to infinity

$AUC_{0\text{-}t}$ – Area under the curve to the last sampling time point

BBB – Blood-brain barrier

BCS – Biopharmaceutics classification system

BHIVA – British HIV association

BLOQ – Below the limit of quantification

BTB – Blood-testis barrier

C_0 – Concentration extrapolated to time zero

CBD – Cannabidiol

CCR5 – C-C Chemokine Receptor 5

CL – Clearance

C_{max} – Maximum drug concentration

CMC – Carboxymethylcellulose

CNS – Central nervous system

CNT – Concentrative nucleoside transporter

CV – Coefficient of variation

CXCR4 – C-X-C Chemokine Receptor 4

DCM – Dichloromethane

DDW – Distilled deionized water

DGAT – Acyl CoA:diacylglycerol acyltransferase

DNA – Deoxyribonucleic acid

DMSO – Dimethyl sulfoxide

DTG – Dolutegravir

EC – Elite-controller

EDTA – Ethylenediaminetetraacetic acid

ESEM – Environmental scanning electron microscope

F – Bioavailability

FaSSIF – Fasted state simulated intestinal fluid

FDA – Food and Drug Administration

FTC – Emtricitabine

GALT – Gut associated lymphoid tissue

gp – Glycoprotein

HAND – HIV-associated neurocognitive disorder

HDL – High density lipoprotein

HEV – High endothelial venule

HBV – Hepatitis B virus

HIV – Human immunodeficiency virus

HIV Env – HIV envelope protein

HPLC-UV – High performance liquid chromatography with ultraviolet detector

HSCT – Hematopoietic stem cell transplantation

IC_{50} – Concentration necessary to achieve 50% inhibition

IDL – Intermediate density lipoprotein

INSTI – Integrase strand transfer inhibitor

IS – Internal standard

IV – Intravenous

LC-MS – Liquid chromatography – tandem mass spectrometry

LDL – Low density lipoprotein

LEC – Lymphatic endothelial cell

LOQ – Limit of quantification

MALT – Mucosa associated lymphoid tissue

MGAT – Acyl CoA:monoacylglycerol acyltransferase

MLNs – Mesenteric lymph nodes

MNs – Microneedles

MTBE – Methyl tert-butyl ether

NMR – Nuclear magnetic resonance

NNRTI – Non-nucleoside reverse transcriptase inhibitor

NRTI – Nucleoside reverse transcriptase inhibitor

OAT – Organic anion transporter

OCT – Organic cation transporter

PBS – Phosphate buffered saline

PCTVs – Pre-chylomicron transport vesicles

PDMS - Polydimethylsiloxane

PEG – Polyethylene glycol

PI – Protease inhibitor

PLA – Polylactic acid

PLGA – Polylactic-co-glycolic acid

PO – Per os/oral

ppm – Parts per million

PVA – Polyvinyl alcohol

PVP – Polyvinylpyrrolidone

PVPVA – Polyvinylpyrrolidone/vinyl acetate

PWH – People with HIV

QC – Quality control

RNA – Ribonucleic acid

SC – Subcutaneous

SD – Sprague-Dawley

STD – Standard deviation

SEM – Standard error of the mean

SIV – Simian immunodeficiency virus

SMEDDS – Self-microemulsifying drug delivery system

SPE – Solid phase extraction

$t_{1/2}$ – Half life

TAF – Tenofovir alafenamide

TDF – Tenofovir disoproxil fumarate

T_{FH} – T follicular helper cell

TLC – Thin layer chromatography

t_{max} – Time to reach maximum drug concentration

UCBT – Umbilical cord blood stem cell transplantation

UPLC – Ultra-performance liquid chromatography

VLDL – Very low density lipoprotein

V_{ss} – Volume of distribution at steady state

v/v – Volume by volume

WHO – World Health Organization

List of Figures

s

List of Tables

Chapter 1 General Introduction

1.1 Human Immunodeficiency Virus

1.1.1 HIV Background

First identified in 1983, human immunodeficiency virus (HIV) affects an estimated 39.0 million people worldwide as of 2022.[1] It is primarily spread through sexual contact or sharing of parenteral drug paraphernalia, although exchange of certain bodily fluids such breast milk[2] can also facilitate spread as well as mother-to-child transmission during pregnancy or childbirth.[3] Worldwide, HIV disproportionately affects injectable drug users, sex workers, men who have sex with men, and transgender women[4] as well as low-income individuals and countries.[5,6]

HIV is a retrovirus that targets CD4+ T cells in order to replicate, which ultimately results in cell death. This leaves people with HIV (PWH) immunocompromised. If left untreated, an HIV infection can progress into acquired immunodeficiency syndrome (AIDS), which is characterized by a severely weakened immune system, leaving infected patients vulnerable to opportunistic infections that may become life threatening. Cumulatively, an estimated 85.6 million people have been infected with HIV and 40.4 million people have died from AIDS-related illnesses.[1]

In addition to AIDS progression, chronic infections, and increased mortality, HIV infections can also result in other comorbidities. This includes cardiovascular conditions, kidney or liver disease, neurocognitive disorders, decreased bone density, and certain cancers.[7] This may be due to side effects of medications, increased representation of risk factors such as use of tobacco, or due to complications of an HIV infection from chronic

inflammation despite treatment with ART.[8] This results in increased healthcare costs for people living with HIV, which can have an impact on both the individual and the healthcare system.

Although HIV has many different subtypes, the most common ones are HIV-1 and HIV-2. Both have their similarities, such as routes of transmission, replication pathways and both types of infection can progress into AIDS.[9] However, HIV-1 and HIV-2 only share 55% sequence identity.[10] HIV-1, which is the more easily transmitted of the two, is the most common subtype worldwide and was responsible for 99.94% of new cases in the United States from 2010 to 2017.[11] However, HIV-2, which is more commonly found in West Africa, has a longer asymptomatic stage[12], a lower mortality rate compared to HIV-1[13], and a slightly different treatment strategy.[14] In addition, individuals with HIV-2 tend to have a lower viral load compared to individuals with HIV-1[15] and may even be undetectable prior to the onset of HIV-2 associated AIDS[12], although this may be due to inaccurate testing for HIV-2 viral load, especially with HIV-2 group B.[16] Because of the many differences between the two subtypes, and as HIV-1 is more prevalent worldwide, this paper will focus on HIV-1.

1.1.2 HIV Replication Life Cycle

HIV requires a host cell to replicate and disseminate. To enter a cell, HIV will bind to a CD4 receptor on the cell membrane surface of a leukocyte using the glycoprotein (gp) 120 subunit of the HIV envelope (HIV Env).[17] This binding causes HIV Env to undergo conformational changes, allowing it to subsequently bind to a co-receptor.[17] Different strains of HIV may target

different co-receptors, although the major ones are C-C Chemokine Receptor 5 (CCR5) and C-X-C Chemokine Receptor 4 (CXCR4).[18] HIV strains are classified based on which co-receptors are used for cell entry: R5 HIV for those that utilize CCR5 and X4 HIV for those that utilize CXCR4.[17] For some strains, both co-receptors can be used. After binding a co-receptor, the other HIV Env subunit, gp41 fusion peptide, is exposed and inserts into the cell membrane and viral contents are unloaded.[17]

In some patients, a CCR5Δ32 mutation manifests as a deletion of 32 base pairs of the CCR5 co-receptor. This mutation ultimately results in an increased innate resistance to HIV strains that need to bind to the CCR5 co-receptor for membrane fusion and cell entry.[19] Some patients with this mutation or patients who have low levels of CCR5 are able to suppress or control viral replication.[20–22] In some patients, this can be achieved even without the need for ART.[23] However, it is also possible for HIV to undergo a tropism-switch to utilize CXCR4 instead of CCR5[24,25], which can leave even patients with the CCR5Δ32 mutation susceptible to viral replication.

After entry into a cell, viral ribonucleic acid (RNA) will undergo reverse transcription using the enzyme reverse transcriptase from the viral core. Reverse transcription converts HIV RNA into deoxyribonucleic acid (DNA), which then enters the cell nucleus to be integrated into host DNA by the enzyme integrase. The host cell will then use this template to produce new HIV RNA and long-chain proteins which must be cleaved by protease before the virus can bud and mature.[26]

1.1.3 Treatment of HIV

Antiretroviral drugs (ARVs) used to treat HIV target each step of viral replication (**Figure 1-1**). Entry inhibitors consist of fusion inhibitors, post-attachment inhibitors, and CCR5 antagonists and prevent the entry of HIV into the host cell. Nucleoside reverse transcriptase inhibitors (NRTIs) are nucleoside analogues that prevent the developing viral DNA strand from elongating due to inhibition of reverse transcriptase. Similarly, non-nucleoside reverse transcriptase inhibitors (NNRTIs) also bind to reverse transcriptase to stop the conversion of viral RNA to DNA. Integrase strand transfer inhibitors (INSTIs) prevent viral DNA integration into host DNA by binding to the enzyme integrase. Lastly, protease inhibitors (PIs) prevent cleavage of polyproteins necessary for viral maturation.

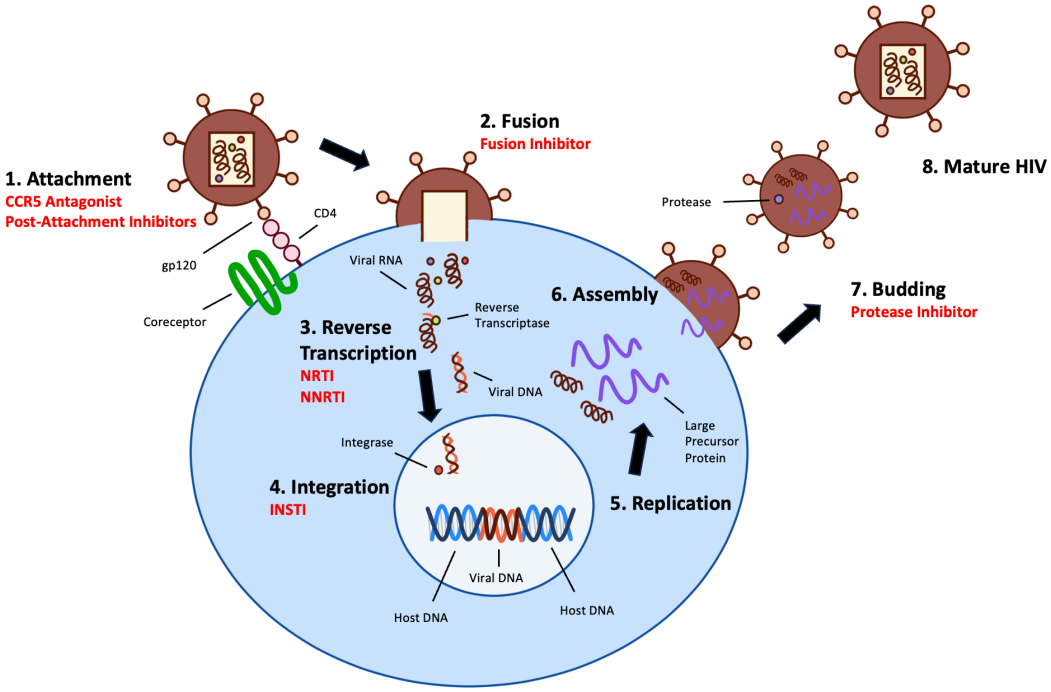

Figure 1-1 *Various ARVs target different stages of the HIV replication cycle. CCR5 antagonists and post-attachment inhibitors target the attachment step, and fusion inhibitors target the fusion step. Next, reverse transcription of viral RNA to DNA occurs, which can be inhibited by NRTIs and NNRTIs. Next, viral DNA is integrated*

into host DNA by the enzyme integrase, which can be inhibited by INSTIs. Following transcription and translation, protease, which can be inhibited by PIs, cleaves HIV polyproteins, allowing the virus to bud and mature. Adapted from HIVinfo.NIH.gov[27]*.*

Antiretroviral therapy (ART) typically consists of a combination, or "cocktail," of ARVs. The World Health Organization (WHO)[28], British HIV Association (BHIVA)[29], and United States[14] treatment guidelines list dolutegravir (DTG) (an INSTI) and an NRTI backbone of tenofovir plus emtricitabine (FTC) or lamivudine (3TC) as first-line therapy. Recently, the clinical trials GEMINI[30] and TANGO[31] have shown success in the treatment of HIV using dual-therapy consisting of DTG and 3TC. Although the WHO guidelines have not yet been updated to reflect this, the United States HIV treatment guidelines were updated in 2021 to include dual-therapy as an acceptable form of first-line therapy in individuals with RNA <500,000 copies/mL and confirmed lack of hepatitis B virus (HBV) coinfection in situations where patients have undergone genotypic resistance testing for reverse transcriptase. As it is an important and effective first-line drug that is used for the treatment of HIV, and other first-line drugs used for HIV such as DTG and FTC have been or will be explored by other members within our lab, this PhD thesis will focus on one of the two drugs approved for dual therapy, lamivudine (3TC).

ART can achieve viral suppression (RNA < 200 copies/mL) if it is successful, with some patients exhibiting an undetectable viral load. In 2022, 71% of PWH had either suppressed or undetectable viral loads.[32] Individuals who have achieved viral suppression have no risk in spreading HIV through

sexual contact.[33] Improvements in life expectancy have been seen over time as advances in treatments continue. Once regarded as a death sentence, the difference in life expectancy between HIV-positive and -negative patients has steadily decreased from 22.1 years in 2000 to 2003 to 9.1 years in 2014 to 2016. The life expectancy differential is even lower at 6.8 years if ART is initiated at higher CD4+ cell counts.[34] Despite this, studies have found that comorbidity-free years for PWH have improved for diabetes and cardiovascular disease, especially in those who initiated ART at higher CD4+ counts.[34] This reflects efforts to address comorbidities in PWH, such as with the REPRIEVE trial, in which pitavastatin was shown to reduce major adverse cardiovascular events in PWH.[35] Although it is important to highlight the great improvements in mortality outcomes in the treatment of HIV, the gap in life expectancy in addition to the little progress regarding comorbidities show that there is still room for improvement.

1.2 T Cells

T cells play an important role in active immunity. The most common types are CD4+, which are also referred to as helper T cells, and CD8+ cells, or cytotoxic T cells.[36] HIV primarily targets CD4+ T cells. Naïve CD4+ T cells are found primarily in lymph nodes and the spleen.[37] Although they are produced in the bone marrow[38], T cells can also replicate through clonal expansion, in which precursor cells proliferate and produce clones. This mechanism allows for the body to produce a robust immune response in response to an infection.[39]

When naïve T cells are activated by antigen, they differentiate into effector T cells, which produce cytokines.[40] These cytokines in turn activate B cells and CD8+ T cells.[41] Effector cells require a high amount of energy to function, and when the pathogen is cleared, the effector cells either undergo apoptosis or further differentiate into resting memory cells, which have a reduced metabolism.[40] These memory cells can be reactivated upon exposure to antigen (**Figure 1-2**).

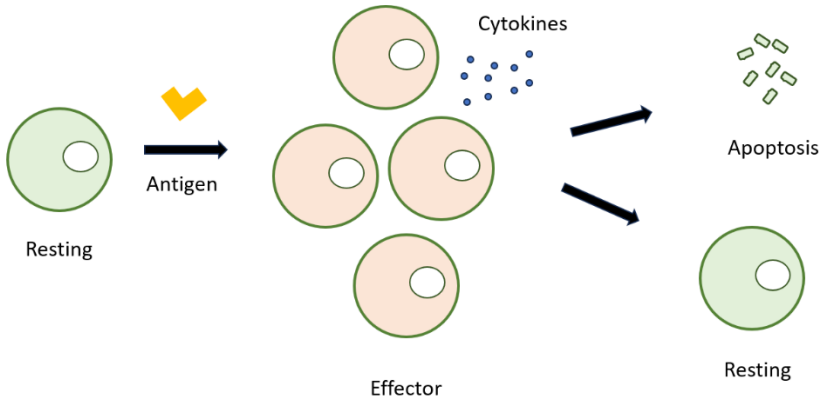

Figure 1-2 CD4+ T cells are activated by antigen and differentiate into effector T cells, which release cytokines that further activate B cells and CD8+ T cells. After the pathogen is cleared, cells undergo apoptosis or transition into the resting phase.

1.3 The HIV Latent Reservoir

While treatment for HIV has come a long way since the 1980's, a cure for HIV remains elusive due to early formation of the HIV latent reservoir. This reservoir persists even with successful use of ART that suppresses viral load in blood.[42] Additionally, increasing the number of antiretrovirals used for treatment, including use of mega-HAART, which consists of five or more drugs, does not reliably reduce the size of the HIV latent reservoir compared to traditional triple-therapy ART.[43] The HIV reservoir is primarily found in

lymphoid tissues, with a large reservoir formed in gut-associated lymphoid tissues (GALT), and can persist despite long-term drug treatment.[44] This is because GALT, which is made up of Peyer's patches, colon and caecal patches, tonsils, appendix, and MLNs[45], has the highest CD4+ cell concentration.[46]

In addition to GALT, other tissues such as other lymph nodes throughout the body, mucosa-associated lymphoid tissues (MALT), and spleen can be a harbour for the latent reservoir, resulting in over 99% of viral RNA-positive cells being found in lymphoid tissues even during treatment with suppressive ART.[47] Other tissues such as the brain[48] and genital tract also contribute to this reservoir.[49] These reservoirs may persist despite viral loads being suppressed in blood because low level replication occurs in reservoirs[50] and because of clonal expansion.[51] In addition, these reservoirs may also experience some cross-infection.[44] While the HIV primarily affects CD4+ T cells, the HIV reservoir also consists of microglial, follicular dendritic cells[52] and other types of macrophages.[53]

The HIV latent reservoir is formed early within days of an initial infection.[42,54] During an acute infection, large amounts of replication occur, primarily in lymphoid tissues, cementing the formation of the latent reservoir.[55] Even in cases where ART is initiated within days of infection, the latent reservoir can already be established.[42,54] This results in a rebound of HIV when ART is discontinued, even in patients who have achieved viral suppression for years.[56] This rebound also occurs in patients with very early initiation of ART[57], although early ART initiation may reduce the size of the

latent reservoir[58,59] and therefore prolong periods of remission before rebound occurs.[60] However, despite being delayed, rebound will most likely occur. Even in the case of the Mississippi baby, a new-born who began ART at 30 hours of age until 18 months, HIV viral load rebounded 27.6 months after ART cessation.[61]

One contributing factor to rebound despite years of successful viral suppression whilst on ART is the longevity of integrated HIV. While cells can be infected at various cellular lifecycle stages, the transitioning period during which a CD4+ T cell converts from the activated phase to the resting memory phase is correlated with higher chance of infection.[62] While active CD4+ T cells display viral proteins and are subject to cytotoxicity, latently infected CD4+ T cells do not, and thus will evade the immune system.[63] Active cells contribute to the majority of viral replication, and although latently infected cells are generally regarded as non-replicative or exhibit inefficient transcription[64], they can be reactivated by antigen and thus become capable of virus-production.[65] This is additionally important because the half-life of free virus is very short in the range of minutes to hours.[66] The half-life of unintegrated viral DNA inside a cell is 1 day[67], and the half-life of an active virus-transcribing cell is about 2 days.[68] In contrast, the half-life of a latently infected resting-memory cell with integrated virus is 43 to 44 months.[69,70] When examining the rate of latent reservoir decay in highly ART-adherent HIV patients, Siliciano et al. determined that it would take 73.4 years for latently infected CD4+ T cells to naturally deteriorate assuming a reservoir size of 10^6 cells.[70] While low-level replication and clonal

expansion that tends to happen in reservoir tissues contribute to the prolongation of the rate of decay, the main contributor to the slow decay of the reservoir is the half-life of resting cells and the rate they are reactivated.[71]

In lymph nodes, the majority of HIV-1 producing cells can be found in germinal centres of the lymph node follicle. The germinal centre is part of the B cell zone near the T cell zone in which B cells undergo clonal expansion following activation by T follicular helper (T_{FH}) cells located in the interfollicular and the B cell zones.[72] The primary affected cells are CD4+ T_{FH} cells in this region (T_{FH} cells outside of the germinal centres represent a minority of productively infected cells).[73] Even in a group of elite-controller (EC) rhesus macaques, T_{FH} cells in germinal centres exhibited ongoing replication. This was due to the lack of CD8+ T cells, which are responsible in EC monkeys for controlling the virus and clearing SIV-infected cells, in this region.[74] In another study, HIV RNA and DNA were found in lymph node germinal centres of human patients on ART.[75] In a separate study on humans, T_{FH} cells in the lymph nodes were found to contain replication-competent and infectious virus in aviraemic patients.[76]

CD4+ T cells are not the only type of cells that make up the HIV latent reservoir. Microglial cells, which are a type of macrophage, express low levels of CD4+ and are the primary contributing cells of the HIV reservoir in the brain.[77] Initially, the brain is infected by CD4+ T cells that migrate across the blood-brain-barrier (BBB).[78] However, the mechanism by which microglial cells are in turn infected is not agreed upon, and microglia may be

infected by free virus or by engulfing HIV+ CD4+ T cells.[79] Infected microglial cells release viral proteins and activate astrocytes, which in turn results in increased extracellular glutamate, resulting in neuron injury.[80] Because of this, PWH can experience cognitive disorders, which can range from asymptomatic impairment to HIV-associated dementia. Microglial cells have relatively long half-lives, with some microglial cells' lifespan being over 20 years.[81]

As microglial cells are primarily responsible for the immune role in the brain, these cells can exhibit a lot of movement within the brain.[82] Thus, microglial cells can be found in all regions of the brain. There is some evidence that they may be found in higher densities in white matter as opposed to grey matter, although this difference was found to be small.[83] Other studies have also found that microglial cell distribution in the brain is generally regular[84], and authors conclude that an even distribution is consistent with microglial cells' surveilling role.[85]

In addition to microglial cells, astrocytes in the brain have been reported to harbour HIV provirus. Although they do not make up the majority of the brain reservoir (it is estimated that only 1-3% of astrocytes are infected in an HIV-positive brain[86]), astrocytes can express low-levels of transcripts without expression protein[86]. Integrated HIV has been found in astrocytes in post-mortem analysis of brains of patients on ART[87]. Astrocytes do not express the CD4 receptor, and infection stems from contact with infected CD4+ cells and receptor-mediated endocytosis.[88] Like microglia, astrocytes tend to be long-lived.[89]

In addition to reported poor penetration of ART into the brain[90], the long lifespans of microglial cells and astrocytes make the brain a challenging site that harbours latent reservoir.

1.4 Patients Who Have Been Cured

There have been cases in which three male and one female PWH have been cured of HIV. In these cases, the patients had additionally been diagnosed with leukaemia or lymphoma, which were initially treated with chemotherapy or radiation. In the cases concerning the male patients, the individuals then underwent hematopoietic stem cell transplantation (HSCT) in which the donor carried two copies of the CCR5Δ32 mutation.[91] Unfortunately, this approach will not work for most patients living with HIV because it is difficult to find a donor match with this mutation, especially as individuals with the CCR5Δ32 mutation are predominantly Caucasian.[92] However, recently, a modified approach was used in a mixed-race female patient, who underwent umbilical cord blood stem cell transplantation (UCBT).[93] This could improve the odds of finding a CCR5Δ32 donor as umbilical cord blood transplantation has less stringent match requirements.[93,94] However, HSCT and UCBT are risky procedures with high morbidity[95,96] and mortality[97] rates. In addition, it is possible for HIV to utilize CXCR4 instead of the CCR5 co-receptor. As a result, these strategies are unlikely to be suitable for a large-scale cure.

1.5 Targeting Lymphatics

1.5.1 Why?

It has previously been shown that lymph nodes and GALT is a source of viral rebound even in patients in suppressive ART.[98] As lymph nodes exhibit low-level HIV replication despite viral suppression by ART in plasma[99,100], it is important that these sites have sufficient exposure to drug therapy. Sufficient drug delivery to sites of replication is important to not only help minimize the size of the latent reservoir, but also to aid in potentially curative strategies such as shock-and-kill or block-and-lock. The shock-and-kill strategy utilizes latency-reversing agents, since active infected cells have much shorter half-lives and are easier to target by the immune system.[101] However, as resting cells are deliberately being reactivated, sufficient ART concentrations at the site of latency reversal will be necessary to prevent additional infection.[102] In the case of block-and-lock, gene transcription of the integrated virus is essentially silenced whilst ART works in conjunction to stop additional spread to uninfected cells.[103] In addition, during an acute infection, early exposure of potential reservoir tissues to high concentrations of ART may be able to help decrease the size of the latent reservoir.[104] Comprehensive targeting to all sites where viral replication occurs will not only help to reduce the size of the latent reservoir during acute infection, but will also be crucial to HIV cure strategies.

1.5.2 How?

Intestinal lymphatics are responsible for transporting ingested fat-soluble vitamins and lipids that are incorporated into large lipoproteins

called chylomicrons (**Figure 1-4**).[105] High density lipoproteins (HDL) and very low density lipoproteins (VLDL) are produced primarily in the liver (although some HDL is produced in the intestines), and VLDL is broken down into intermediate density lipoproteins (IDL) in peripheral tissues which are then broken down into low density lipoproteins (LDL) in the liver.[106] In contrast, chylomicrons are produced in intestinal epithelial cells. Following ingestion, triglycerides are broken down by lingual lipase in the mouth preferentially at the sn-3 position, although it may cleave at the sn-1 position as well (**Figure 1-3**).[107] Tri- and diglycerides are further broken down in the stomach by acid and gastric lipases.[108] In the duodenum, up to 70% of lipid digestion occurs [109], and diglycerides can be more efficiently (due to bile salt emulsification) be broken down into sn-2 monoglycerides by pancreatic lipase (with the help of co-lipase), which is also specific for the sn-1 and sn-3 positions.[107] Micelles with free fatty acids and monoglycerides must then pass through the unstirred water layer of the jejunum where they are transported inside intestinal epithelial cells.[109] Free fatty acids are intracellularly esterified into fatty acyl-CoAs by acyl-CoA synthetase and, along with monoglycerides, are then resynthesized into diglycerides with acyl CoA:monoacylglycerol acyltransferase (MGAT) and subsequently triglycerides with acyl CoA:diacylglycerol acyltransferase (DGAT).[110] Triglycerides then form pre-chylomicrons in the endoplasmic reticulum and are transported via pre-chylomicron transport vesicles (PCTVs) to the Golgi complex, where chylomicrons are assembled.[111] Chylomicrons then enter the lamina propria, where they are then taken up by lacteals.

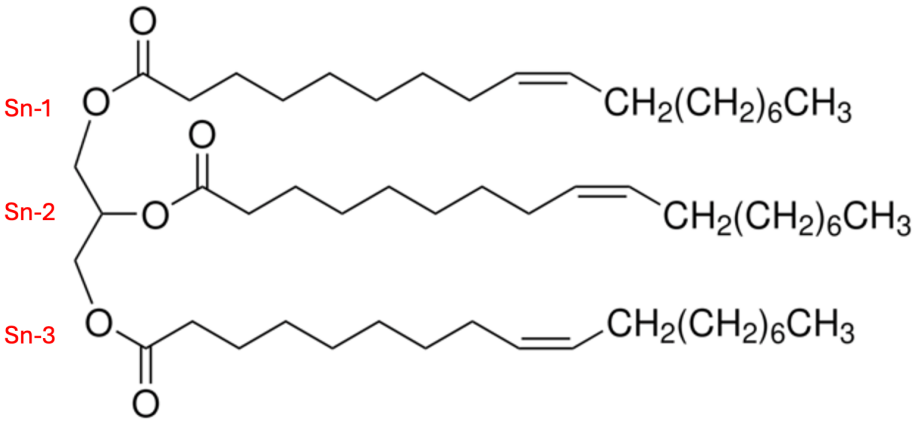

Figure 1-3 *A triglyceride with three oleic acid moieties (triolein). The sn-2 position is in the middle of the structure.*

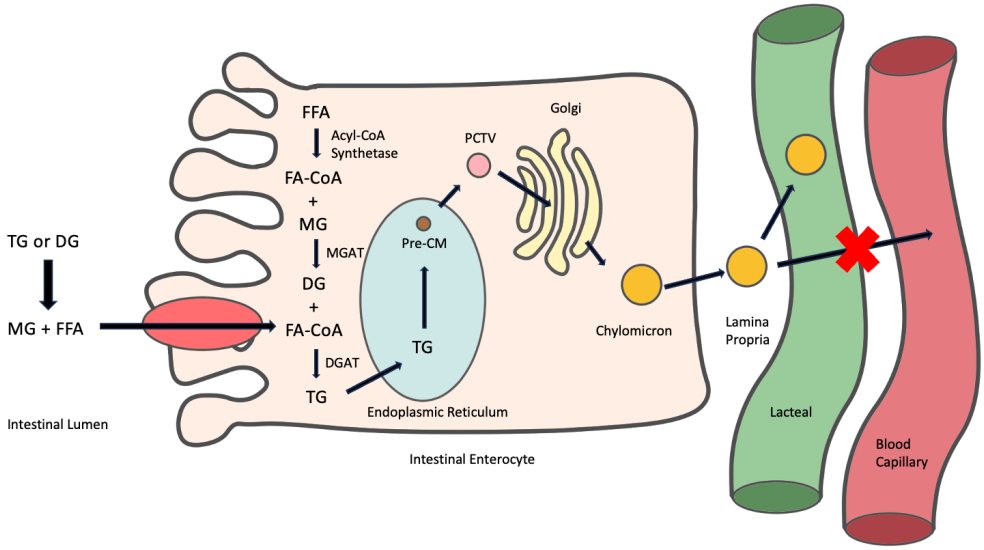

Figure 1-4 *Following initial breakdown of triglycerides by lingual lipase in the mouth or gastric lipase and acid in the stomach, triglycerides or diglycerides are further broken down into free fatty acids and monoglycerides in the intestinal lumen. These are transported into the intestinal enterocyte where triglycerides are resynthesized, and chylomicrons are produced. Chylomicrons then exit the intestinal enterocyte into the lamina propria, where they are further transported into lacteals as they are too large to enter blood capillaries. TG, triglyceride; DG, diglyceride; MG, monoglyceride; FFA, free fatty acid; FA-CoA, fatty acyl-CoA; MGAT, acyl CoA:monoacylglycerol acyltransferase; DGAT, acyl CoA:diacylglycerol acyltransferase; Pre-CM, pre-chylomicron; PCTV, pre-chylomicron transport vesicle.*

Orally administered drugs are usually preferentially transported into blood capillaries as opposed to lymphatics (**Figure 1-5**). This is due to blood

having a flow rate that is 100 to 500 times faster than that of lymph fluid.[112] However, lymph capillaries have highly permeable button-like junctions[113] whereas blood capillary's tight zipper-like junctions do not allow for the passage of larger particles. These button-like junctions allow for chylomicrons, which are usually between 200 to 600 nm in diameter but can range in size up to 1000 nm[114], to be transported selectively into lymph capillaries. To take advantage of this mechanism, drugs can be designed with physicochemical properties that allow them to be incorporated into chylomicrons when they are produced in intestinal epithelial cells for direct transport into lymphatics. In order for a drug to associate with chylomicrons, the drug must be highly lipophilic, generally with a log $D_{7.4} > 5$ and a triglyceride solubility > 50 mg/mL.[115] In addition, a variety of other physiochemical properties also factor into whether a drug will associate with chylomicrons.[116]

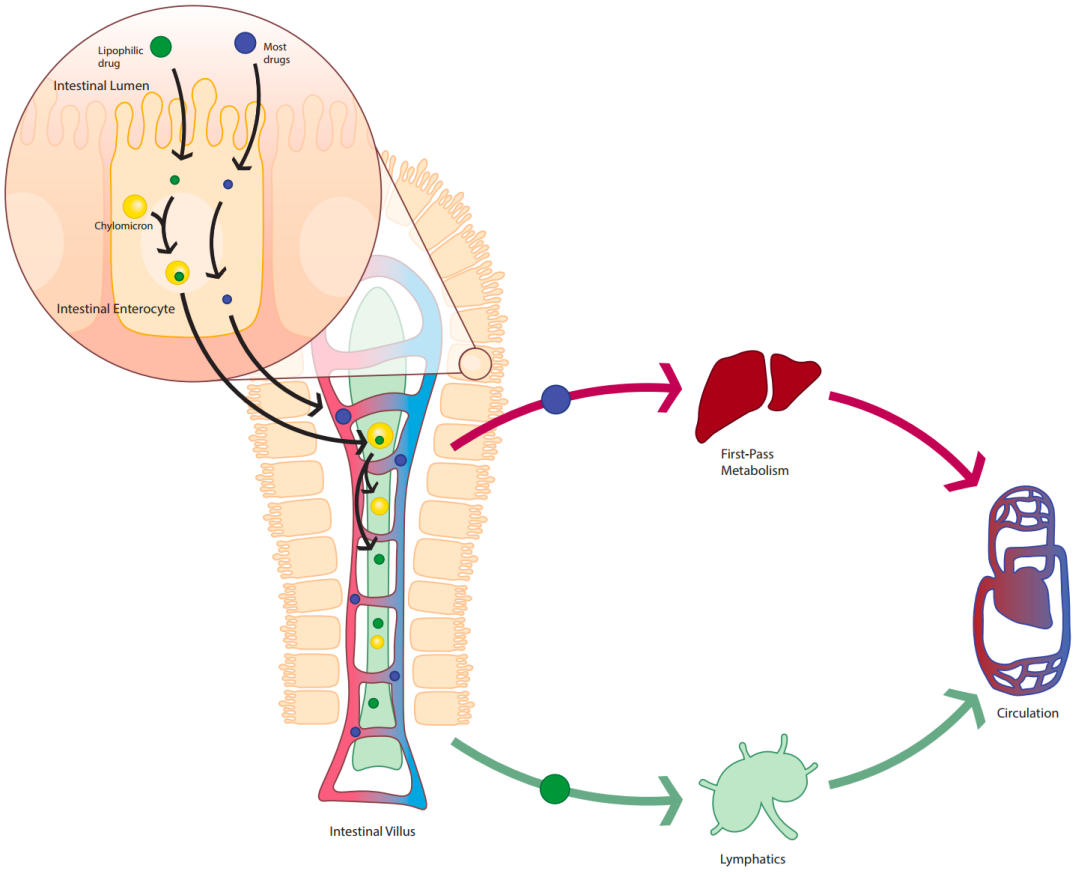

Figure 1-5 *Small molecule drugs like 3TC that do not exhibit association with chylomicrons are not expected to be transported into intestinal lymphatics to any significant extent. Instead, they are expected to be transported straight into blood, where they will undergo first-pass hepatic metabolism before entering general systemic circulation.*

Although lipophilic drugs' intestinal lymphatic uptake can be improved with simple methods such as administration with vegetable oils[117], this approach may not work for other drugs that are less lipophilic and do not associate with chylomicrons. For more hydrophilic drugs, there are differing strategies that work to varying degrees of success that aim to deliver drug into intestinal lymphatics such as nanoparticles[118] or self-microemulsifying drug delivery systems (SMEDDS).[119] In addition, there are a variety of prodrug approaches that aim to increase the lipophilicity of the drug molecule in order to deliver drugs into intestinal lymphatics including

triglyceride mimetics[120,121], alkyl fatty-acid esters[122,123], and self-immolating prodrugs.[124,125]

In peripheral lymphatics, selective uptake is based on size, due to the button-like junctions in lymph capillaries[113] that allow for the passage of larger particles (**Figure 1-6**). Smaller particles and molecules with a size < 10 nm should preferentially transport into blood capillaries when administered subcutaneously or transdermally due to the much faster flow rate of blood compared to lymph fluid.[126,127] Larger particles and molecules with a size of 10 to 80 nm will transport into lymph capillaries due to the larger button-like junctions in lymph vessels.[126,128] Particles larger than 100 nm tend to diffuse more slowly into lymphatics (if at all)[129], but due to their larger size, they will tend to accumulate in lymph nodes once they are absorbed.[128] By controlling the size of the molecule or particle that is injected either subcutaneously or microneedles (MNs), the transport of drug into target-tissues can be manipulated. Preferential lymph targeting via MNs or SC injection has been accomplished with polymer[130] or lipid[131] nanoparticles, liposomes[132], or nanocrystals.[133]

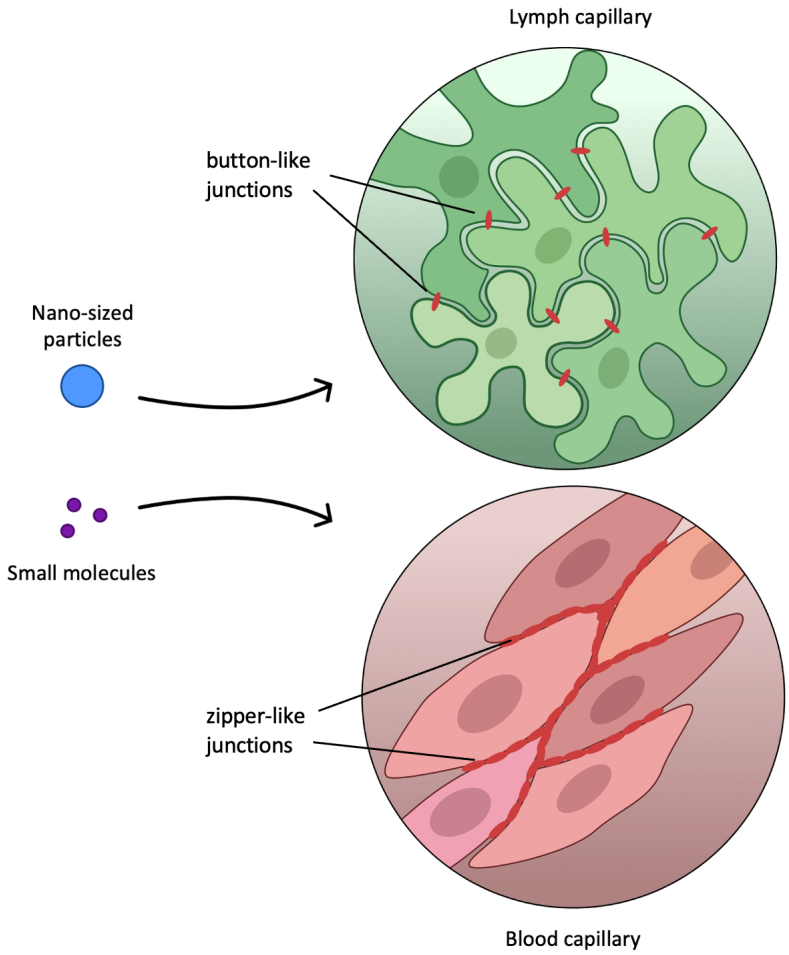

Figure 1-6 *In the periphery, small molecules will be transported into blood capillaries due to a quicker flow rate of blood compared to lymph fluid. Nano- or micro-sized particles will preferentially transport into lymphatics due to larger button-like junctions.*

1.6 Lamivudine (3TC)

3TC (**Figure 1-7**) is a nucleoside analogue of cytidine and inhibits HIV reverse transcriptase. Approved by the FDA in November 1995[134], 3TC is a relatively old drug compared to FTC and tenofovir disoproxil fumarate (TDF) which were approved in the 2000s, and compared to DTG and tenofovir alafenamide (TAF) which were approved in the 2010s (**Figure 1-8**). However, 3TC has remained a mainstay in the first-line treatment of HIV. This is important as 3TC is much cheaper than the comparable cytidine-analogue,

FTC.[14] The use of dual-therapy DTG-plus-3TC regimens (as opposed to traditional three-drug regimens) additionally translates into extra cost savings.[135] Whilst the situation has been improving over the past couple decades, socioeconomic inequity is still a large hurdle in the worldwide effort against HIV.[136] With COVID-19 contributing to financial burdens, especially in low- or middle-income countries[4], it is important to consider the cost of ART to ensure effective therapy is available to all, and effective low-cost drugs like 3TC are essential.

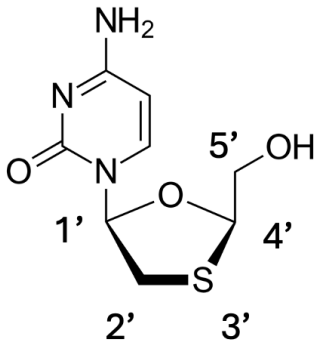

Figure 1-7 *The structure of 3TC, an analogue of cytidine. 3TC lacks a 3'-OH group, which prevents viral DNA elongation.*

The mechanism of action for 3TC is as a nucleoside analogue of cytidine. It is, as most nucleoside analogues are, a prodrug itself and must be phosphorylated at its 5'-OH group (**Figure 1-7**) into 3TC-monophosphate (3TC-MP) and an additional two times into its triphosphate form (3TC-TP) before it is ready to be incorporated into the growing HIV DNA strand by reverse transcriptase. However, as 3TC's ribose is missing its 3'-OH group, further elongation of viral DNA is not possible. Since HIV-1 reverse transcriptase is inaccurate, error-prone and lacks a proofreading function[137] (unlike human DNA polymerase[138]), NRTIs like 3TC are effective against viral

replication without disrupting regular DNA replicative activity and serve as a backbone to HIV treatment.

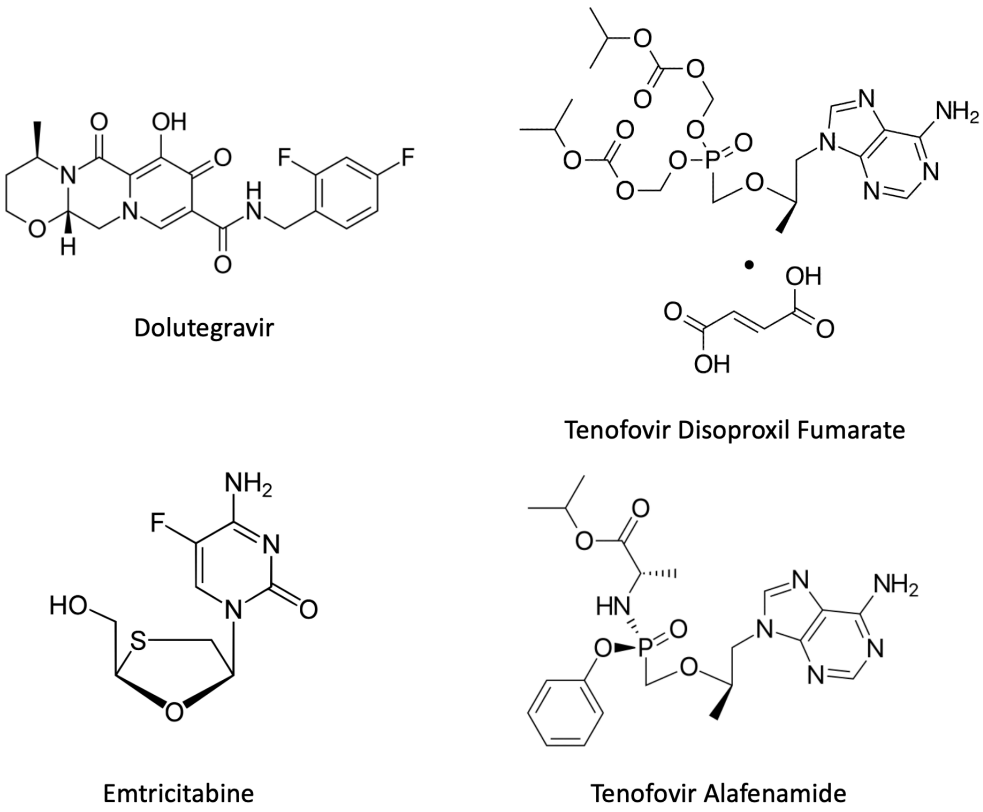

Figure 1-8 *Other antiretrovirals used in the first-line treatment of HIV. Dolutegravir (DTG) is an integrase strand transfer inhibitor. Emtricitabine (FTC), tenofovir disoproxil fumarate (TDF), and tenofovir alafenamide (TAF) are reverse transcriptase inhibitors.*

HIV resistance against lamivudine involves a M184V mutation of HIV reverse transcriptase. This mutation allows for preferential

incorporation of deoxycytidine triphosphate into viral DNA instead of 3TC-TP. The M184V mutation allows for deoxycytidine triphosphate selectivity 20 to 100 times more than the wild type HIV variant.[139] M184V is rarely found in treatment-naïve patients and is therefore determined to be developed due to drug pressure with NRTIs.[140] Interestingly, even in patients who have this reverse transcriptase mutation, lamivudine can still maintain

moderate antiviral efficacy. This could be due to synergistic effects with other antiretrovirals[141] or due to inability of the M184V variant to remove 3TC-MP once it is incorporated.[142] In addition, the M184V variant may decrease HIV's ability to replicate and may decrease transmissibility of the virus.[140] Lastly, as resting lymphocytes maintain low levels of triphosphate nucleotides, the availability of cytidine triphosphate relative to 3TC-TP is decreased, suggesting that 3TC may be more effective against the M184V variant in resting cells.[143]

As with other nucleoside analogues, 3TC is very hydrophilic, with a clog P of -0.71 (ACD/I-Lab, Advanced Chemistry Development, Toronto, ON, Canada). Because of 3TC's hydrophilic physiochemical properties, it is not expected to associate with chylomicrons following oral administration. As a result, its transport into intestinal lymphatics following oral administration, especially GALT and mesenteric lymph nodes (MLNs), is expected to be low. This is a concern as GALT and MLNs are the primary site of acute HIV replication as well as the latent reservoir.

Due to the one-way flow of the lymphatic system, drugs transported directly into the intestinal lymphatics following oral administration will end up flowing through the mesenteric duct, cisterna chyli, thoracic duct and ultimately drain into blood circulation via the left subclavian vein.[144] This flow pattern means that drug that was directly transported into intestinal lymphatics would not be able to reach other lymph nodes outside of this flow path. In order to deliver drug to these lymph nodes, lymph capillaries in the periphery can be targeted using either subcutaneous or transdermal

administrations with targeting methods utilizing particle sizes outlined in section 1.3.2. In this case, 3TC can then be formulated into dissolvable microneedle (MN) patches using these targeting methods to be administered to the extremities. While the one-way flow of lymph fluid still applies, drug transported into lymph capillaries located in the extremities will pass through draining lymph nodes, ultimately returning to blood through the right lymphatic duct or thoracic duct emptying into the right or left subclavian vein, respectively.[145] Because of this, combining both oral and subcutaneous or transdermal methods for targeting intestinal and peripheral lymphatics, respectively, could be beneficial to ensuring high concentrations of drug in lymph nodes throughout the body.

1.7 Aims

The overall aim of this project was to deliver 3TC into sites of the HIV reservoir in lymph nodes throughout the body. We aimed to achieve this by combining two routes of administration: oral administration to target the MLNs, and subcutaneous (SC) or transdermal administration to target other draining lymph nodes throughout the body. A secondary aim of this project was to observe the different concentrations of 3TC in the brain, spleen, testes, and lungs, which are other tissues that harbour HIV latent reservoir. By doing so, early initiation and increased concentrations of ARV could help to decrease the size of the forming latent reservoir. In addition, exposure of the lymph nodes to sufficient concentrations of ARV could minimize any low-level replication that occurs in this tissue. Lastly, delivering ARV to

tissues where latently infected cells can be found would be helpful to use in conjunction with curative strategies that utilize latency reversing agents in order to prevent additional new infections.

The first aim was to deliver 3TC to MLNs. For oral administration targeting, we first designed and synthesized highly lipophilic ester prodrugs that could associate with chylomicrons in intestinal enterocytes. These prodrugs could then take advantage of the fact that intestinal lymphatics are responsible for chylomicron transport, and the prodrugs could preferentially target the MLNs. The designed prodrugs must be stable in the intestinal environment but must also release parent drug quickly once they reach the lymphatics. Synthesized prodrugs underwent *in vitro* testing for association with artificial chylomicrons, stability in fasted state simulated intestinal fluid (FaSSIF) and rat plasma, and solubility in triglycerides to evaluate if they were suitable candidates for *in vivo* experiments. The delivery of parent drug 3TC to lymph nodes and other tissues harbouring HIV reservoir following oral, subcutaneous, and IV dosing was also analysed to understand the tissue penetration capabilities of 3TC.

The second aim was to target 3TC to peripheral lymphatics. We fabricated dissolvable MN patches for this purpose. These patches underwent *in vitro* testing to determine if 3TC-loaded MN patches could be a viable method for delivering drug into draining lymph nodes. Testing included drug loading, rigidity of needles and fracture force, insertion studies and Franz cell diffusion studies with porcine skin.

In addition, we performed pharmacokinetic studies for 3TC. Using time points for animal sacrifice determined from the results of the pharmacokinetic studies, we then assessed the biodistribution of 3TC in lymph nodes, brain sections, lung, spleen, and testes through *in vivo* experiments using male Sprague-Dawley rats following oral lipid-free, oral lipid-based, SC and intravenous (IV) administrations.

To support these studies, a sensitive bioanalytical method for the detection of 3TC and its prodrugs in biological matrices using high performance liquid chromatography with a UV detector (HPLC-UV) was developed and partially validated.

Chapter 2 Materials & Methods

2.1 Materials

Lamivudine (CAS: 134678-17-4, Batch: CAT6499-2) was purchased from ChemShuttle (Hayward, CA, USA). Synthetic cannabidiol (CBD) was purchased from THC Pharm (Frankfurt, Germany). Vinyl stearate, oleic acid, vinyl acetate, lipase B, Intralipid® 20%, propylene glycol, polyethylene glycol (PEG) 400, glycerol, sodium carboxymethyl cellulose (MW 90,000) (CMC), sesame oil, Dulbecco's phosphate buffered saline (PBS), potassium bromide, glacial acetic acid, PBS tablets and serum triglyceride determination kit were purchased from Sigma-Aldrich (Merck, St. Louis, MO, USA). High performance liquid chromatography (HPLC) grade ammonium acetate and methyl tert-butyl ether (MTBE) were purchased from Honeywell (Charlotte, NC, USA). HPLC grade methanol and acetonitrile (ACN) were purchased from Fisher Scientific (Hampton, NH, US). Next Advance (Troy, NY, USA) green and pink RINO® bead lysis kits were purchased from Thistle Scientific (Glasgow, UK). Kollidon® VA 64 was provided by BASF (Ludwigshafen, Germany).

2.2 Bioanalytical Methods for Determination of 3TC

All samples underwent the same sample preparation process. Proteins were precipitated by adding 450 µL of cold (-20 °C) ACN to 150 µL of sample and 15 µL of internal standard (IS), which was 50,000 ng/mL cannabidiol (CBD) solution in methanol. Samples then underwent further extraction by adding 4.5 mL of MTBE, vortexing for 10 minutes, and subsequent centrifugation at 1160 *g* at 10 °C for an additional 10 minutes. All liquid was collected and completely evaporated under nitrogen at 40 °C (Techne Dri-Block Heater DB-3D, Cambridge, UK). Samples were

reconstituted with 100 µL of 40% methanol in water (v/v) and transferred into HPLC vials.

All samples were analysed using an HPLC system equipped with a UV detector (Waters Alliance 2695 & Waters 996 Photodiode Array Detector, Waters, Milford, MA, USA). Separation was achieved using a Waters Atlantis dC18 Column, 5 µm particle size, 4.6 x 250 mm (Waters, Milford, MA, USA), at 45 °C. The autosampler was kept at 5 °C and 40 µL of the sample was injected into the HPLC system.

The gradient mobile phase (**Table 2-1**) consisted of ammonium acetate 10 mM buffer adjusted to a pH of 6 with acetic acid in the A line and methanol in the B line. The flow rate was set at 0.6 mL/min. The chromatographies were monitored at 270 nm for 3TC and its prodrugs and at 236 nm for IS (CBD). The retention times of the analytes were 16.6, 47.5, 41.7 and 32.7 minutes for 3TC, 3TC-stearate, 3TC-oleate and CBD, respectively.

Table 2-1 *Gradient of HPLC mobile phases for elution of parent drug 3TC, its prodrugs and CBD.*

3TC		**3TC-stearate & 3TC-oleate**	
Time (min)	**Mobile Phase (Ammonium Acetate Buffer:Methanol)**	**Time (min)**	**Mobile Phase (Ammonium Acetate Buffer:Methanol)**
0 - 17	88:12	0 - 17	88:12
17 - 22	88:12 to 10:90	17 - 22	88:12 to 8:92
22 - 32	10:90	22 - 47	8:92
32 - 37	10:90 to 88:12	47 - 52	8:92 to 88:12
37 - 43	88:12	52 - 58	88:12

2.3 Validation of Sensitivity, Linearity, Accuracy and Precision of HPLC-UV Method

Linearity of calibration curves, sensitivity of the limit of quantification (LOQ) and accuracy and precision were determined following the guidance of the FDA Bioanalytical Method Validation.[146] Briefly, a calibration curve was prepared with five replicates of the LOQ calibrators. To validate the sensitivity of the assay, the accuracy and precision must be validated for at least five LOQ replicates. To confirm accuracy, the observed concentrations for at least five LOQ calibrators would need to have a less than 20% error relative to the nominal concentrations. The precision of the five LOQ replicates was confirmed by a coefficient of variation (CV) under 20%. To validate the linearity of the calibration curve, all other calibrators would need to show less than 15% relative error.

The LOQ and low, medium and high quality controls (QCs) were run in five replicates on three different days for validation of the assay's inter-day accuracy and precision. The relative error would need to be less than 20% for the LOQ and 15% for the other QCs to confirm accuracy. The CVs were also calculated for each concentration and would need to be less than 20% for the LOQ and 15% for the other QCs to validate the method's precision.

2.4 Stability of Biological 3TC Samples in -80 °C and 37 °C Conditions

The stability of biological samples containing 3TC in -80 °C storage conditions were tested by adding 15 µL of 10,000 ng/mL 3TC stock solution

in methanol into 135 µL of blank rat plasma in triplicate. This resulted in a final rat plasma concentration of 1,000 ng/mL of 3TC. These samples were stored in a -80 °C freezer. After eight weeks, samples were removed and analysed for 3TC concentration by HPLC-UV.

Triplicates of samples prepared in the same way as described above were also incubated at 37 °C for 24 hours to test the stability of 3TC under heated conditions. Samples were analysed by HPLC-UV.

2.5 Design and *In Silico* Analysis of Physicochemical Properties of 3TC and Prodrugs

3TC-stearate and 3TC-oleate were designed as fatty-acid ester prodrugs of 3TC. The extent of association with chylomicrons was predicted using a previously described *in silico* model.[116] 3TC, 3TC-stearate and 3TC-oleate structures were loaded into ACD/I-Labs (Advanced Chemistry Development Inc., Toronto, Canada), and the corresponding physicochemical properties were then incorporated into the *in silico* model to obtain values that predicted affinity to chylomicrons. The following values were used: $LogD_{7.4}$, $LogP - LogD_{7.4}$, polar surface area, hydrogen-bond acceptors, freely rotatable bonds, density, molar volume, and hydrogen-bond donors (**Table 2-2**).

Table 2-2 *Physicochemical properties and corresponding coefficients to be used when calculating the predicted association with chylomicrons.*

Physicochemical property	Coefficient
$LogD_{7.4}$	0.299879
$LogP - LogD_{7.4}$	− 0.238127
PSA	− 0.00855215
H-bond acceptors	− 0.184359
FRB	0.0805226
Density	1.45337
Molar volume	0.00545912
H-bond donors	0.0823094
Constant	− 5.24138

The equation to calculate the predicated percentage association with chylomicrons is as follows:

$$\%\ Chylomicron\ Association = \frac{10^{\sum(Physicochemical\ property * Coefficient) + Constant}}{1 + 10^{\sum(Physicochemical\ property * Coefficient) + Constant}}$$

2.6 Synthesis of 3TC-stearate and 3TC-oleate

Vinyl stearate was purchased from Sigma-Aldrich (Merck, St. Louis, MO, USA). Vinyl oleate was synthesized using a previously described method[147]. Briefly, oleic acid was added to an excess of vinyl acetate, 0.01 equivalents of cyclooctadiene iridium chloride dimer and 0.03 equivalents of sodium acetate and refluxed in a three-neck round bottom flask at 100 °C overnight under nitrogen (**Figure 2-1**). Vinyl oleate was then purified by column chromatography using a PuriFlash column, 50 µm Si-HP, 12 g (Interchim, Montluçon, France) with a 20 to 50% gradient of dichloromethane (DCM) in cyclohexane in an Isolera Four flash chromatography system (Biotage, Hengoed, UK).

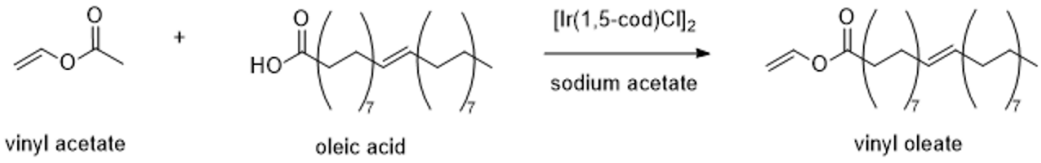

Figure 2-1 *Schematic for the synthesis of vinyl oleate. This reaction was refluxed overnight at 100 ℃.*

Prodrug synthesis was achieved using a previously described enzymatic reaction[148] with minor adjustments (**Figure 2-2**). Four equivalents of vinyl stearate or vinyl oleate were added to 2 mmol of 3TC and 300 mg of lipase B derived from *Candida antarctica* yeast immobilized on Immobead 150. This mixture was stirred at 50 °C overnight in 10 mL of a 4:1 mixture of pyridine and cyclohexane.

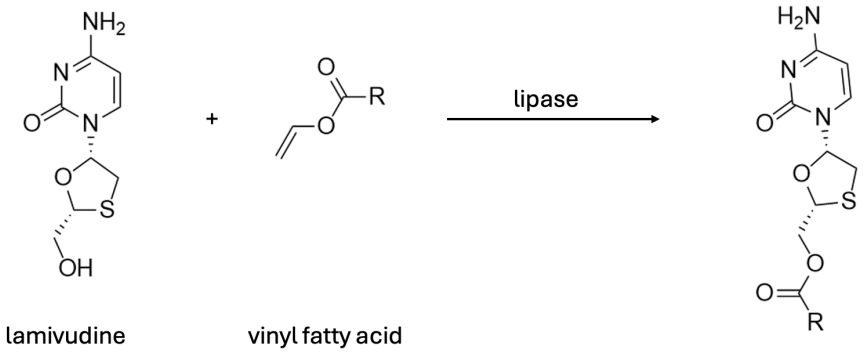

	R
3TC-stearate	$-(CH_2)_{16}CH_3$
3TC-oleate	$-(CH_2)_7CH{=}CH(CH_2)_7CH_3$

Figure 2-2 *Reaction scheme for the lipase synthesis of 3TC-stearate and 3TC-oleate. This reaction was stirred overnight at 50 ℃.*

The mixture was cooled to room temperature and lipase B was removed through vacuum filtration. Purification of 3TC-stearate was achieved through trituration as 3TC-stearate is insoluble in methanol.

Methanol was then removed via evaporation. Purification of 3TC-oleate was achieved by two rounds of column chromatography using ISOLUTE® SPE columns (Flash Silica II 5g/25mL) (Biotage, Hengoed, UK). The first column system was 70% cyclohexane in ethyl acetate and the second column system was 5% methanol in ACN. The purified fractions were pooled, and solvent was removed via evaporation. Trace 3TC was removed via trituration with water. Water was completely removed from 3TC-oleate by freeze drying.

((5-(4-amino-2-oxopyrimidin-1(*2H*)-yl)-1,3-oxathiolan-2-yl)methyl stearate (3TC-stearate). Vinyl stearate (8 mmol, 4.0 eq., 2484 mg), lamivudine (2 mmol, 1.0 eq., 460 mg) and lipase B (300 mg) were stirred in pyridine (8 mL) and cyclohexane (2 mL) at 50 °C for 16 hours. The lipase B was removed by vacuum filtration. 3TC-stearate was purified through trituration with methanol in 30% yield as a colourless solid. ^{1}H NMR (400 MHz, $CDCl_3$): δ 7.7 (d, 1H, *J* = 7.5 Hz), 6.3 (t, 1H, *J* = 5.3 and 4.2 Hz), 5.7 (d, 1H, *J* = 7.5 Hz), 5.3 (dd, 1H, *J* = 5.6 and 3.4 Hz), 4.6 (dd, 1H, *J* = 12.2 and 5.6 Hz), 4.3 (dd, 1H, *J* = 12.2 and 3.4 Hz), 3.6 (dd, 1H, *J* = 12.2 and 5.4 Hz), 3.1 (dd, 1H, *J* = 12.1 and 4.1 Hz), 2.3 (t, 2H, *J* = 7.6 Hz), 1.5-1.7 (m, 2H, *J* = 7.3 Hz), 1.2-1.4 (m, 28H), 0.9 (t, 3H, *J* = 6.7 Hz). HRMS-ESI (*m/*z): $[M+H]^+$ calculated for $C_{26}H_{45}N_3O_4S$, 495.72; found, 496.3.

(5-(4-amino-2-oxopyrimidin-1(*2H*)-yl)-1,3-oxathiolan-2-yl)methyl (*E*)-octadec-9-enoate (3TC-oleate).

Vinyl oleate (8 mmol, 4.0 eq., 2468 mg), lamivudine (2 mmol, 1.0 eq., 460 mg) and lipase B (300 mg) were stirred in pyridine (8 mL) and cyclohexane (2 mL) at 50 °C for 16 hours. The lipase B was removed by vacuum filtration. 3TC-oleate was purified with silica gel column chromatography in 30% yield as a colourless solid. ^{1}H NMR (400 MHz, $CDCl_3$): δ 7.7 (d, 1H, *J* = 7.7 Hz), 6.3 (t, 1H, *J* = 4.7 and 4.9 Hz), 5.7 (d, 1H, *J* = 7.3 Hz), 5.3 (m, 3H, *J* = 5.5 Hz), 4.6 (dd, 1H, *J* = 5.7 and 5.7 Hz), 4.3 (dd, 1H, *J* = 3.5 and 3.5 Hz), 3.6 (dd, 1H, *J* = 5.3 and 5.3 Hz), 3.1 (dd, 1H, *J* = 4.1 and 4.1 Hz), 2.3 (t,

2H, *J* = 7.5 and 7.5 Hz), 2.0 (m, 4H, *J* = 5.7 Hz), 1.5-1.6 (m, 6H, *J* = 7.5 Hz), 1.2-1.3 (m, 20H, *J* = 16.7 Hz), 0.9 (t, 3H, *J* = 6.5 and 7.1 Hz). HRMS-ESI [*m/z*]: $[M+H]^+$ calculated for $C_{26}H_{43}N_3O_4S$, 493.71; found, 494.2.

2.7 Characterization of Prodrugs

All reactions were monitored with thin layer chromatography (TLC) using Silica gel 60 F_{254} plates (Merck, Darmstadt, Germany).

In addition, a LC-MS/MS (liquid chromatography – tandem mass spectrometry) was used to monitor the reactions. A Shimadzu UFLCXR module (Shimadzu, Kyoto, Japan) with an Applied Biosystems API 2000 (Applied Biosystems, Waltham, MA, USA) equipped with a Phenomenex Gemini-NX C18 column, 3 µm particle size, 50 x 2 mm (Phenomenex, Macclesfield, UK) at 40 °C were used. The UV channels were monitored at wavelengths 220 nm and 254 nm. The mobile phase flow rate was 0.5 mL/min. The mobile phase gradient program is outlined in **Table 2-3**.

Table 2-3 Gradient program for LC-MS/MS used to monitor prodrug reactions.

Time	**Mobile Phase (0.1% Formic Acid in Water:0.1% Formic Acid in Acetonitrile)**
Pre-equilibration (1 min)	95:5
0 – 2 min	95:5 to 2:98
2 – 4 min	2:98
4 – 4.5 min	2:98 to 95:5
4.5 – 5.5 min	95:5

Prodrugs were dissolved into chloroform-*d* for characterization by ^1H nuclear magnetic resonance (NMR) (Bruker 400 Ultrashield Spectrometer,

Billerica, MA, USA) spectra recorded at 400 MHz at ambient temperature. Chemical shifts (δ) were reported as parts per million (ppm) relative to chloroform-*d* (^{1}H, δ = 7.26 ppm[149]). ^{1}H NMR data were reported as chemical shift, integration, multiplicity (s = singlet, d = doublet, t = triplet, m = multiplet) and coupling constant (*J*). The spectra were analysed using Topspin 4.1.3 (Bruker, Billerica, MA, USA).

All reagents and solvents were purchased from Merck (Gillingham, UK) and Fisher Scientific (Leicestershire, UK).

2.8 *In Vitro* Association of 3TC and Prodrugs with Intralipid®

Drug association with chylomicrons was determined using previously described methods.[150] 3TC and prodrug association with chylomicrons was assessed *in vitro* using Intralipid® 20% that was adjusted to a triglyceride concentration of 1 mg/mL using PBS. The concentration of triglycerides was measured using a serum triglyceride determination kit (Sigma, Gillingham, UK) according to manufacturer's instructions and a BioTek FL600 plate reader (BioTek Instruments, Winooski, VT, USA).

A 0.1 mM stock solution of 3TC or 3TC-oleate was prepared in 1% ethanol in propylene glycol (v/v), and a stock solution of 3TC-stearate was prepared in 5% dimethyl sulfoxide (DMSO) in propylene glycol (v/v). Stock solutions were spiked into triglyceride-adjusted Intralipid® to a final drug concentration of 1.75 µM, which was stirred at 170 rpm for one hour at 37 °C. A volume of 1 mL of this emulsion was then transferred to a polyallomer ultracentrifuge tube. Then, on top of the incubated Intralipid®, a density gradient was layered using a syringe with PBS that was adjusted to the

following densities using KBr: 1.006, 1.019, and 1.063 g/mL. Volumes of 2, 4, and 4 mL were used, respectively, for each density layer. After ultracentrifugation (SORVALL Ultracentrifuge, TH-641 Rotor, 268,350 *g*, 35 min, 15 °C), the white floating chylomicron layer (approximately 1 mL) was collected using glass Pasteur pipette and analysed by HPLC-UV for presence of drug.

To calculate the percentage of association with chylomicrons, the amount of drug recovered in the chylomicron layer was divided by the amount of drug spiked into the Intralipid®.

2.9 *Ex Vivo* Association of 3TC with Natural Rat Chylomicrons

Animal welfare and all experimental procedures were reviewed and approved by the University of Nottingham Ethical Review Committee under the Animals [Scientific Procedures] Act 1986. Male Sprague-Dawley rats ranging from 300 to 350 g purchased from Charles River UK. They were housed at Bio Support Unit, University of Nottingham. Animals were kept in an environmentally controlled room (12:12 h light-dark cycle) with free access to food and water for at least four days before gathering chylomicrons. To gather rat chylomicrons, rats were given oral gavages of 0.5, 0.3, and again 0.3 mL of sesame oil for 3 subsequent hours to facilitate intestinal chylomicron production. An hour after the final dose of sesame oil, rats were sacrificed by terminal blood collection. Blood was then centrifuged at *13,000 g* for 10 minutes and plasma collected. The plasma was then adjusted to a density of 1.1 g/mL using KBr. The density gradient was layered on top of the plasma using standards adjusted to 1.006, 1.019, and

1.063 g/mL. The plasma and gradient were ultracentrifuged as previously described in section 2.8. Chylomicrons were separated and the concentration of triglycerides was measured using a serum triglyceride determination kit (Sigma, Gillingham, UK) and a BioTek FL600 plate reader (BioTek Instruments, Winooski, VT, USA). The chylomicrons were then adjusted using PBS to a triglyceride concentration of 1 mg/mL. The triglyceride-adjusted chylomicrons were stored at 4 °C for a maximum of 24 hours.

The triglyceride-adjusted natural rat chylomicrons and 3TC were then incubated and stirred at 37 °C. Following incubation, the density gradient was layered on top of the chylomicrons and subsequently ultracentrifuged as described in section 2.8. Floating rat chylomicrons (approximately 1 mL) were then separated and analysed by HPLC-UV for presence of drug.

2.10 *In Vitro* Prodrug Stability in Rat Plasma and FaSSIF

Prodrugs were assessed for stability in rat plasma and FaSSIF matrices. FaSSIF was made following previously described formulations[151] of 3 mM sodium taurocholate, 0.75 mM lecithin, 8.7 mM sodium hydroxide, 28.65 mM monosodium phosphate and 105.9 mM sodium chloride in water adjusted to a pH of 6.5. To this mixture, 20 IU/mL of porcine esterase was added.[124,125,152,153] Rat plasma or FaSSIF were incubated at 37 °C for 5 minutes. Then, 10 µL of 1 mM prodrug stock solution of either 3TC-stearate or 3TC-oleate in DMSO or methanol, respectively, was added to 990 µL rat plasma or FaSSIF and further incubated at 37 °C at 200 rpm in an orbital shaker incubator (Thermo Scientific MaxQ4000, Waltham, MA, USA). 150 µL

of the mixture was taken at pre-determined time points and mixed directly into 450 µL of cold ACN for reaction termination and protein precipitation. 15 µL of IS was added and samples were prepared and analysed using HPLC-UV. Each experiment was performed in triplicate.

The elimination rate constant (*k*) was calculated by plotting the natural logarithm of the concentration of drug against the time points and obtaining the slope. The half-life was calculated using the equation $t_{1/2} = -0.693/k$.

2.11 Triglyceride Solubility of 3TC and its Prodrugs

The solubility of 3TC, 3TC-stearate, and 3TC-oleate in triglycerides was determined using sesame oil as a representative vehicle for long-chain triglycerides. An excess of 3TC or 3TC-stearate was dissolved into sesame oil and stirred at 37 °C for 72 hours. 3TC-oleate was stirred in sesame oil for 72 hours at room temperature. The mixtures were then filtered in Costar Spin-X Centrifuge Tubes (Fisher Scientific, Loughborough, UK) for 5 minutes at 2400 *g.* The filtrate was then diluted 10 times in acetone, another 10 times in ethanol and a further 10 times in methanol. The final dilution was analysed by means of HPLC-UV. Each experiment was performed in triplicate.

2.12 Animals

Animal welfare and all experimental procedures were reviewed and approved by the University of Nottingham Ethical Review Committee under the Animals [Scientific Procedures] Act 1986. Male Sprague-Dawley rats ranging from 300 to 350 g purchased from Charles River UK were used for all *in vivo* studies. They were housed at Bio Support Unit, University of

Nottingham. Animals were kept in an environmentally controlled room (12:12 h light-dark cycle) with free access to food and water for at least six days before starting any procedures prior to jugular vein cannulation studies, or four days before biodistribution studies.

For all animal studies, animals were fasted overnight prior to the start of study, but rats were allowed free access to water. Rats were fasted for a maximum of 16 hours before food was returned.

2.13 Jugular Vein Cannulation Surgery

Rats' jugular veins were cannulated according to previously described protocols.[124,125,154] Rats were sedated under inhaled 2.5% isoflurane in oxygen anaesthesia. Fur was shaved on the right dorsal neck-to-upper thorax and on the midline of the ventral neck. The shaved areas were cleaned with 2% chlorhexidine wipes (Clinell®. GAMA Healthcare Ltd, London, UK). Ophthalmic lubricating ointment was applied to the eyes to prevent dryness. Four mL of saline and 1 mg/kg of meloxicam were injected subcutaneously into the ventral trunk. The rats were then wrapped with Glad® Press'n Seal® cling film and transferred to the operating theatre.

Rats were placed on a heating pad and the nose was placed in a mask with a flow of 2.5% isoflurane in oxygen. With the dorsal side facing up, the pulse of the rat was identified before surgical incision. Following blunt dissection, the jugular vein was then identified and isolated from surrounding fatty and connective tissues using cotton swabs. An incision was made at the ventral shaved area, and a metal pin was used to create a subcutaneous "tunnel" from the ventral to the dorsal incision. A cannula

made of silastic-polyethylene was inserted into this "tunnel." Using a pair of iris micro scissors, an incision was made on the jugular vein and 2.5 cm of the silastic end of the cannula was inserted into the vein towards the heart. The cannula was then secured with silk suture and the dorsal incision was closed. On the ventral side, the cannula was anchored onto the muscle using suture and Tygon® tubing, then the ventral incision was closed. The cannula's integrity was verified, and 0.7 mL of 100 IU/mL heparinized saline was pushed to flush the cannula. The cannula was then cut to allow approximately 4 cm protrusion from the ventral incision and closed with a metal pin. Rats were allowed two nights for recovery prior to pharmacokinetics studies. Cannulas were flushed with 1 mL/kg of 100 IU/mL heparinized saline the morning after surgery and evening prior to the study.

2.14 *In Vivo* – Pharmacokinetics Studies

3TC formulations used in *in vivo* studies were prepared in 70% propylene glycol, 20% water and 10% ethanol by volume for oral and IV formulations, and in 100% sterile water for SC formulations. Formulations were prepared in concentrations of 30 mg/mL, 10 mg/mL, and 30 mg/mL for oral, IV, and SC administrations, respectively.

The dose of 3TC for oral administration in rats was chosen by allometric scaling from the Food and Drug Administration (FDA)-approved human dose for HIV (300 mg once per day) using an assumed average human weight of 62 kg.[155] This was calculated using the following equation:

*Animal dose (mg/kg) = Human dose (mg/kg) * Conversion Factor*. In this case, the human-to-rat dose conversion factor was 6.2.

Orally dosed rats were separated into two groups: oral lipid-free and oral lipid-based. The oral lipid-based administration group was given an oral gavage of 1 mL/kg sesame oil followed by 30 mg/kg of oral 3TC formulation, whereas lipid-free animals were only given the drug formulation without oil. Lastly, all animals were then administered 1 mL of water via oral gavage. Blood was sampled through the jugular cannula at 0, 30, 60, 90, 120, 180, 300, 420, and 540 minutes.

The intravenously dosed rats were administered 10 mg/kg of IV 3TC formulation as a bolus dose into the previously surgically inserted jugular cannula. The cannula was then flushed with 1 mL/kg of 100 IU/mL heparinized saline. Blood was sampled through the jugular cannula at 0, 5, 15, 30, 60, 120, 180, 240, and 300 minutes.

Subcutaneously dosed rats were injected with 10 mg/kg of the SC 3TC formulation at the right side of the base of the tail. Blood was sampled through the jugular cannula at 0, 5, 10, 15, 30, 60, 120, 180, and 240 minutes.

At each sampling time point for all administration groups, 0.3 mL of blood was collected from the cannula into Eppendorf vials containing 3K ethylenediaminetetraacetic acid (EDTA). Following blood sampling, cannulas were flushed with 0.3 mL of 100 IU/mL heparinized saline. The blood was centrifuged at 3,000 *g* at 10 °C for 10 minutes, and the plasma was collected to be sample prepared and analysed via HPLC-UV as described in section 2.2.

All pharmacokinetic parameters were calculated with Phoenix WinNonlin 6.3 (Certara, Princeton, NJ, USA) using non-compartmental analysis.

2.15 *In Vivo* – Biodistribution Studies

Animals in biodistribution studies were dosed in the same way as in pharmacokinetic studies as described in section 2.14.

Time points for biodistribution studies were determined based on pharmacokinetic studies performed in section 2.14. Times for animal sacrifice by carbon dioxide chamber were designed to be around the t_{max} for oral and SC administrations. Oral-administration biodistribution sacrifice times were 30, 60, 90, and 120 minutes. SC-administration biodistribution sacrifice times were 15, 30, and 60 minutes. Since IV administration pharmacokinetic profiles do not have a t_{max}, sacrifice times were chosen to be the same as the SC study to allow for ease of comparison and to track tissue concentrations throughout the distribution phase. As such, animals in the IV group were also sacrificed at 15, 30 and 60 minutes.

Immediately following sacrifice, lymph fluid was sampled from the mesenteric lymph duct and 1 mL blood drawn from the vena cava in orally dosed animals. Lymph fluid was collected in an Eppendorf containing K3-EDTA (1.5 M) to prevent clotting and kept on ice for a maximum of 3 hours until lymph fluid components could be separated. Blood was collected into an empty Eppendorf tube and allowed to coagulate at room temperature. To separate serum, the Eppendorf tubes were centrifuged at 3,000 *g* at 10 °C for 10 minutes and the supernatant was collected.

In orally dosed animals, the following lymph nodes were then collected: mesenteric, cervical, axillary, brachial, iliac, and popliteal. Due to the site of the SC injection, for SC and IV dosed animals, inguinal nodes were additionally gathered, and all lymph nodes (except mesenteric) were separated into nodes found on the left or right (injection) side of the body. Lymph nodes were isolated from visceral tissue in all animals using previously described methodology.[125,154] All lymph nodes were weighed. Water was added to MLNs at a ratio of 1:3 (w/v) and the mixture was homogenized using a Polytron® PT 10-35 GT homogenizer (Kinematica, Malters, Switzerland). All other lymph nodes were placed in green bead homogenizer RINO® tubes and sufficient water to obtain at least 150 µL of sample was added. The lymph nodes and water inside the RINO® tubes were homogenized using a Bullet Blender 24 Gold (Next Advance, Troy, NY, USA).[156]

The brain was collected from each rat and further separated into the following sections: olfactory bulb, cerebellum, medulla, hippocampus, frontal lobe, striatum, temporal lobe, occipital lobe and parietal lobe. All sections of the brain were weighed. Water was added to the cerebellum, medulla, frontal lobe, temporal lobe, occipital lobe and parietal lobe at a ratio of 1:3 (w/v) and the mixture was homogenized using a Polytron® PT 10-35 GT homogenizer (Kinematica, Malters, Switzerland). The olfactory bulb, hippocampus and striatum were placed in pink bead homogenizer RINO® tubes and sufficient water added to obtain at least 150 µL of sample. These

brain sections and water inside the RINO® tubes were homogenized using a Bullet Blender 24 Gold (Next Advance, Troy, NY, USA).

The other tissues collected for analysis were the testes, lungs and spleen. All tissues were weighed, and water was added at a ratio of 1:3 (w/v). The mixture was homogenized using a Polytron® PT 10-35 GT homogenizer (Kinematica, Malters, Switzerland).

All blood samples, lymph fluid samples and homogenates were then sample prepared following methodology outlined in section 2.2 and analysed via HPLC-UV.

2.16 Separation and Analysis of Lymph Fluid Components

Immediately following the oral-administration biodistribution studies, in lymph fluid samples with greater than 30 µL collected, 5 µL was separated to be analysed as "whole lymph". The remainder was then centrifuged at 420 *g* at 10 °C for 10 minutes to pellet the cells. The supernatant was collected, and a density gradient was built and subsequently ultracentrifuged to separate out the chylomicrons layer as described in section 2.8. The chylomicrons layer was analysed by HPLC-UV for presence of 3TC. The remaining gradient (with chylomicrons removed) was then evaporated at 40 °C under nitrogen overnight to dryness and then reconstituted with 1 mL of water. This fraction consisting of lymph without both cells and chylomicrons was considered to be the "fluid only" compartment of lymph and analysed by HPLC-UV. The cell pellet was resuspended in PBS and centrifuged again. After the second centrifugation, the PBS layer was discarded and 200 µL of fresh PBS was added for a final

cell suspension. The final cell suspension was then analysed by means of HPLC-UV for presence of drug.

The “whole lymph” concentration taken in the first step of this section was used to calculate mass recovery percentages for each compartment: “fluid only,” “cells” and “chylomicrons.”

Lymph fluid samples with less than 30 µL collected were analysed by HPLC-UV directly and did not undergo the separation procedure described.

2.17 Microneedle Patch Fabrication

Polyvinylpyrrolidone/vinyl acetate (PVP/VA) MN patches were fabricated using a previously described method using previously fabricated 10 x 10 array of obelisk-shaped polydimethylsiloxane (PDMS) moulds (300 µm x 300 µm x 1000 µm, L x W x H per needle)[157] with some minor alterations. The needle matrix was made by mixing 2 mL of either blank, 30 mg/mL or 60 mg/mL 3TC solution in water, 0.324 g of Kollidon® VA 64 and 40 µL of PEG 400. After ensuring the PVP/VA was dissolved, the mixture was degassed. Using a positive placement pipette, the mixture was pipetted into the PDMS moulds and centrifuged at 4000 RPM for 15 minutes to ensure each needle mould was filled with matrix solution. After centrifugation, excess needle matrix was then removed. Possible bubbles were removed by vacuum pump, and needles were left to dry in a desiccator at room temperature and pressure for 3 days.

The backing layer matrix was made by dissolving 0.4 g CMC into 7.6 mL of water and 50 µL of glycerol. After degassing, 200 µL of backing layer matrix was pipetted into the moulds with dried needle matrix. The moulds

were then centrifuged at 3500 RPM for 10 minutes. Again, bubbles were removed using a vacuum pump, and patches were left to dry in a desiccator at room temperature and pressure for an additional 4 days.

MN patches were then demoulded carefully to ensure that there was no needle breakage.

2.18 Visualization of Microneedle Patches

MN patches were initially characterized under a Zeta Profilometer (KLA-Tencor, Milpitas, CA, USA) to ensure that needles were of an obelisk shape and that needles were not broken during the demoulding process. Patches were subsequently characterized under an environmental scanning electron microscope (ESEM) (Quanta 650, FEI Company, Hillsboro, Oregon, USA) in low vacuum mode.

2.19 Microneedle Patch Fracture Force

To ensure that the MNs would be robust enough for skin insertion, the mechanical strength of the MNs were tested using a texture analyser (TA.XTPlus, Stable Micro Systems, Surrey, UK) using a previously described method.[158] After attaching the MN patch onto a cylindrical probe using double-sided tape, the patch underwent a strain rate test with the following parameters: 50 kg load cell, Strain Rate 20%/sec, Pre-Test Speed 10 mm/sec, Post-Test Speed 10 mm/sec, Trigger Force 0.02 N. The fracture force was then calculated as N/needle. Experiments were carried out in quadruplicate.

2.20 Microneedle Patch Insertion Tests

MN patches underwent Parafilm M® insertion tests using a previously described method.[159] Eight sheets of Parafilm M® were layered

and MNs fabricated in section 2.17 were pressed using thumb pressure manual insertion. Each layer of Parafilm M® were then visualized under a Zeta Profilometer (KLA-Tencor, Milpitas, CA, USA) and the number of needle punctures per patch per layer were counted and converted into a percentage of the number of punctures per the number of needles. This experiment was performed in quadruplicate.

Patches then underwent porcine skin insertion tests. Without damaging the skin, hairs were trimmed using clippers. Loaded MN patches were then pressed into skin for 10 seconds using thumb pressure. Following removal of the patch, methylene blue dye was applied to the skin and allowed to sit for one hour. Excess dye was removed and visually inspected for formation of micro-channels. Skin was then cross-sectioned using a cryostat (CM3050 S, Leica, Wetzlar, Germany) and visualized under a Zeta Profilometer (KLA-Tencor, Milpitas, CA, USA). The dyed channels were then measured. This was performed in quadruplicate.

2.21 Microneedle Patch Drug Loading

3TC loading was determined by dissolving one patch into 1 mL of water. This was then diluted 100 times and then underwent sample preparation as outlined in section 2.2. This was performed in quadruplicate. These samples were then analysed by HPLC-UV.

2.22 Microneedle Patch Franz Cell Diffusion

Pig skin was first prepared by scraping off as much SC fat as possible and hair was removed using clippers. The skin was then cut into pieces just large enough to fit a MN patch. Blank patches and patches loaded with 3TC

were then inserted into the skin using thumb force and held in place using tape. The skin and patch were then placed in a Franz diffusion cell, which was held together using a clamp. The receptor compartment was filled with PBS. The Franz diffusion cell was then placed into a water bath heated to 36.5°C and stirred with a magnetic stirring bar for 24 hours.

After 24 hours, the skin and patch were removed from the Franz diffusion cell and the PBS receptor fluid was removed for analysis. The tape holding the patch and the residual MN patch itself was removed from the skin and collected into a glass scintillation vial. The surface of the Franz diffusion cell glass was swabbed with a 3% v/v Teepol®-soaked sponge and also placed into a glass scintillation vial. 10 mL of water was then added to the vials with patch residue or sponge and vortexed for 10 minutes followed by sonication for 30 minutes. The contents were left to soak overnight and subsequently vortexed and sonicated again before analysis via HPLC-UV for 3TC content.

The remaining pig skin was cut into small pieces and weighed before diluting six times with water and undergoing homogenization using a Polytron® PT 10-35 GT homogenizer (Kinematica, Malters, Switzerland). The homogenate then underwent sample preparation as described in section 2.2. All samples were analysed via HPLC-UV.

2.23 Statistical Analysis

Statistical analysis was done on Prism 9 (GraphPad, Boston, MA, USA). All data are shown as mean ± standard error of the mean (SEM) except for chapter 6, in which data are shown as mean ± standard deviation

(STD). Statistical significance was determined using one-way ANOVA followed by Tukey's test for analysis of three or more groups, one-way ANOVA followed but Dunnett's test for analysis in which there was a control group, mixed-effects model followed by Šídák's multiple comparisons test for analysis of two groups, or t-tests.

Chapter 3 HPLC-UV Method Development for the Determination of 3TC Biological Samples

3.1 Introduction

Initially approved by the US Food and Drug Administration (FDA) in 1995, 3TC is a relatively older but still very commonly used drug. As a result, there are several studies that have reported HPLC-UV methods for the determination of this drug in biological samples. However, many of these published methods are for different species, such as rabbit[160] or human[161–163], and therefore would not translate to rat plasma. In methods that did utilize rat plasma, limits of quantification (LOQ) were rather high at 125 - 200 ng/mL. [164,165] Other assays that had lower LOQs ranging from 5 - 50 ng/mL utilized ultra-performance liquid chromatography (UPLC) or LC-MS methods[166–168], which are more expensive, especially for resource-limited settings.

In order to accurately plot a pharmacokinetic profile and capture the elimination phase (and therefore elimination half-life), our bioanalytical assay must be able to quantify low concentrations of 3TC in plasma. In addition, a higher LOQ of 125 - 200 ng/mL could be an issue in future biodistribution studies because a minimum of three times the tissues' weight in water is added during homogenization, resulting in a chromatography concentration that is four times lower than the actual tissue concentration. This could be problematic in the analysis of tissues with especially low concentrations or in smaller tissues with low mass that may need the addition of more water relative to tissue weight in order to reach the minimum sample volume. In such situations, a bioanalytical method with a higher LOQ may not be able to quantify the concentrations of

drug. Because of this, it was necessary to develop a sensitive assay that would be able to quantify drug at much lower concentrations.

To ensure accurate and humane pharmacokinetic studies, a maximum of 15% of the animal's total blood can be taken as samples[169]. Rats have a total volume of about 64 mL/kg of whole blood.[170] As about 50% of the sample volume of whole blood can be recovered as plasma post-centrifugation, the approximate maximum plasma volume that can be sampled would be 1.44 mL from a 300 g rat. As a result, in order to obtain the minimum eight time-points for a pharmacokinetic study, each sample would have to be a maximum of 180 µL of plasma. Thus, for the purposes of this thesis, an HPLC-UV method for the bioanalysis of 3TC would have use less than 180 µL rat plasma per sample whilst quantifying low concentrations.

This method would also need to be able to detect high concentrations of 3TC. In previously published pharmacokinetic studies performed in rats, concentrations found at the t_{max} in oral administration studies and the first time point in IV administration studies were found to be quite variable. Reported oral C_{max} ranged from around 1200 to 110,000 ng/mL[171–174] and 5-minute blood collection time points in IV administration studies ranged from 3,500 to 16,000 ng/mL[166,175] when adjusted for dose. However, due to differences employed by other studies regarding concentration analysis methods, rat species, and drug combinations, 10,000 ng/mL seemed like a reasonable upper limit of quantification.

Lastly, in addition to 3TC, which is very hydrophilic, the HPLC-UV method would need the ability to be easily modifiable to simultaneously quantify highly lipophilic prodrugs. Being able to quantify both 3TC and its prodrugs in a single bioanalytical method would be time saving compared to developing separate assays to be run separately for the prodrugs. In addition, being able to obtain both 3TC and prodrug concentrations from one HPLC-UV assay would be able to decrease the volume of plasma sample needed for each time point.

3.2 Experimental Design

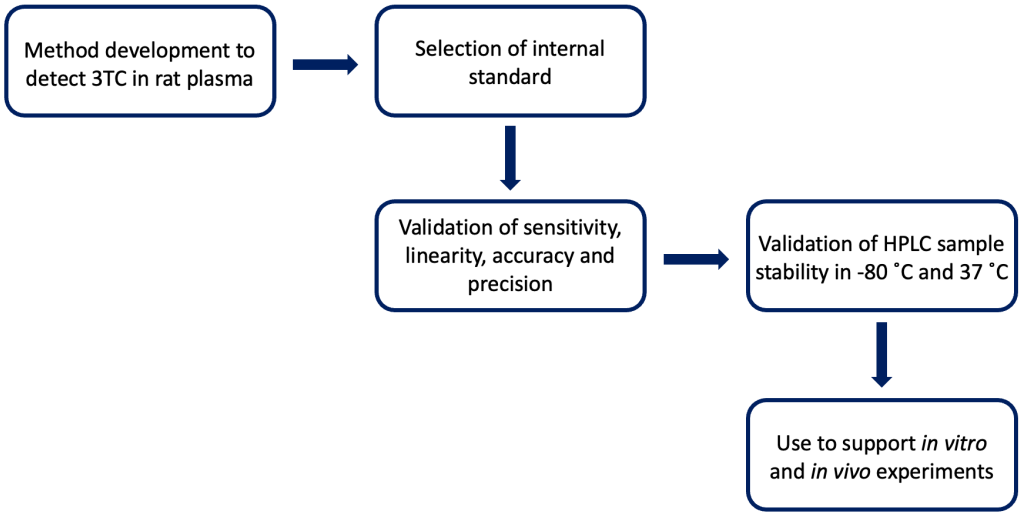

Figure 3-1 *Schematic outlining the workflow for the development and validation of an HPLC-UV method for 3TC in rat plasma. 3TC, lamivudine; HPLC, high performance liquid chromatography.*

The preparation of samples and the HPLC-UV method parameters are described in section 2.2.

Linearity of calibration curves, sensitivity of the LOQ and accuracy and precision were determined following methods described in section 2.3.

Stability of biological samples of 3TC in -80 °C and 37 °C conditions were determined as described in section 2.4.

3.3 Results and Discussion

The HPLC-UV machine available for this project was a Waters Alliance 2695 & Waters 996 Photodiode Array Detector (Waters, Milford, MA, USA). The sample carousel chamber was kept at 5 °C. Highly hydrophilic drugs like 3TC can be difficult to retain in reverse-phase columns as there is usually very little interaction between such molecules and an 8-carbon or 18-carbon chain bonded to silica. As a result, higher percentages of the aqueous component in the mobile phase are necessary in order to promote polar drug retention in the column. Unfortunately, traditional reverse-phase columns can experience phase dewetting when used with mobile phases with high water content[176], resulting in a loss of retention. However, Waters Atlantis columns utilize difunctionally bonded silanes and are designed to be able to be used with 100% water mobile phase. Because of this, a Waters Atlantis dC18 Column, 5 µm particle size, 4.6 x 250 mm (Waters, Milford, MA, USA) was chosen for this project.

Due to 3TC's log D chart (**Figure 3-2**), the buffer chosen was 10 mM ammonium acetate adjusted to a pH of 6. Since 3TC is a weak base, this would ensure that 3TC was maximally unionized, therefore maximizing UV absorbance and the area under the chromatography's drug peak. In addition, using a buffer instead of water would be beneficial to ensure consistent pH and minimize variation. Although the Waters Atlantis column could support a maximum of pH 7, adjusting the ammonium acetate buffer

to this pH would require ammonia. As the use of acetic acid is safer than ammonia and the peak area of 3TC was not notably different between a pH of 6 and 7, this method was developed utilising a buffer pH of 6.

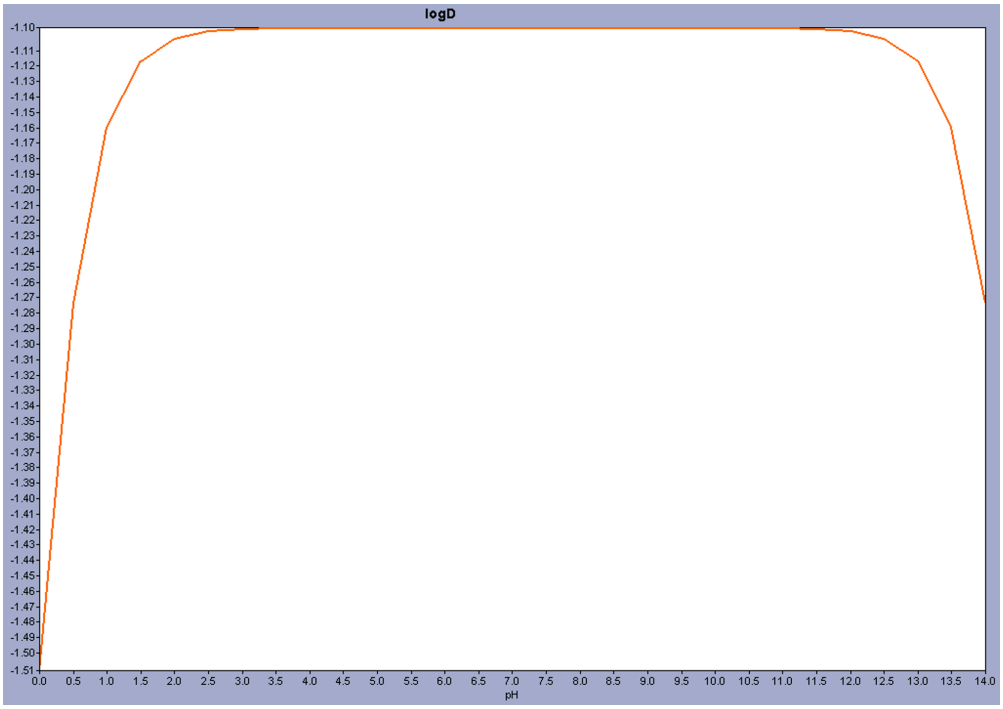

Figure 3-2 *Log D chart at different pH for 3TC generated with MarvinSketch (ChemAxon, Budapest, Hungary).*

In order to test the retention of 3TC in the Atlantis column, a stock solution of 5,000 ng/mL in 50% methanol was prepared. Each injection was for a volume of 40 µL. This volume was chosen because assuming a sample reconstitution volume of 100 µL, an HPLC sample injection of 40 µL would allow for two injections per reconstitution. This would provide for a second chance in the case of an injection error or any other HPLC run error. The stock solutions were processed at varying mobile phase compositions ranging from 10 to 40% methanol in buffer with a column temperature of 45 °C (**Figure 3-3**). An initial flow rate was chosen to be 1 mL/min. Unfortunately, even at a relatively low organic mobile phase composition at

20% methanol in buffer, the retention of 3TC was poor at less than 5 minutes.

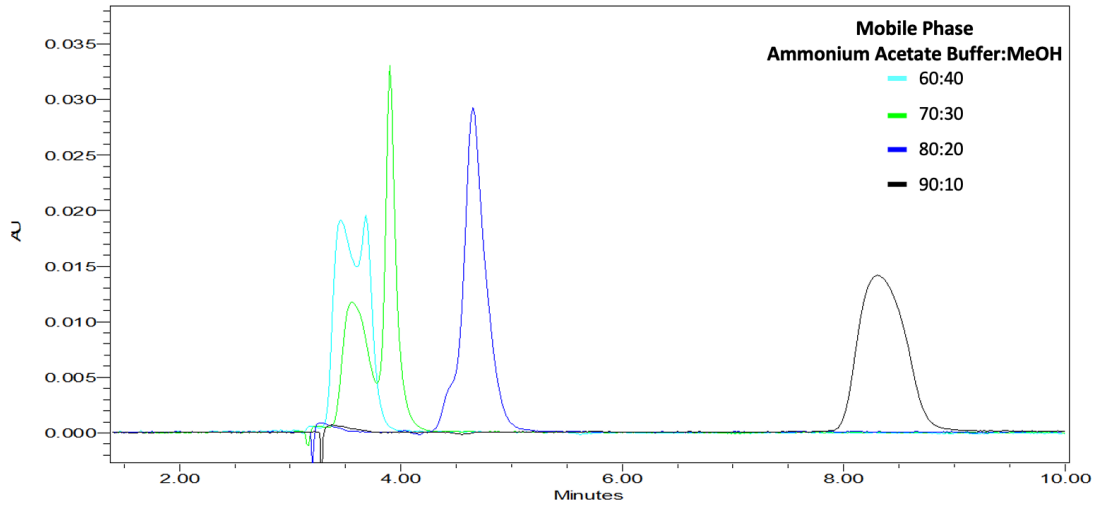

Figure 3-3 *Chromatographies of an injection of 5,000 ng/mL 3TC solution in 50% methanol at isocratic methods with a column temperature of 45 ℃ and flow rate of 1 mL/min of varying mobile phase compositions. The drug retention was poor, even at low-organic mobile phase compositions.*

In order to increase retention, the flow rate of the mobile phase was next decreased to 0.8 mL/min. A stock solution of 1,000 ng/mL of 3TC in 50% methanol was injected. This was compared to a blank preparation of 100 µL rat plasma, which underwent protein precipitation with methanol and liquid-liquid extraction with MTBE. This volume of rat plasma was initially chosen in an attempt to maximize the number of time points In an effort to minimize the number of time-points achievable in pharmacokinetic studies. The mobile phase was set at an isocratic 80:20 ratio of ammonium acetate buffer:methanol. Unfortunately, this did not result in separation of the drug peak and rat plasma peaks (**Figure 3-4**).

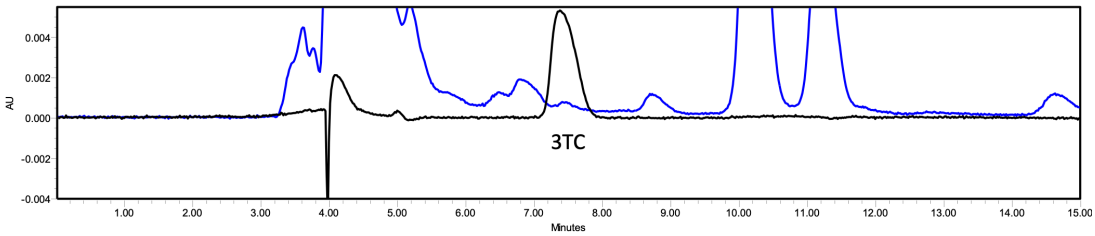

Figure 3-4 *An overlay of a chromatography of 1,000 ng/mL of 3TC solution in 50% methanol (black) and blank rat plasma (blue) with a column temperature of 45 ℃ and a flow rate of 0.8 mL/min. The mobile phase was an isocratic 80:20 ratio of ammonium acetate buffer:methanol. 3TC, lamivudine.*

In order to further increase retention, the flow rate was adjusted 0.6 mL/min. However, using the 80:20 isocratic buffer:methanol method, this still did not result in complete separation of the drug peak from the rat plasma peaks. The aqueous phase of the mobile phase mixture was gradually incrementally increased until potentially acceptable separation of the 3TC peak and rat plasma peaks was achieved at 88% ammonium acetate buffer and 12% methanol. The retention time of 3TC using these parameters was 16.6 minutes (**Figure 3-5A**).

Initially, nitrogen-evaporated samples were reconstituted using 100 µL of 50% methanol in water. However, using this reconstitution solvent, the peak shape of 3TC was found to be poor with severe shouldering when the mobile phase during 3TC elution was 88:12 ammonium acetate buffer:methanol (**Figure 3-5A**). The poor peak shape caused drug peak interference with background rat plasma peaks, and it was hypothesized that improving the peak shape could result in peak separation. This shouldering was addressed by changing the reconstitution solvent to be more similar to the mobile phase during drug elution as shown in **Figure 3-5**. As such, the reconstitution solvent was changed from 50% methanol in

water to 40% methanol in water. Although the peak shape could likely be further improved by decreasing the methanol content to 12% in water, there was concern that a reconstitution solvent that had too little methanol would not be able to solubilize highly lipophilic prodrugs that would be synthesized in the future. As a result, the reconstitution solvent was kept as 40% methanol in water to achieve an acceptable peak shape whilst maintaining as high as possible methanol content to maintain prodrug solubility.

Initially, protein precipitation was performed used cold methanol. However, this resulted in a small rat plasma peak at 18 minutes as shown in **Figure 3-5**. Although this rat plasma peak eluted after the 3TC drug peak, this configuration would not allow for any shift in chromatography and potentially could cause some interference at higher 3TC concentrations. When the protein precipitation solvent was changed to cold acetonitrile, the rat plasma peak at 18 minutes no longer appeared (**Figure 3-6**). As a result, cold acetonitrile was used for protein precipitation for the remainder of this project.

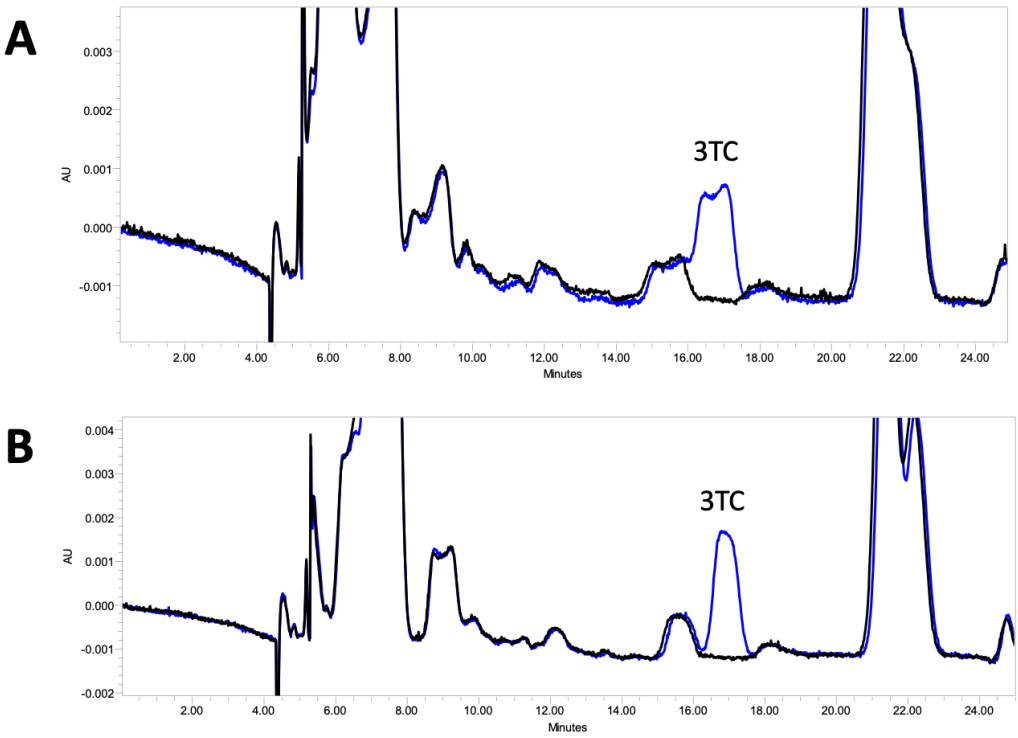

Figure 3-5 *Chromatographies showed peak shouldering when the reconstitution medium consisted of 50% methanol in water (A). This shouldering was drastically reduced with a reconstitution medium of 40% methanol in water (B). The mobile phase at this phase of the method gradient is 88% ammonium acetate buffer and 12% methanol. Blank rat plasma is displayed in black, and rat plasma with 3TC at a concentration of 1,000 ng/mL is displayed in blue. 3TC, lamivudine.*

When using 100 µL of sample, the 3TC was undetectable in rat plasma below 50 ng/mL. This was deemed to be too high as the sample preparation process of most tissues involves adding 3 times the tissue weight in water for homogenization, resulting in dilution. In addition, previously performed pharmacokinetic studies suggested that a lower LOQ may be beneficial to ensure an accurate representation of the elimination phase.[166,171–173] As a result, the volume of sample was increased to 150 µL of rat plasma. This sample volume was deemed acceptable as it would allow for nine time-points in a pharmacokinetic study.

Using this method of 150 µL of sample in 88% ammonium acetate buffer and 12% methanol at 0.6 mL/min with the column at 45 °C, the lowest detectable concentration was 15 ng/mL (**Figure 3-6**). If validated, an LOQ of 15 ng/mL would allow for the quantification of as low as 60 ng/g in tissues samples in which the volume of water was added at a 1:3 ratio (w/v) for homogenization.

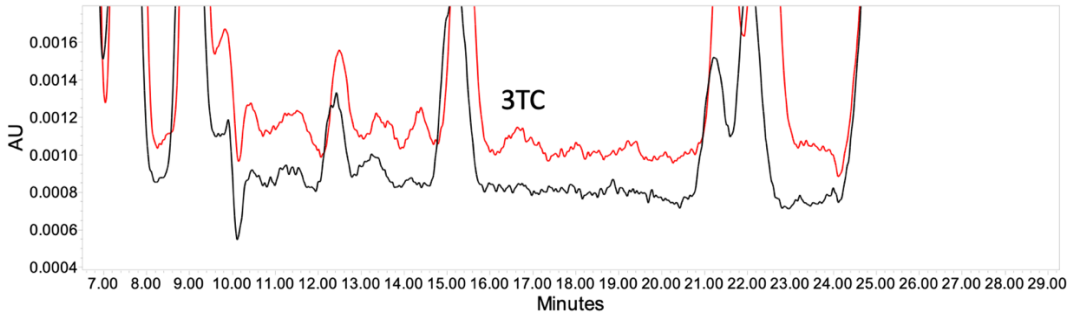

Figure 3-6 *A closeup of a chromatograph of blank rat plasma (black) and 15 ng/mL 3TC (red) at wavelength 270 nm. The retention time of 3TC is 16.6 minutes.*

Because the HPLC-UV method would need to elute highly lipophilic prodrugs, the mobile phase was changed from an isocratic method to a gradient starting from 12% methanol in buffer to 90% methanol in buffer immediately after the elution of 3TC. In addition to eluting prodrugs, high percentages of methanol would also help to flush the column and decrease carryover of background noise from the rat plasma. The percentage of methanol during this step of the gradient could easily be adjusted for the elution and quantification of lipophilic prodrugs.

Next, an IS was picked. Although the chosen IS is usually structurally similar to the analyte of interest, the IS in this method was chosen to be a lipophilic compound due to the expectation that the HPLC-UV method

would be used for the analysis of both 3TC and its highly lipophilic prodrugs. Additionally, CBD was previously used as an IS within our lab for methods analysing lipophilic prodrugs, and was shown to be stably extracted by MTBE[123,124]. CBD was ultimately chosen as the chromatography showed no interfering peaks when read at 236 nm (**Figure 3-7**).

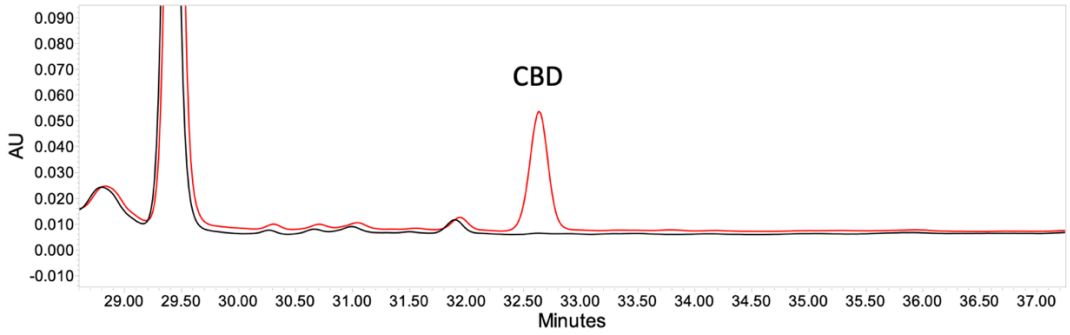

Figure 3-7 *A closeup of a chromatograph of blank rat plasma (black) and CBD (red) at wavelength 236 nm. The retention time of CBD is 32.7 minutes. CBD, cannabidiol.*

Calibration curves were then tested with five replicates of the LOQ according to the FDA Bioanalytical Method Validation Guidance for Industry (**Table 3-1**).[146] Chromatographies from these calibration curves are shown in **Figure 3-8**. To verify the sensitivity of the LOQ, each LOQ calibrator needed to be verified for accuracy and precision. As each LOQ calibrator showed less than 20% error when comparing observed to nominal concentration, the LOQ's accuracy was confirmed (**Table 3-1**). The CV for these five replicates was calculated to be 12.53%, which confirmed the precision of this LOQ (**Table 3-1**). As a result, this calibration curve was concluded to be sensitive for the quantification of 15 ng/mL of 3TC in rat plasma. In addition, each other non-LOQ calibrator was within 15% relative error, confirming the linearity of the calibration curve from 15 to 10,000 ng/mL.

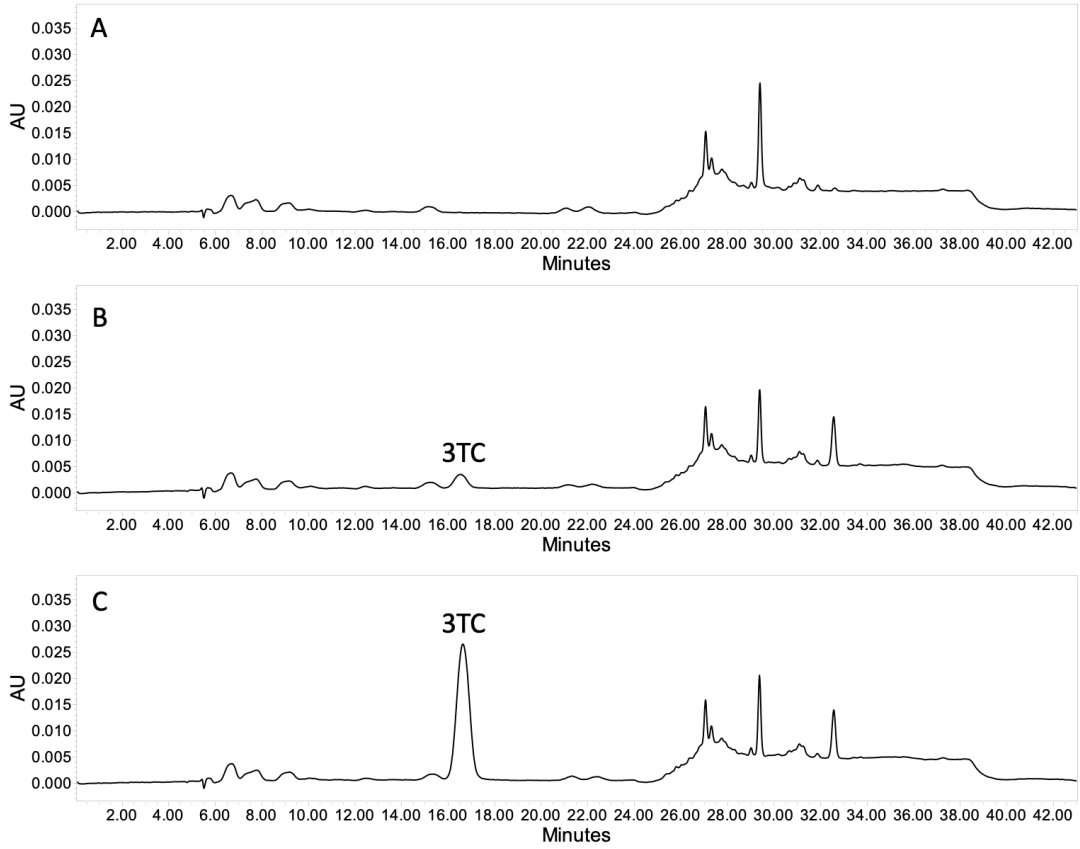

Figure 3-8 *HPLC-UV chromatographies from a calibration curve of 3TC in rat plasma with the column oven at 45 ℃ read at 270 nm. A) Blank rat plasma, B) rat plasma + 1,000 ng/mL 3TC and C) rat plasma + 10,000 ng/mL 3TC. 3TC, lamivudine.*

Table 3-1 *Confirmation of the sensitivity and linearity of the calibration curve.*

Nominal Concentration (ng/mL)	Observed Concentration (ng/mL)	Accuracy, (Relative Error, %)	Precision, (Coefficient of Variation, %)
15	13.47	-10.20	
15	17.18	14.54	
15	13.03	-13.14	12.53%
15	13.78	-8.14	
15	12.96	-13.63	
25	22.25	-11.02	-
50	55.10	10.19	-
100	105.55	5.55	-
250	257.09	2.84	-
500	524.43	4.89	-
1000	948.69	-5.13	-
2500	2673.57	6.94	-
5000	5096.09	1.92	-
10000	9744.29	-2.56	-

Using QC data of four replicates of each QC level per run on three different days, the inter-day accuracy for this method was validated as the relative errors were shown to be less than 20% for the LOQ and 15% for the low, medium and high QC for all samples. The inter-day precision of this method was validated as the CV values were less than 20% for the LOQ and 15% for the low, medium and high QC for all samples.

In addition, the stability of 3TC-containing samples in rat plasma were tested in the -80 °C freezer. After eight weeks, the percent of drug recovery was found to be 102% ± 4% (mean ± STD). This shows that 3TC in a biological matrix is stable and that animal samples from *in vivo* studies may be stored in the -80 °C freezer for up to eight weeks before analysis without 3TC degradation.

The stability of 3TC-contained samples in rat plasma was also tested in 37 °C for 24 hours. The recovery after 24 hours was found to be 98% ± 3% (mean ± STD), showing that 3TC is stable for 24 hours under heated conditions simulating normal body temperatures. This result is consistent with previous studies that show that 3TC is thermally stable.[177]

This HPLC-UV method was determined to be sensitive, accurate and precise for the detection of 3TC at a range of 15 to 10,000 ng/mL in rat plasma with a sample volume of 150 µL. While this method requires more sample volume compared to another published HPLC-UV method for the quantification of 3TC in rat plasma by Chimalakonda *et al*. which used 100 µL[164], our method allowed to quantification of 3TC at concentrations over eight times lower at 15 ng/mL compared to 125 ng/mL. This may have been due to the sample preparation technique in which only 100 µL of supernatant (out of 240 µL of samples-plus-solvent) was collected following protein precipitation. This will have decreased the amount of drug recovered.

A different published HPLC-UV method by Alnouti *et al*. similarly used 100 µL of rat plasma as a sample volume but was only able to achieve a LOQ of 200 ng/mL.[175] This may be due to the differences in HPLC-UV injection volume, as only 15% (15 µL out of 100 µL total) of the reconstitution from the Alnouti *et al*. method was injected, whereas 40% (40 µL out of 100 µL total) of the reconstitution was injected in the method developed in this project. In addition, Alnouti *et al*. used a solid phase extraction (SPE) which only resulted in 60-78% recovery of 3TC.[175] In

addition, SPE can be expensive compared to liquid-liquid extractions. In contrast, the extraction technique employed in this project, in addition to being cost effective, allowed for the extraction of more 3TC. The tradeoff for higher 3TC extraction and a lower LOQ was that in this PhD project's method, increased retention was required to separate the 3TC peak from interfering rat plasma peaks, which resulted in a high drug elution time of over 16 minutes. In contrast, the Alnouti *et al*. method resulted in 3TC eluting at 9 minutes as the SPE technique helped to remove interfering rat plasma peaks. A faster elution time could be beneficial when processing large amounts of samples.

Using this method allows for nine sample points for a robust pharmacokinetic study and allows for most tissues (in which three times the tissue's weight in water is added for homogenization) to be detected in concentrations as low as 60 ng/g. In addition, it was able to be easily modified in order to simultaneously quantify highly lipophilic prodrugs. This was determined to be acceptable for the purposes of this project.

Chapter 4 Lymphatic Targeting Potential of 3TC and its Distribution into Tissues Harbouring HIV Reservoir

4.1 Introduction

Because the intestinal lymphatics are a major site for HIV replication, it is important that antiretrovirals (ARVs) are able to penetrate into these tissues. However, as 3TC is a highly hydrophilic drug, it is not expected to transport directly into intestinal lymphatics following oral administration to a significant extent.

One of the ways to promote direct transport of 3TC into mesenteric lymph nodes (MLNs) following oral administration is by synthesizing highly lipophilic prodrugs. These prodrugs can associate with chylomicrons when they are produced in intestinal enterocytes in the presence of long-chain lipids. Chylomicrons are then transported into intestinal lymphatics. Previous studies have shown success in targeting MLNs through such prodrugs.[120,121,124,125,178] Although there are various types of lipophilic prodrug strategies including self-immolating or triglyceride mimetic prodrug mechanisms, a simpler fatty-acid prodrug approach was taken in this study. Within our group, the fatty-acid ester prodrug approach had shown some success in *in vitro* experiments with high association with chylomicrons as well as quick prodrug conversion in rat plasma whilst maintaining a prolonged half-life in fasted state simulated intestinal fluid (FaSSIF). In addition, some preliminary work within our group performed showed that unsaturated fatty acid ester prodrugs of dolutegravir (DTG) designed to increase DTG uptake into MLNs had significantly increased solubility in sesame and olive oils compared to saturated fatty acid ester prodrugs (**Figure 4-1**). Unsaturated fatty acid DTG prodrugs also were shown to have

faster release of parent drug in stability assays with plasma and FaSSIF compared to saturated fatty acid prodrugs. To test if these trends regarding saturated and unsaturated fatty acid ester prodrugs was reproducible with other parent drugs, both saturated and unsaturated fatty acids were used as ester moieties for 3TC prodrugs.

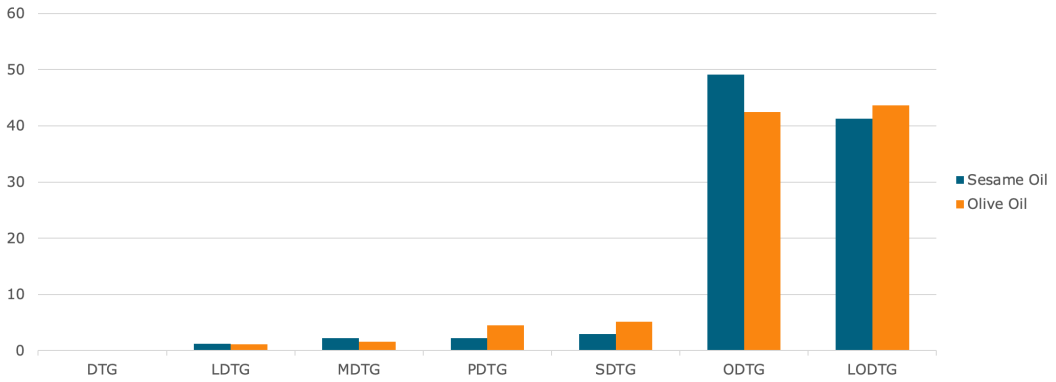

Figure 4-1 *Preliminary work within our lab showed that unsaturated fatty acid ester prodrugs of dolutegravir exhibited higher solubility in sesame oil and olive oil compared to saturated fatty acid ester prodrugs. Oleic and linoleic acid are unsaturated fatty acids, whereas lauric, myristic, palmitic, and stearic acids are saturated fatty acids. DTG = dolutegravir; LDTG = lauric dolutegravir, MDTG = myristic dolutegravir, PDTG = palmitic dolutegravir, SDTG = stearic dolutegravir, ODTG = oleic dolutegravir, LODTG = linoleic dolutegravir.*

3TC, without any nano-formulation, is also not expected to transport into peripheral lymphatics following subcutaneous or intramuscular administrations due to the faster flow in blood capillaries compared to lymph capillaries. In addition to being a means to increase the delivery of 3TC into MLNs as outlined in section 1.3.2, lipophilic prodrugs could also be used to target peripheral lymphatics through nano-sized materials. A simple way to make nanoparticles or nanocrystals is by nanoprecipitation[179], which involves dissolving a drug in an organic solvent with a low boiling point that is miscible with water. As the mixture stirs and the organic solvent

evaporates, a drug that is insoluble in water will precipitate. Unfortunately, as 3TC is highly water soluble[180], nanocrystalization will not be possible using this technique, and nanoparticle drug loading for hydrophilic drugs is typically low[181,182]. A prodrug that is insoluble in water and has a short half-life inside the lymphatics to quickly release the parent drug could be a simple way to enable a nanoprecipitation technique to make nano-sized materials that deliver 3TC.

In this section, synthesized fatty acid ester prodrugs of 3TC will be assessed by *in vitro* analysis to determine whether they could be good candidates for oral delivery for the purpose of targeting MLNs, or candidates for nanoprecipitation for fabrication of prodrug nanocrystals. **Figure 4-2** shows the conversion process of the fatty acid ester prodrug into the parent drug, 3TC.

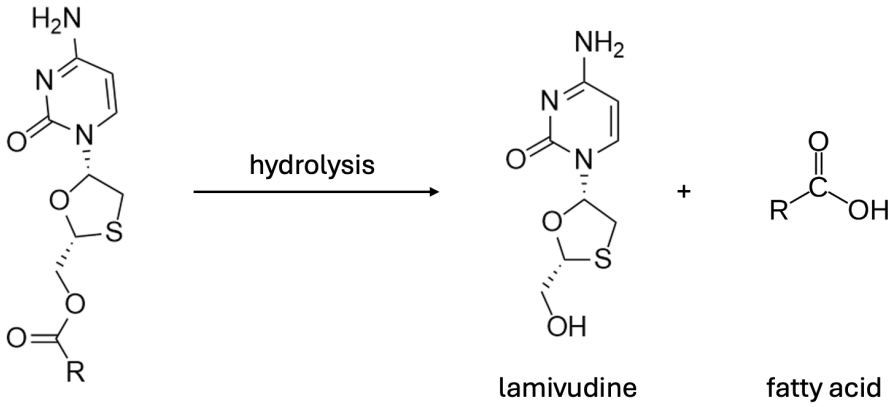

Figure 4-2 *The conversion of a lamivudine fatty acid ester prodrug into the parent drug through hydrolysis.*

Additionally, in this study, the biodistribution properties of 3TC formulated as a solution in Sprague-Dawley rats was examined. These

biodistribution studies were designed based off results from pharmacokinetic studies that were performed first. In addition to lymph nodes (**Figure 4-3**), other tissues that can harbour HIV latent reservoir were examined: brain, testes, spleen and lungs.[47]

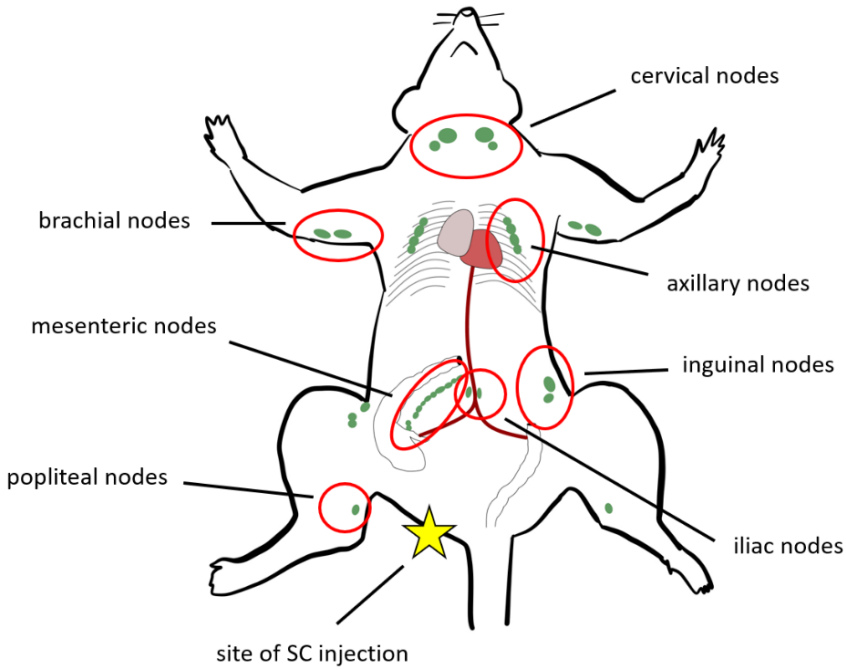

Figure 4-3 *The locations of the lymph nodes that were collected in this study.*

As with lymph nodes, the brain is an important tissue that harbours HIV latent reservoir.[47] A recent study quantified HIV provirus in the frontal cortex, which showed that levels of provirus in patients on suppressive ART had similar levels to those who were viremic.[183] This may be the result of low concentrations of ARVs reaching the brain. Because of the blood brain barrier (BBB), which consists of endothelial cells with tight junctions surrounded by pericytes and astrocytes helping to regulate what can pass through[184], it can be difficult for drugs to effectively penetrate the brain tissue. Various studies have shown lower concentrations of various ARVs in

the central nervous system (CNS) compared to blood.[90,185–188] As microglial distribution in the brain is relatively uniform, it is important for ARVs to be able to penetrate all portions of the brain. In this study, the concentrations of 3TC in different sections of the brain were examined to determine the extent of drug distribution and if distribution is heterogenous or homogenous.

The testes also act as tissues that harbour HIV reservoir.[189] Additionally, as the spleen is an important lymphatic organ, it also is a contributor to the HIV reservoir.[190] Lungs, which also are home to mucosa associated lymphoid tissue (MALT), are also a site of latent reservoir.[191] Even after treatment with suppressive antiretroviral therapy (ART), the testes, spleen and lungs are found to harbour both viral RNA[47] and DNA.[192] Thus, it is important to understand the ability of ARVs such as 3TC to penetrate into these tissues.

4.2 Experimental Design

4.2.1 *In Silico*, *In Vitro*, *Ex Vivo* and Chemical Synthesis

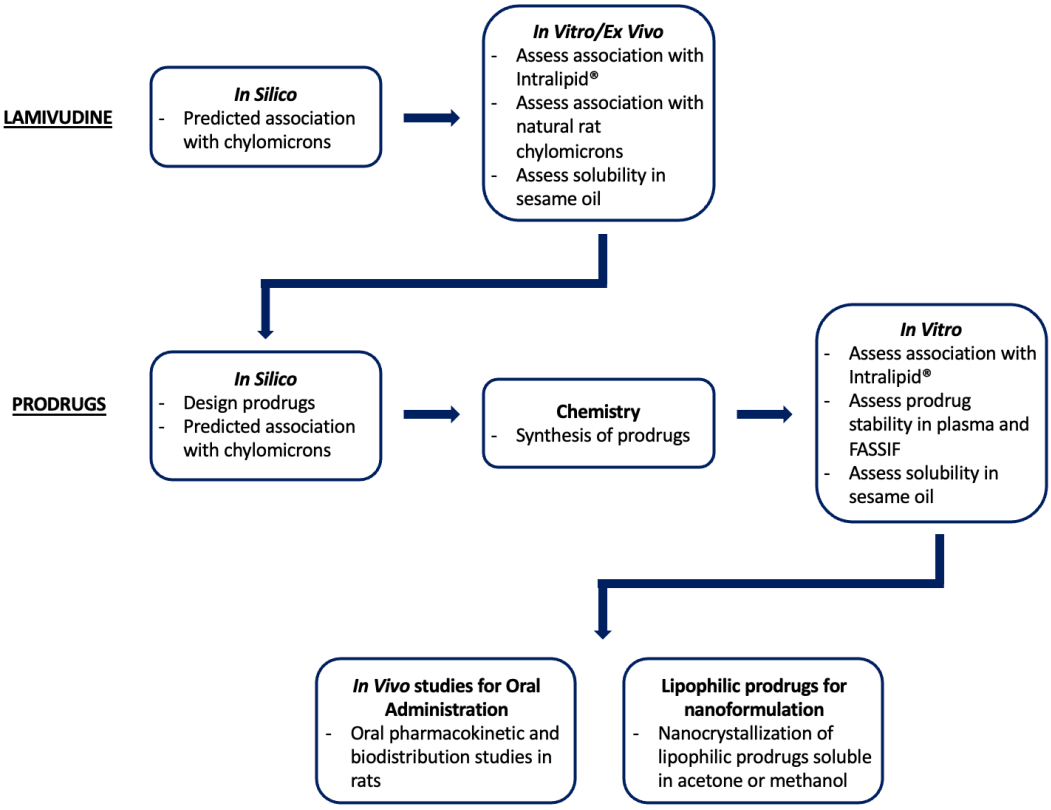

Figure 4-4 *Schematic outlining the procedure for the design, synthesis and in vitro assessment of prodrugs. FaSSIF, fasted state simulated intestinal fluid. FaSSIF, fasted state simulated intestinal fluid.*

The *in silico* predictions of drug association with chylomicrons was determined using a previously described model as described in section 2.5. The association with artificial chylomicrons in the form of Intralipid® is outlined in section 2.8. If *ex vivo* association with natural rat chylomicrons was carried out, the procedure for gathering these chylomicrons from rats is detailed in section 2.9.

The synthesis of the prodrugs 3TC-stearate and 3TC-oleate are described in section 2.6. The characterization methods of the prodrugs are described in section 2.7.

In vitro conversion of prodrugs in rat plasma and FaSSIF is detailed in section 2.10.

The solubility of 3TC and its prodrugs in triglycerides was determined based on methods outlined in section 2.11.

4.2.2 *In Vivo* Experiments in Sprague-Dawley Rats

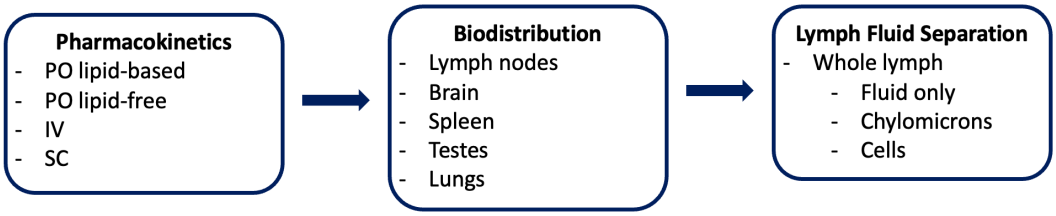

Figure 4-5 *Schematic outlining the procedures in* in vivo *studies. PO, per os/oral; IV, intravenous; SC, subcutaneous.*

The methodology for jugular cannulation surgery is outlined in section 2.13, and the methodology for pharmacokinetics studies in rats is outlined in section 2.14.

The biodistribution methodology can be found in section 2.15.

All samples were prepared and analysed via HPLC-UV following procedures outlined in section 2.2.

4.3 Results and Discussion

4.3.1 Lymphatic Targeting Potential of 3TC and its Prodrugs

3TC was first input into ACD/I-Lab and its predicted physicochemical properties were entered into a previously described *in silico* model[116] to predict association with chylomicrons. As expected, due to its hydrophilicity,

3TC was not predicted to associate with chylomicrons and had a < 1% predicted association, suggesting that lipophilic prodrugs would be needed to achieve targeted delivery of 3TC to MLNs following oral administration.

Ester prodrugs were designed in ACD/I-Lab and physicochemical properties were input into the *in silico* model. Two long-chain fatty acid ester prodrugs, 3TC-stearate and 3TC-oleate utilizing 18:0 and 18:1 fatty acid moieties, respectively (**Figure 4-6**), were chosen because they had the shortest fatty acid chains with acceptable predicted association with chylomicrons. The results from the *in silico* prediction are presented in **Table 4-1**. 3TC-stearate was predicted to have a moderate association with chylomicrons at 47.13% and was chosen for prodrug synthesis and testing. Although the *in silico* model only predicted low-to-moderate association at 36.86% with chylomicrons, the oleic acid prodrug moiety was additionally chosen for synthesis. This was due to preliminary data within our own lab that suggested that unsaturated fatty acid prodrugs exhibit higher triglyceride solubility and achieve faster conversion in rat plasma compared to saturated fatty acid prodrugs.

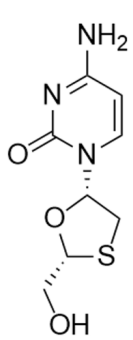

lamivudine

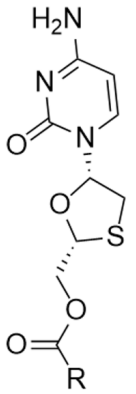

	R
3TC-stearate	$-(CH_2)_{16}CH_3$
3TC-oleate	$-(CH_2)_7CH{=}CH(CH_2)_7CH_3$

Figure 4-6 *The chemical structures for 3TC and its prodrugs.*

Table 4-1 *The* in silico *model association with chylomicrons predictions for 3TC, 3TC-stearate and 3TC-oleate.*

Parameter	3TC	3TC-stearate	3TC-oleate
Log $D_{7.4}$	-1.08	6.74	6.35
Log P	-0.71	8.04	7.53
Log P – Log $D_{7.4}$	0.37	1.3	1.18
Polar Surface Area ($Å^2$)	113.45	119.52	119.52
H-bond Acceptors	6	7	7
Freely Rotatable Bonds	2	20	19
Density (g/cm^3)	1.73	1.16	1.15
Molar Volume (cm^3)	132.2	427.1	427
H-bond Donors	3	2	2
Predicted Association with Chylomicrons	**0.01%**	**47.13%**	**36.86%**

3TC-stearate was initially attempted to be synthesized with a lipase reaction utilising unmodified stearic acid instead of vinyl stearate. This reaction did not yield any appreciable product, and as a result vinyl stearate was used instead. Vinyl stearate was commercially available to purchase to be used to synthesize 3TC-stearate using lipase.[148] 3TC-stearate proved to be generally insoluble in a variety of organic solvents (although it was soluble in dicholoromethane [DCM] and sparingly soluble in dimethyl sulfoxide [DMSO]) and thus was simply purified through trituration with methanol.

Unlike vinyl stearate, vinyl oleate was not commercially available and instead was synthesized using a previously described method[147], which was outlined in section 2.6. This method was chosen as the iridium catalyst had high affinity to the silica in the column, resulting in a simple purification method for vinyl oleate. Ultimately, synthesis of 3TC-oleate was also successful using lipase, as well. Compared to 3TC-stearate, 3TC-oleate was much more readily soluble in a variety of solvents including methanol, and as a result purification through column chromatography was necessary.

Next, 3TC was tested for association with chylomicrons. Intralipid®, which is a lipid emulsion typically used to administer calories and fats intravenously, was used as artificial chylomicrons as an initial screening due to similar particle size and composition to chylomicrons. It has previously been shown that Intralipid® association is a good predictor of a drug's association with natural rat chylomicrons[123–125,193], and it is used as a screening tool to minimize the number of rats sacrificed from which natural

chylomicrons are gathered. The HPLC-UV chromatography for Intralipid® association samples were below the limit of quantification (LOQ) and 3TC was not detected in the chylomicron layer. As the LOQ could detect as low as 3% association, this result suggested that 3TC would not have any significant association with chylomicrons. In order to verify this, the association with natural extracted rat chylomicrons was tested. As with Intralipid®, 3TC was undetected in the chylomicron layer, and association was therefore less than 3%. In addition, the HPLC-UV chromatography for 3TC solubility in sesame oil did not show detectable peaks, meaning solubility was < 0.015 mg/mL. As association with chylomicrons and solubility in triglycerides are strong predictive factors of a drug's intestinal lymphatic bioavailability following oral administration[194], these data suggest that 3TC would not be transported into intestinal lymphatics to any significant extent.

Next, the prodrugs' association with chylomicrons was assessed. 3TC-stearate and 3TC-oleate exhibited an Intralipid® association of 85.6% and 61.1%, respectively (**Table 4-2**). The experimental association was nearly twice as high for both prodrugs compared to the *in silico* model. This discrepancy may be due to the way the *in silico* model was designed and the structure of the prodrugs. The 3TC prodrugs have a very hydrophilic end with the parent drug along with a very long lipophilic alkyl chain with the fatty acid moiety. The drugs used for the development of the *in silico* model do not have structures similar to this. Although one of the drugs used to validate the model, amphotericin B, does have hydrophilic and hydrophobic

regions, its ultimately very low log P (1.16) and log D (-1.41) may have contributed to its fitting in to the model. This is in contrast to 3TC-stearate and 3TC-oleate, which have hydrophilic and hydrophobic regions, but are ultimately extremely lipophilic. None of the highly lipophilic molecules used in the development of this model have this structure pattern.

Table 4-2 In vitro *and* ex vivo *analysis of 3TC and prodrug parameters. 3TC exhibited below the limit of quantification (BLOQ) association with Intralipid®, association with natural rat chylomicrons and solubility in sesame oil. Data are displayed as mean ± STD.*

Parameter	3TC	3TC-stearate	3TC-oleate
Intralipid® Association (%)	< 3	85.6 ± 3.0	61.1 ± 2.6[a] *
Rat Chylomicrons Association (%)	< 3	-	-
Rat Plasma $t_{1/2}$ (min)	-	27.4 ± 1.3	1.7 ± 0.1[a] ***
FaSSIF $t_{1/2}$ (min)	-	86.3 ± 3.0	9.5 ± 0.3[a] ***
Sesame Oil Solubility (mg/mL)	< 0.015	0.3 ± 0.03	2.5 ± 0.2[a] ***

FaSSIF, fasted state simulated intestinal fluid.

[a] Unpaired t-test was used for statistical analysis, *p < 0.05, ***p < 0.001 compared to the corresponding experimental value for 3TC-stearate

As expected, as 3TC-stearate has a slightly higher cLog P than 3TC-oleate, the association with Intralipid® was found to be higher in 3TC-stearate than 3TC-oleate. However, the chylomicrons association for both prodrugs was found to be significantly improved when compared to unmodified 3TC. However, there is some published literature about amphiphilic molecules that are able to self-assemble or self-gelate.[148,195–197] In order to ensure that the prodrug found in the white floating chylomicron

layer was not due to self-assembling or self-gellification and subsequent floating, a control group was tested in which the association experiment was performed and incubated with PBS only without the addition of Intralipid®. The top 1 mL of fluid was collected after ultracentrifugation, and prodrugs were not found in this top layer in these control groups. This suggests that any drug found in the chylomicron layer in the association experiments performed with Intralipid® was, indeed, due to drug association with chylomicrons.

Next, the stability of the prodrugs in rat plasma and FaSSIF were tested. This was in order to ensure that the prodrugs would convert quickly enough once they reached lymphatics but would be stable enough to not be converted in the intestines before being absorbed into the enterocytes. Rat plasma was used as a surrogate for lymph fluid due to the volume of biological matrix necessary to perform these stability experiments. One of the purposes of *in vitro* screening is to reduce the use of animals in *in vivo* studies and to ensure that prodrugs that progress into *in vivo* studies are good candidates. A minimum of 3 mL of biological matrix is needed to perform conversion assays for one prodrug, and obtaining mesenteric lymph fluid from rats by non-surgical means typically results in less than 100 µL per animal. In keeping with the values of the 3R's of animal research[198] by reducing the number of animals impacted and because conversion of a prodrug in rat plasma has previously been shown to be a good indicator for conversion in lymph fluid[124,125], plasma was used instead of lymph for

conversion assays as many prodrugs could be screened with blood from one rat.

3TC-stearate had elimination half-lives of 27.4 ± 1.3 and 86.3 ± 3.0 minutes in rat plasma and FaSSIF, respectively (**Table 4-2**). 3TC-oleate had a much lower stabilities in both media with half-lives of 1.7 ± 0.1 and 9.5 ± 0.3 minutes in rat plasma and FaSSIF, respectively (**Table 4-2**). An unpaired t-test showed that 3TC-oleate has significantly faster conversion in both rat plasma and FaSSIF compared to 3TC-stearate. The prodrugs' solubilities in sesame oil were found to be 0.3 ± 0.03 and 2.5 ± 0.2 mg/mL, for 3TC-stearate and 3TC-oleate, respectively (**Table 4-2**). An unpaired t-test showed that the solubility of 3TC-oleate in sesame oil was significantly higher than 3TC-stearate.

One study conducted with 3TC-stearate examined the half-life of the prodrug in PBS with 10% foetal bovine serum.[199] In this study, Li *et al*. found this half-life to be about 19 minutes. This is similar to the half-life that we have observed in rat plasma.

Quicker release of parent drug for the unsaturated fatty acid moiety prodrug compared to the saturated fatty acid moiety prodrug has been observed in other studies examining alkyl ester prodrugs.[123] In a study by Chu *et al*., oleic acid ester prodrugs of DTG had much quicker conversion in both rat plasma and FaSSIF compared to the stearic acid ester prodrug. The impact of an unsaturated versus saturated fatty acid moiety on half-life may be due to the placement and geometry of the double bond.[201] In this paper, Van Kuiken and Behnke show that a double-bond at the carbon position 6, 9

or 11 increases lipase activity. Oleic acid's double bond is positioned at the 9-carbon position, resulting in 3TC-oleate's instability in biological matrix. This may also be due to the bond angle as lipase appears to prefer the smaller 141° angle of the "kink" in oleic acid as opposed to the 181° straight structure of saturated fatty acids[201]. Although Van Kuiken and Behnke found that oleic acid (and linoleic acid) can increase the activity of pancreatic lipase in the presence of bile salts due to a shift in pH, this increased activity is not observed with the bile salt taurocholate, which is what was used in the formulation of FaSSIF used in this project.

The addition of the double-bond in the unsaturated oleic acid fatty acid moiety also had an impact on drug solubility, resulting in an over eight times higher solubility of 3TC-oleate in sesame oil compared to 3TC-stearate. This pattern can be found in other fatty acid ester prodrugs[123] in which oleic acid moiety ester prodrugs of DTG had higher sesame oil solubility than stearic acid moiety ester prodrugs. The hypothesis for this phenomenon is that this occurrence is due to the fatty acid makeup of sesame oil, which is composed of 35.9 to 42.3% oleic acid compared to only 4.8 to 6.1% stearic acid.[202]

3TC-oleate was also more soluble in a range of organic solvents including methanol, whereas 3TC-stearate was not. Unsaturated free fatty acids are more polar than their saturated counterparts. As a result, they are more soluble in methanol.[203] The properties of the fatty acid ester moieties on the prodrugs are likely affecting the solubilities of the prodrugs, as well.

Unfortunately, however, despite the increased solubility of 3TC-oleate in sesame oil compared to 3TC-stearate, the solubility in triglycerides was still well below the 50 mg/mL indicative of lymphatic uptake. In addition, it would be impossible to dose rats with the necessary amounts of prodrugs solubilized in sesame oil. As the allometrically scaled oral dose of 3TC for rats is 30 mg/kg, an equivalent 3TC-oleate dose would be 64 mg/kg. In a 300-gram rat, this would be a 3TC-oleate in sesame oil dose of nearly 26 mL, which is not feasible as rat stomach capacity is only 3.4 mL[204] and maximum suggested oral dose is 10 ml/kg.[205] In addition, because rats do not have gallbladders, oil digestion in rats is limited as the function of the gallbladder is to concentrate and store bile acid emulsifiers, further rendering this dose unfeasible.

Ultimately, because the solubilities of both prodrugs in sesame oil were too low and because 3TC-oleate converted too quickly in FaSSIF, these prodrugs were not considered as candidates for oral *in vivo* studies. As a result, experiments for the association of these prodrugs with natural rat chylomicrons were not conducted to reduce the number of rats sacrificed.

However, although these prodrugs are not suitable for oral administration and intestinal lymphatic targeting, it is possible that 3TC-oleate could be used for peripheral lymphatic targeting. Because 3TC-oleate was soluble in a variety of organic solvents but insoluble in water, a simple solvent evaporation method[206] could be used to nanoprecipitate 3TC-oleate and create nanocrystals. As the half-life for 3TC-oleate is very quick in rat plasma at less than 2 minutes, an injection of a formulation containing 3TC-

oleate nanocrystals could be a quick way to increase concentrations of parent drug 3TC into peripheral lymph nodes.

4.3.2 Pharmacokinetics of 3TC following oral, IV and SC administrations

The plasma concentration-time profiles of 3TC following oral (with both lipid-based and lipid-free formulations), IV and SC administrations are shown in **Figure 4-7**, and calculated pharmacokinetic parameters are shown in **Table 4-3**. Oral co-administration with sesame oil did not have a significant impact on the plasma concentration-time profile or pharmacokinetic parameters of 3TC.

The pharmacokinetic profiles for IV and oral dosing are generally consistent with previously published data. As expected for a highly hydrophilic drug, the half-life is short ranging from 41 to 93 minutes depending on the route of administration (**Table 4-3**). This is comparable to other studies, which reported half-lives of 93 to 133 minutes following oral administration[172–174,207] and 27 to 64 minutes following IV administration.[166,175,208]

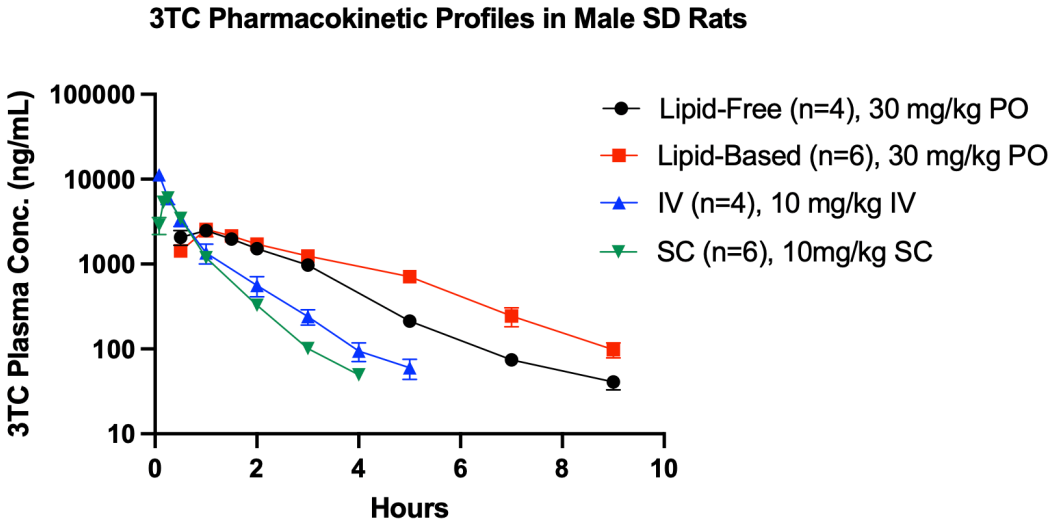

Figure 4-7 *Pharmacokinetic profiles of 3TC following oral lipid-free, lipid-based, IV and SC administrations. Animals administered oral lipid-free (n=4) and lipid-based (n=6) formulations were given 30 mg/kg of 3TC via oral gavage. Animals administered IV (n=4) and SC (n=6) formulations were given 10 mg/kg of 3TC parenterally. Data are reported as mean ± SEM. 3TC, lamivudine; SD, Sprague-Dawley; PO, per os/oral; IV, intravenous; SC, subcutaneous.*

Table 4-3 *Pharmacokinetic parameters of 3TC, mean ± SEM.*

		Oral		
Parameter	**IV (n=4)**	**Lipid-Free (n=4)**	**Lipid-Based (n=6)**	**SC (n=6)**
$t_{1/2}$ (min)	52 ± 2	80 ± 4	93 ± 4	41 ± 4
C_0 or C_{max} (ng/mL)	15487 ± 1375	2484 ± 354	2577 ± 457	6179 ± 537
t_{max} (min)	-	60	60 or 90	10 or 15
$AUC_{0\text{-}t}$ (ng/mL*min)	375929 ± 53567	388515 ± 41776	495161 ± 48944	244983 ± 10384
$AUC_{0\text{-}inf}$ (ng/mL*min)	380474 ± 54395	393212 ± 41999	508683 ± 49048	248043 ± 10411
CL (mL/kg/min)	29 ± 5	-	-	-
V_{ss} (mL/kg)	1318 ± 244	-	-	-
F (%)	-	34.4%	43.9%	65.2%

$t_{1/2}$, half-life; C_0, concentration extrapolated to time zero; C_{max}, maximum observed concentration; t_{max}, time to reach C_{max}; $AUC_{0\text{-}t}$, area under the curve from time zero to the last sampling time point; $AUC_{0\text{-}inf}$, area under the curve from time zero to infinity; CL, clearance; V_{ss}, volume of distribution in steady state; F, bioavailability

[a] Calculated based on the $AUC_{0\text{-}t}$

The SC administration pharmacokinetic study showed quick absorption of 3TC, with a t_{max} of 15 minutes in five rats and 10 minutes in one rat. In SC studies performed in other species, however, the t_{max} is found to be higher at 36 minutes for macaques.[209] Other subcutaneously injected nucleoside analogues exhibit a similar pattern in other species, with most ranging from 30 to 50 minutes in dogs or humans[210–212], although one study with azacytidine in human patients found a t_{max} at 15 minutes.[212] This difference could be due to the area being injected. The injection site at the base of the tail has less available volume compared to the traditional SC

injection site at the back over the shoulders or in the flank of a rat, where large amounts of excess skin allow for tenting around the dose. As a result, due to the excess skin, there may be less pressure exerted onto the volume of injected drug. We had tried to account for this by using a solely water-based formulation, as well as increasing the formulation concentration to decrease the dose volume. However, this may not have been enough to offset the pressure differences. There is evidence to support the idea that the site of SC injection can alter the pharmacokinetic profiles of drugs, including t_{max}[213]. Additionally, there is some evidence that increased surface-to-volume exposure of subcutaneously injected drug may increase absorption[214]; as such, the absorption from a site such as the base of tail may be increased compared to a site such as the back. This difference in t_{max} may also simply be attributed to use of a different drug in the case of the studies with other nucleoside analogues, or a difference in species in the case of the study by Bourry *et al*.

Ultimately, the time points chosen for animal sacrifice for SC administration biodistribution studies were 15, 30 and 60 minutes in order to capture the t_{max} and drug distribution phases. The IV administration biodistribution studies were designed with the same animal sacrifice time points for ease of comparison and to capture the distribution phase.

The t_{max} for the oral administrations was found to be 60 minutes except for one rat which received an oral lipid-based formulation, which was found to have a t_{max} at 90 minutes. This is generally consistent with other pharmacokinetic studies performed in rats which have found the t_{max} to be

60 to 105 minutes.[172–174,207] Thus, the biodistribution studies were designed around these time points and the sacrifice times were chosen at 30, 60, 90 and 120 minutes to best characterize the absorption phase.

4.3.3 Biodistribution of 3TC following oral, IV and SC administrations into lymph nodes

The concentration in the MLNs in the oral lipid-based administration group was found to be significantly higher than in other lymph nodes (**Figure 4-8**). In addition, the concentration of 3TC in MLNs was found to be 2 to 3 times higher than the concentration found in serum. Even at 120 minutes, which was approximately the end of the absorption phase, the tissue-to-serum ratio for MLNs was 1.5. This finding was contrary to what our *in vitro* data predicted, as 3TC had undetectable association with both artificial and natural rat chylomicrons and was practically insoluble in triglycerides.

To test whether this result would be reproducible in animals that were not given sesame oil and therefore have reduced chylomicron production compared to the oral lipid-based administration group, a biodistribution study was performed at the same time points in an oral lipid-free group. This study yielded largely similar results, with the MLNs having significantly higher concentrations than nearly all other lymph nodes at 30, 60 and 90 minutes. However, unlike the oral lipid-based group, the higher 3TC concentration found in the MLNs following lipid-free administration loses significance at 120 minutes. This could be due to the high variability in concentrations found in the peripheral nodes in the oral lipid-free 120-minute group. Despite the lack of significance compared to other lymph

nodes, the oral lipid-free tissue-to-serum ratio for MLNs at 120 minutes was 1.4 and was comparable to the oral lipid-based administration group ratio at the same time point (1.5). In addition, similar to the oral lipid-based group, the concentrations of 3TC found in MLNs in the oral lipid-free administration group were just over twice as high as serum at 30, 60 and 90 minutes. This suggests that the mechanism by which 3TC is transported into MLNs is likely not due to association with chylomicrons as the administration of lipids (and therefore extent of chylomicron production) did not affect concentration of 3TC in MLNs.

In order to shed light on the possible mechanism of 3TC transport into MLNs, lymph fluid collected from the superior mesenteric lymph duct was analysed for concentrations of 3TC in whole lymph-fluid, as well as in separated "compartments" comprising of chylomicrons, cells and fluid-only (**Figure 4-10**). Due to high concentrations of 3TC in lymph fluid, concentrations could be quantified in sample volumes as little as 5 µL using the developed HPLC-UV assay. The "whole lymph" concentrations were all similar or higher compared to MLNs and were used to calculate the percentage of drug recovery found during lymph fluid compartment analysis. After 5 µL of whole lymph was taken for analysis, the remaining fluid was centrifuged to pellet the cell content. To ensure that there were no cells in the supernatant and that the pelleted cells were alive, a trypan blue stain, which cannot penetrate intact live cell membranes[215], was used. **Figure 4-10** data was generated using lymph fluid from various animals in the oral lipid-free and lipid-based groups in which enough lymph fluid (≥ 50

µL) was obtained to undergo centrifugation to remove cells followed by ultracentrifugation to remove chylomicrons. The oral administration animals used to compile these data were as follows: lipid-based oral administration, 120 minutes animals 2 and 3; lipid-free oral administration, 30 minutes, animals 1, 2, 3, and 4; lipid-free oral administration, 60 minutes, animals 1, 2, and 3; lipid-free oral administration, 90 minutes, animal 3; and lipid-free oral administration, 120 minutes, animal 4. Visualization of the resuspended pellet and supernatant following a trypan blue stain confirmed the presence of live cells in the pelleted cell layer only (**Figure 4-9**).

Out of the 11 animals in which enough lymph fluid was obtained to undergo "compartment" separation, only one sample had any detectable 3TC in the chylomicrons layer following ultracentrifugation. In this one sample, the percent of drug recovered in the chylomicrons layer was only found to be 1%. This is consistent with our *in vitro* and *ex vivo* association experiments, which found that 3TC had < 3% association with chylomicrons. This highly suggests that the mechanism by which 3TC is transported into lymph is not related to association with chylomicrons.

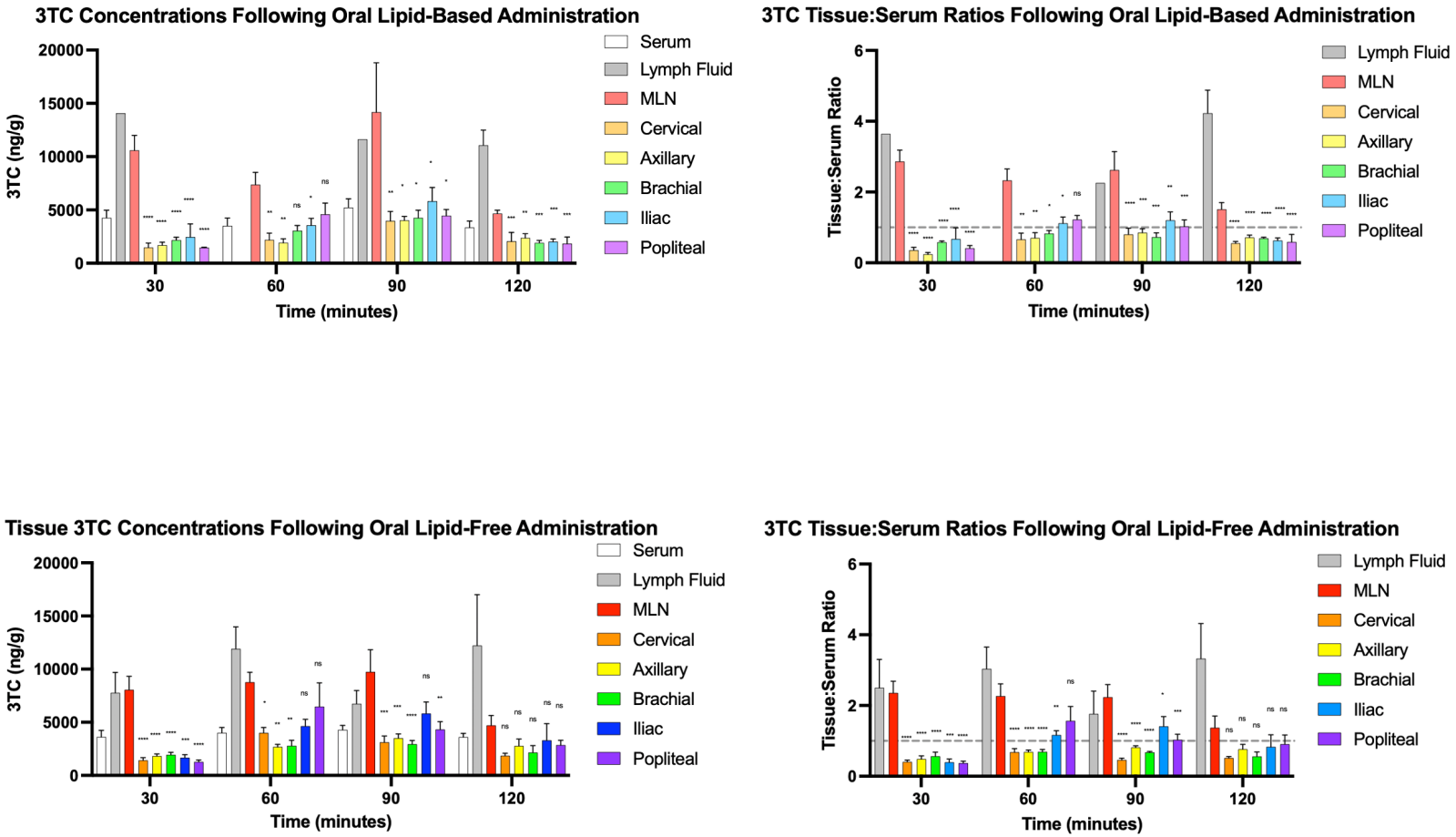

Figure 4-8 *The distribution of 3TC into lymph nodes following 30 mg/kg oral lipid-based (A and B) and 30 mg/kg oral lipid-free (C and D) administrations (mean ± SEM). For lipid-based, n = 4, 5, 6 and 5 for 30, 60, 90 and 120 minutes respectively. For lipid-free, n = 5, 4, 5 and 4 for 30, 60, 90 and 120 minutes respectively. One-way ANOVA followed by Tukey's test was used for statistical analysis. Asterisks denote significance against MLNs. *p < 0.05, **p < 0.01, ***p < 0.001, ****p < 0.0001, ns-p > 0.05. 3TC, lamivudine.*

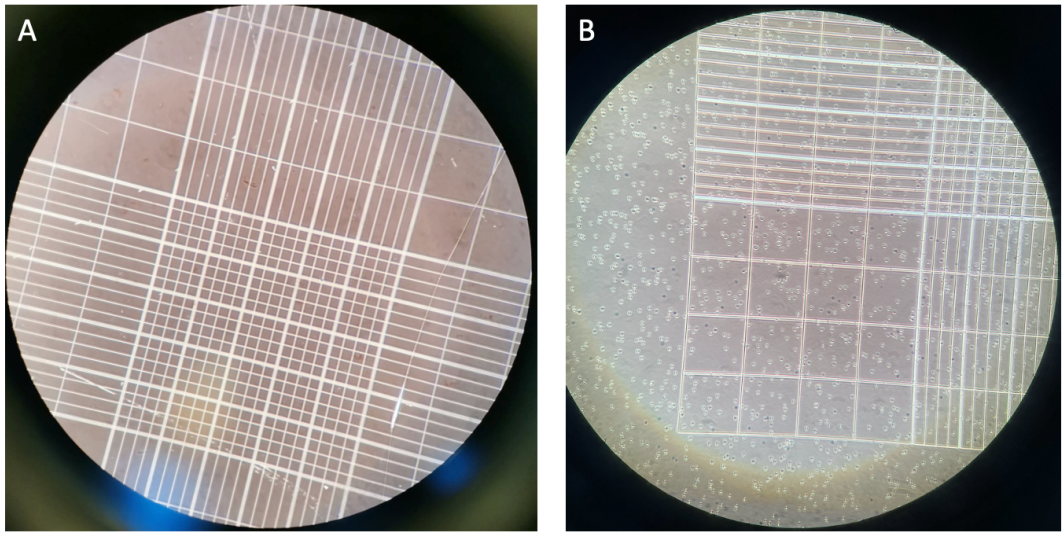

Figure 4-9 *Lymph fluid after centrifugation. A) The lymph fluid supernatant stained with trypan blue shows that there are no cells present. B) The resuspended cell pellet stained with trypan blue shows live cells with intact cell membranes.*

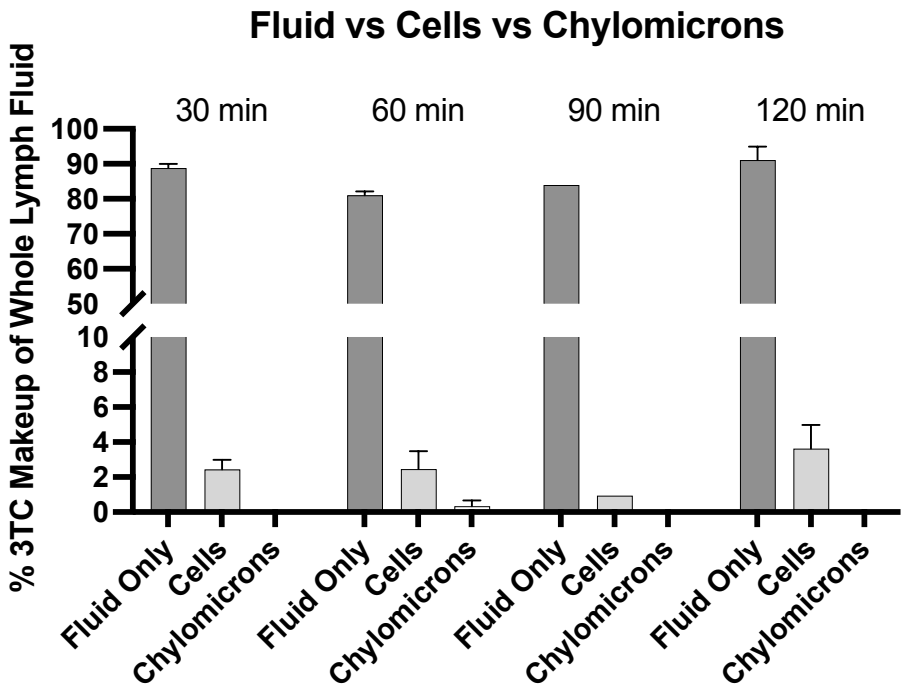

Figure 4-10 *Recovery of 3TC in cell-free chylomicron-free lymph fluid, cells and chylomicron compartments as a percentage contribute to whole lymph. Data are represented as mean ± SEM. N = 4, 3, 1 and 3 for 30, 60, 90 and 120 minutes respectively. 3TC, lamivudine.*

The cell compartment and fluid-only compartments were then analysed by HPLC-UV. As 90% of cells in efferent lymph (such as from the mesenteric lymph duct) entered through high endothelial venules (HEVs)[216],

measuring drug content in efferent lymph cells could be a good indicator of whether the high lymph fluid concentrations were due to redistribution from blood via cell migration. However, most of the 3TC was found in the fluid-only compartment, which contained 80-91% of the drug in lymph fluid for all time points. In contrast, while the cell compartment did appear to contain more 3TC compared to the chylomicron layer, the cells only attributed for 1-4% of drug found in lymph fluid. This suggests that the mechanism by which 3TC is transported into lymph nodes and fluid is not due to high concentrations inside cells that enter the lymphatics from blood. This finding is consistent with existing data regarding intracellular concentrations of 3TC, especially in lymph node cells compared to peripheral blood mononuclear cells (PBMCs).[217] This is not limited to lymphocytes, and low intracellular concentrations of 3TC compared to extracellular concentrations can be found in other matrices such as seminal fluid.[218]

Following oral administration, excluding MLNs, the mean concentrations in lymph nodes were 1,921 to 6,477 ng/mL at the t_{max} of 60 minutes. By 120 minutes, the mean range for non-MLN concentrations was 1,834 to 3,310 ng/mL. Depending on the clade or group of HIV-1, IC_{50} values for 3TC ranges from 0.7 to 3,450 ng/mL.[180] This suggests that, depending on the clade or group of HIV, concentrations of 3TC in non-MLN lymph nodes following oral administration may be reasonable for suppressing replication, especially in combination with other forms of ART. In order to increase

coverage for different HIV clades or groups, an increase in delivery of 3TC may be beneficial.

Next, SC injections of 3TC solubilized in water were tested to see if this phenomenon of lymphatic drainage could be reproduced peripherally. According to current literature, this should not be the case due to the higher flow rate of blood in capillaries compared to lymph fluid.[126,127] In order to test this, lymph nodes were harvested from rat cadavers following subcutaneous administration and separated into nodes found on the left side of the body and nodes found on the right side (except for the MLNs, which are not bilateral). This was because the SC injection was administered at the base of the tail on the right side. By separating lymph nodes into left- and right-sides, the movement of 3TC inside lymphatics could be better tracked. The inguinal nodes were also gathered in addition to all the other lymph nodes gathered in the oral-administration biodistribution studies. This is because at the base of the tail where the drug was administered, the primary draining lymph nodes were expected to be the inguinal nodes.[144,219]

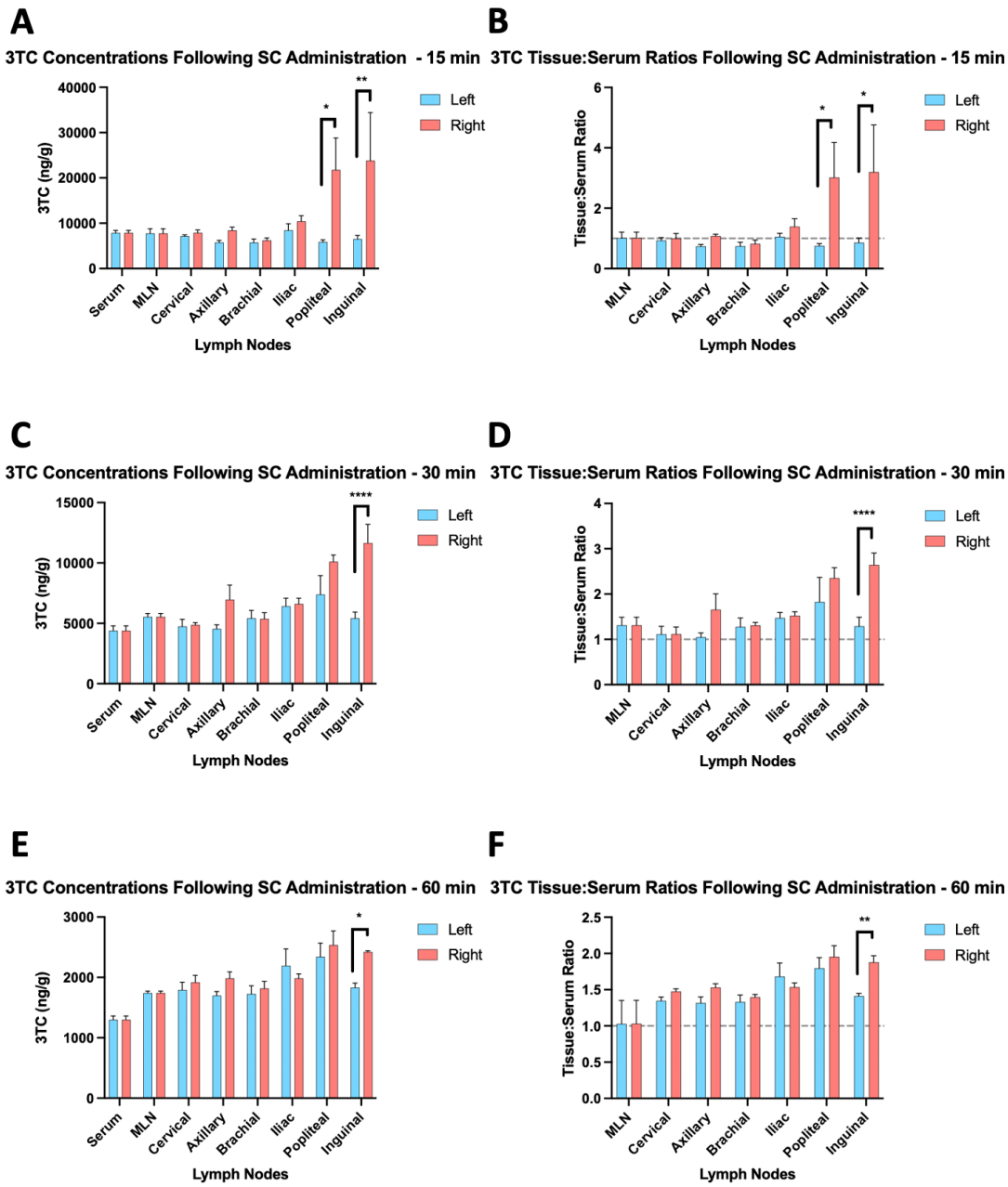

Figure 4-11 *The distribution of 3TC into left- and right- side lymph nodes (except for MLNs) following a 10 mg/kg SC administration at the base of the tail at 15 minutes (A and B), 30 minutes (C and D) and 60 minutes (E and F) (mean ± SEM, n = 4 for each time point). Mixed effects model followed by Šídák's multiple comparisons test was used for statistical analysis. *p < 0.05, **p < 0.01, ***p < 0.001, ****p < 0.0001. SC, subcutaneous; 3TC, lamivudine; MLN, mesenteric lymph node.*

At 15 minutes, the concentrations found in the right-side inguinal and popliteal nodes was found to be significantly higher compared to the left-side nodes. This pattern carried on to the 30- and 60-minute time point,

in which the right-side inguinal nodes contained more drug compared to the left-side nodes (**Figure 4-11**).

Literature by Tilney shows that the site of SC injection at the base of the tail should be drained by the inguinal node[144], which explains the difference in concentrations between the left- and right-inguinal nodes at all time points. However, at 15 minutes, we also observed a difference between the left- and right-popliteal nodes. When comparing the primary draining lymph nodes that Tilney describes versus the placement of our SC injection, it is possible that the site of injection is at the border of the inguinal-drained-region versus the inguinal-plus-gluteal-drained-region on the tail (**Figure 4-12**). Considering that the popliteal node efferently drains the gluteal node[144], the significantly higher right-side popliteal node concentration we observed may be due to initial draining at the gluteal node and subsequent draining into the popliteal node.

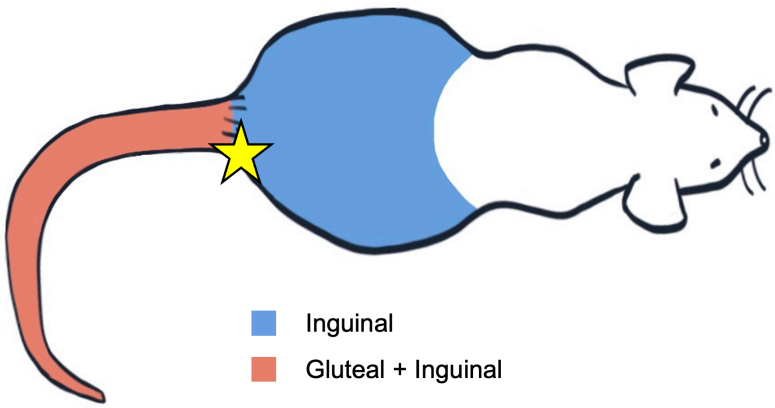

Figure 4-12 *The site of the SC injection is marked with a yellow star. This drawing is based off of images from Tilney's 1971 publication Patterns of Lymphatic Drainage in the Adult Laboratory Rat.*[144]

Although not statistically significant, it is also worth noting that the axillary node, which drains the inguinal node, exhibits higher concentrations on the right side compared to the left at 30 minutes. The lack of significance may be because lymph nodes are vascularized tissues. HEVs allow not only for cell migration into lymph nodes, but also for solute and fluid exchange between lymph nodes and blood circulation.[220] As such, some drug in the lymph fluid may be lost to lower-concentration blood via exchange through HEVs in the inguinal lymph node chain before reaching the axillary nodes.

In addition, by 60 minutes post-SC-dose, the concentrations of 3TC in the draining inguinal and popliteal nodes were more similar to the concentrations in other non-draining lymph nodes. One potential benefit to administering 3TC subcutaneously would be to achieve concentrations in lymph nodes throughout the body. A sustained-release device or formulation could be beneficial in order to maintain prolonged high ARV concentrations that may be necessary to fully inhibit HIV replication in lymph nodes.

To confirm that the difference in 3TC concentration in the right- and left-side draining nodes was, indeed, due to lymphatic drainage instead of redistribution from blood, an additional biodistribution study following IV administration was performed.

Following an IV 3TC dose, the lymph nodes on the left- and right-sides did not show any significant difference at any time point (**Figure 4-13**). As distribution into lymph nodes after an IV dose can only be due to redistribution from blood, the lack of difference between left and right sides

underscores the differences that were observed in draining lymph nodes following an SC injection.

In addition, there were no differences in concentrations or tissue:serum ratios between the types of lymph nodes at all time points (**Figure 4-13**). These data also demonstrate that the high concentrations of 3TC found in MLNs following oral administration are also not due to blood redistribution and are likely due to direct lymphatic transport from the gut.

To the best of our knowledge, this is the first report of a solution of a highly hydrophilic small molecule showing significant direct uptake into intestinal lymphatics following oral administration and comparison to concentrations in other non-intestinal lymph nodes. Previous studies show that drugs with moderate-or-low lipophilicity and negligible association with chylomicrons [124,125,221,222] exhibit poor intestinal lymphatic transport following oral administration. In these previous studies, the concentration of drugs in intestinal lymphatics was lower than in serum.

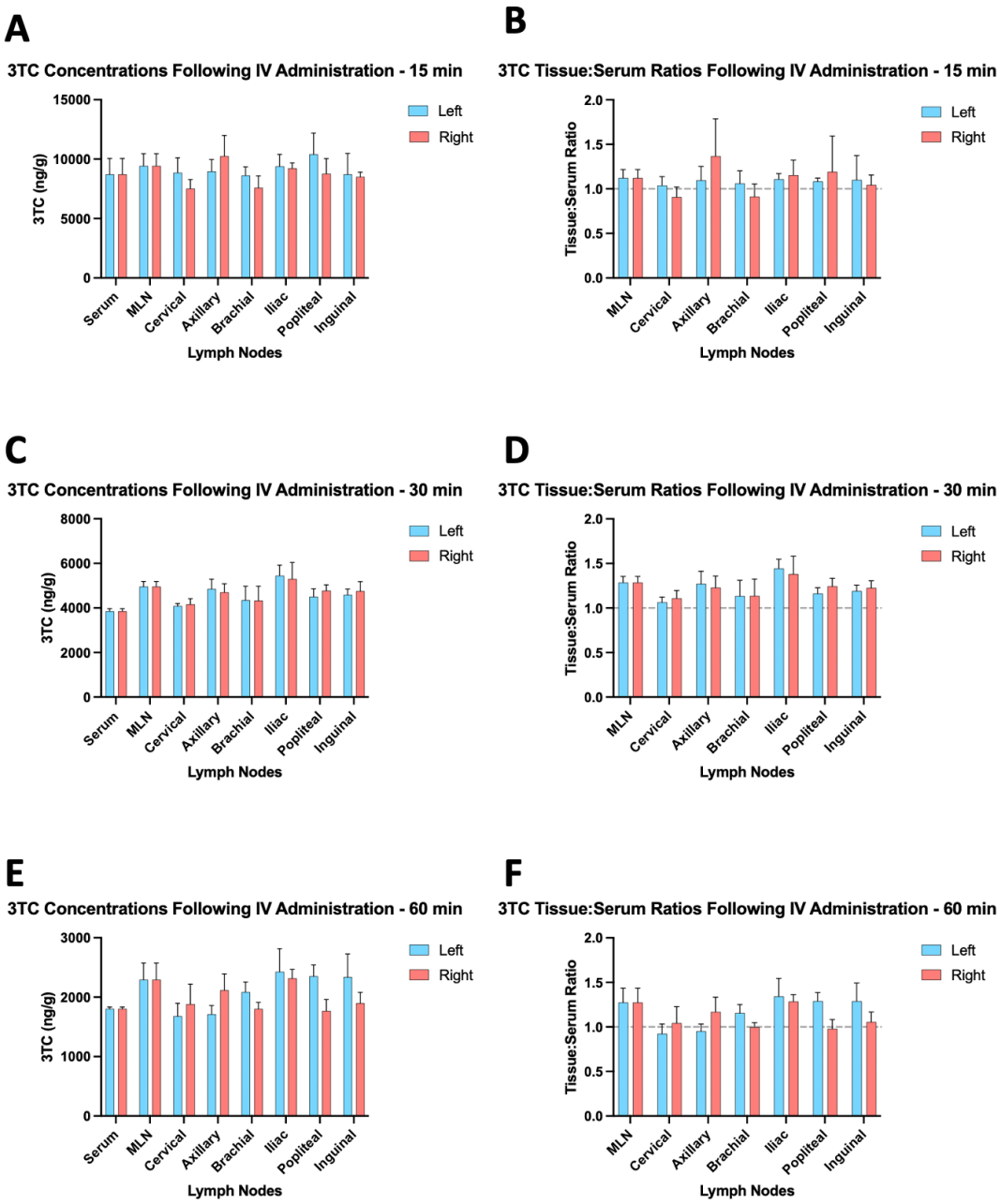

Figure 4-13 *The distribution of 3TC into left- and right- side lymph nodes (except for MLNs) following a 10 mg/kg IV administration at 15 minutes (A and B), 30 minutes (C and D) and 60 minutes (E and F) (mean ± SEM, n = 4 for each time point). Mixed effects model followed by Šídák's multiple comparisons test showed that there were no statistical differences between left- and right-side nodes for all nodes at all time points.*

To contrast, one study examining the highly hydrophilic drug levodopa showed concentrations in intestinal lymph fluid slightly higher than plasma at t_{max} following oral administration.[223] Another study examined

MLNs following oral administration of nucleoside reverse transcriptase inhibitors (NRTIs) tenofovir disoproxil fumarate (TDF) and emtricitabine (FTC) and found higher concentrations in MLNs compared to plasma at 24 hours post-dose. In the same study, another anti-HIV drug, dolutegravir (DTG), showed a low MLN tissue:plasma [222] (this trend is reflected in another study that examines concentrations of DTG in MLNs after an oral dose[123]). The authors hypothesized that NRTIs penetrate into tissues at higher concentrations compared to DTG due to lower molecular weight and protein binding, thus allowing drug to redistribute away from blood.[222] Whilst this may contribute to higher distribution of 3TC into lymph nodes following IV administration, this does not explain why we found about twice as high concentrations in MLNs compared to other lymph nodes in oral-administration biodistribution studies.

Regarding SC dosing, one previous study in mice examined lymph nodes' concentrations of various ARVs and found high concentrations of all drugs in pooled inguinal, axillary and cervical lymph nodes following SC administration.[224] Interestingly, out of all the drugs tested in that study, the drug with the highest penetration into lymph nodes following SC administration was TDF, another NRTI, which had a tissue:serum ratio of 21.0. A different prodrug of tenofovir, tenofovir alafenamide (TAF), was also assessed, but tissue:serum ratios achieved were much lower than TDF, although the tissue:serum ratio was still relatively high at 1.9.

Another SC administration study also found higher tissue:serum ratios of NRTIs FTC and tenofovir[225], although sacrifice times in that study do

not appear to be designed around the absorption phase. The authors checked for several common drug transporter proteins and corresponding gene expression in lymph nodes but did not find any in substantial quantities. As a result, they concluded that the high concentrations found in lymph nodes was due to passive diffusion. However, of the transporters tested, proteins for organic cation transporter (OCT) 3, for which 3TC is a substrate for, were detected in non-human primates (NHPs), albeit in low quantities, in lymph nodes. It was also found that mouse gene expression for OCT3 was higher than found in NHPs. To note, a separate study found low-to-undetectable gene expression for other HIV drug transporters (multidrug resistance-associated protein [MRP] 2, organic anion transporting polypeptide [OATP] 1B1, organic anion transporter [OAT] 1, concentrative nucleoside transporter [CNT] 1 and equilibrative nucleoside transporter [ENT] 2) yet observed expression of transporter proteins.[226] Although not transporters, another study also found that levels of mRNA expression are not a great predictor of the levels of expression of various types of monocyte proteins.[227]

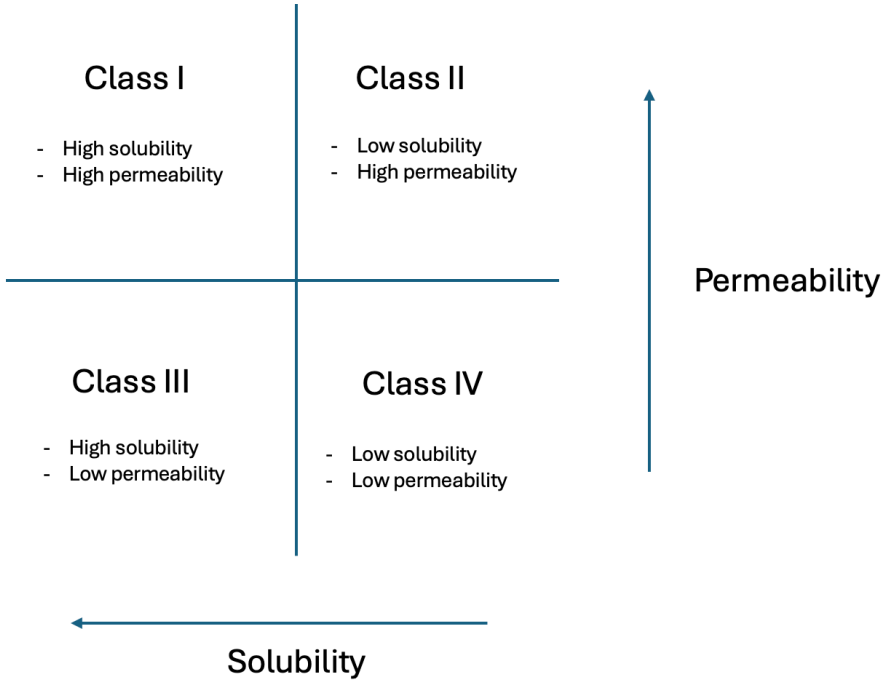

Figure 4-14 *The biopharmaceutical classification system (BCS). 3TC is a BCS Class III drug.*

There appears to be a pattern for all of these previous studies. Levodopa, which achieved a slightly higher concentration in intestinal lymph compared to plasma [223], is absorbed from the intestine via transporters $b^{0,+}$ AT-rBAT, LAT2-4F2hc, and TAT1.[228] FTC is BCS Class III and can utilize CNT1 transporters to achieve uptake by intestinal enterocytes.[229,230] Although tenofovir prodrugs do not appear to utilize transporters for intestinal absorption, both TDF and TAF are BCS Class III drugs with low permeability. These drugs achieved high concentrations in lymph nodes or lymph in previous studies [222–225]. This contrasts with lopinavir, bexarotene, mycophenolic acid and DTG, which also showed low tissue:serum ratios in MLNs[125,221,222], are BCS Class II drugs exhibiting high passive membrane permeability[231–233] and do not rely on transporters for bioavailability.

BCS Class III drugs such as 3TC suffer from poor permeability and typically rely on transporters instead of passive diffusion for intestinal absorption following oral administration.[234] Highly hydrophilic drugs, such as 3TC, usually stay mostly in the central compartment or other highly perfused organs and have a low volume of distribution.[235] In our pharmacokinetic studies, 3TC's volume of distribution is 1.318 L/kg, which is relatively high given the drug's hydrophilicity. This high volume of distribution is closely reflected in human data.[236] CNT 1 and OCT3, which 3TC is a substrate for[237,238], can be found on the luminal side of intestinal enterocytes[230], allowing for 3TC to penetrate these cells, leading to a relatively high oral bioavailability. Indeed, OCT3 was one of the few transporters in which Burgunder *et al*. found protein expression in low-but-detectable quantities in NHPs[225]; presence of CNT1 was not examined. Because observed concentrations of drug in lymph nodes were often slightly higher compared to serum in IV-administration biodistribution studies we hypothesize that 3TC at least in part enters the lymphatics through transporters on HEVs in lymph nodes, although further studies will be necessary to confirm this hypothesis.

Transporters could also help to explain the large variability in lymph node concentrations exhibited in *in vivo* experiments. There is some evidence that some polymorphisms in genes that encode for transporters can alter 3TC drug concentrations.[239,240]

Although concentrations in draining lymph nodes were around 3 times higher compared to serum in SC-dosed biodistribution studies, it is

worth noting that in terms of mass-balance, it is still likely that more of the drug injected was taken up into blood compared to lymph. Lymph nodes are small-size tissues and even low drug quantities distributed there could lead to high concentrations. It is possible that hydrophilic molecule 3TC may exhibit relatively slower permeability into blood capillaries compared to drugs that exhibit higher permeability. Because of this, it is possible that drug may build up in the lamina propria or SC space. Therefore, more 3TC may be available to be passively transported into lymph capillaries compared to other highly permeable drugs that enter blood capillaries more quickly. Enough 3TC is passively transported directly into draining lymphatics to result in high tissue:serum ratios. The passive absorption mechanism at the lymph capillaries (in contrast to a proposed active transport mechanism at HEVs) is supported by a study conducted using FTC (structurally very similar to 3TC), which observed low concentrations inside human lymphatic endothelial cells (LECs) in *in vitro* studies.[241] Further studies are necessary to confirm whether this is the case for 3TC as well.

Despite high concentrations of 3TC in MLNs following oral administration and penetration into all other lymph nodes, viral deoxyribonucleic acid (DNA) and ribonucleic acid (RNA) can still be found in lymphatic tissues in patients on suppressive ART regimens that include 3TC.[242] This may be due to several reasons. Firstly, drug concentrations of 3TC have been found to be lower in lymph node cells compared to PBMCs.[217] Secondly, ARV distribution within the lymph node may have an impact on viral replication. A recent study showed ARV distribution in lymph

nodes is heterogenous, and different drugs may penetrate different regions.[243] Sites with low concentrations may exhibit viral replication and result in newly infected cells.[244] Lastly, recent studies show that clonal cellular proliferation is the main contributor to HIV-1 persistence in lymph nodes.[245] Unfortunately, ARVs such as 3TC do not stop clonal proliferation.[246] To fully address HIV reservoir expansion in lymph nodes, there will be a need to: 1) address low intracellular ARV concentrations in lymph nodes 2) explore ARV targeting to all sections of the lymph node and 3) develop new drug therapy to stop reservoir growth through clonal expansion.

Our studies show that an SC injection of a simple aqueous solution formulation of 3TC can achieve concentrations 3 times higher in draining lymph nodes compared to serum. Although current literature frequently cites the need for nanoformulations of small molecules to target drainage of intramuscular, SC or transdermal doses into the lymphatics instead of blood[126,127], our SC -administration biodistribution studies show that this is not always necessary.

As the T cell zone can be found in the lymph node paracortex[216], it is important for ARVs to penetrate this area. The lymph node conduit system connects afferent lymph flow from the subcapsular sinus to the paracortex and is made up of microchannels with further size restrictions due to a network of collagen.[247] This conduit system filters particles > 70 kDa, limiting access to the paracortex.[248] Since small molecules may more effectively target the T cell zone compared to nanoformulations, it could be useful to

understand the mechanism by which 3TC is drained into peripheral lymphatics. Understanding this mechanism could be useful in delivering other ARVs to injection-site-draining lymph nodes through SC administration.

4.3.4 Biodistribution of 3TC following oral, IV and SC administrations into the brain

In addition to lymph nodes, the concentrations in different parts of the brain were analysed. As oral lipid-based administration biodistribution studies were the first to be carried out, the concentrations for the corresponding brains were analysed as whole tissue. Lower concentrations of 3TC were found in the brain compared to serum (**Figure 4-14**). This was to be expected as 3TC is hydrophilic, and drugs that can passively permeate through the BBB are lipophilic small molecules.[249] As such, 3TC is likely relies on transporters to be distributed into the brain.[250] However, as 3TC is a substrate for the P-gp efflux transporter[180], the small amount of drug that is able to pass through the BBB may quickly be effluxed out.[251]

As mentioned previously, depending on the clade or group of HIV-1, IC_{50} values for 3TC ranges from 0.7 to 3,450 ng/mL.[180] The results from our biodistribution study show that following oral-lipid based administration, in the brain, the concentrations of 3TC will cover the lower end of the IC_{50} at the dose used, and thus may be at concentrations effective enough to inhibit more susceptible clades of HIV-1. However, this coverage only accounts for the lower < 10% of the IC_{50} range, with our mean C_{max} in whole brain at 222

ng/g. The penetration of lamviudine into brain tissue is not high enough to addequately inhibit HIV replication.

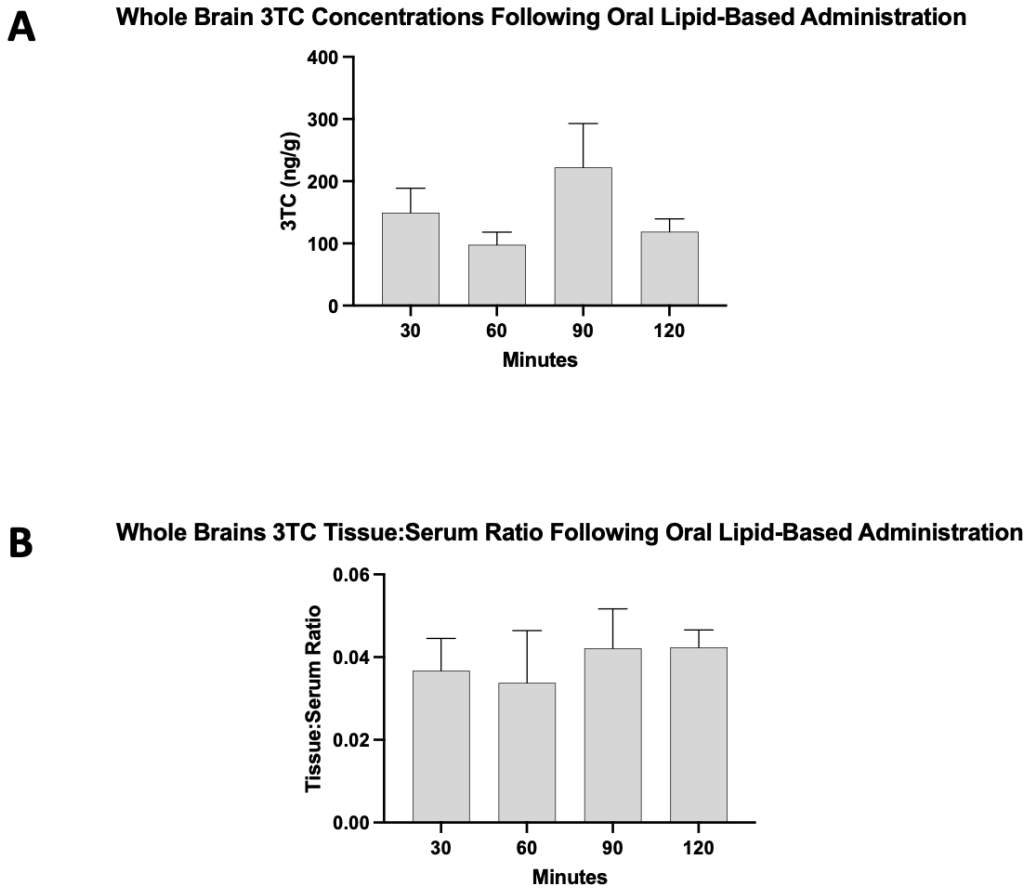

Figure 4-15 *Distribution of 3TC into the whole brain following 30 mg/kg lipid-based oral administration of 3TC shown in A) concentration and B) tissue:serum ratio. (Mean ± SEM, n = 4, 4, 6 and 4 for 30, 60, 90 and 120 minute groups, respectively.) 3TC, lamivudine.*

Next, different sections of the brain were analysed to test if distribution of 3TC was homogenous or heterogenous. If heterogenous, it is possible that some areas of the brain could have sufficient coverage, whilst other regions are left susceptible to replication. In the next biodistribution in the oral lipid-free group, the brain was dissected into nine separate sections before analysing concentrations. Except for the olfactory bulb and

hippocampus at 60 minutes, there were no statistical differences in concentration between different brain sections at any time (**Figure 4-15**).

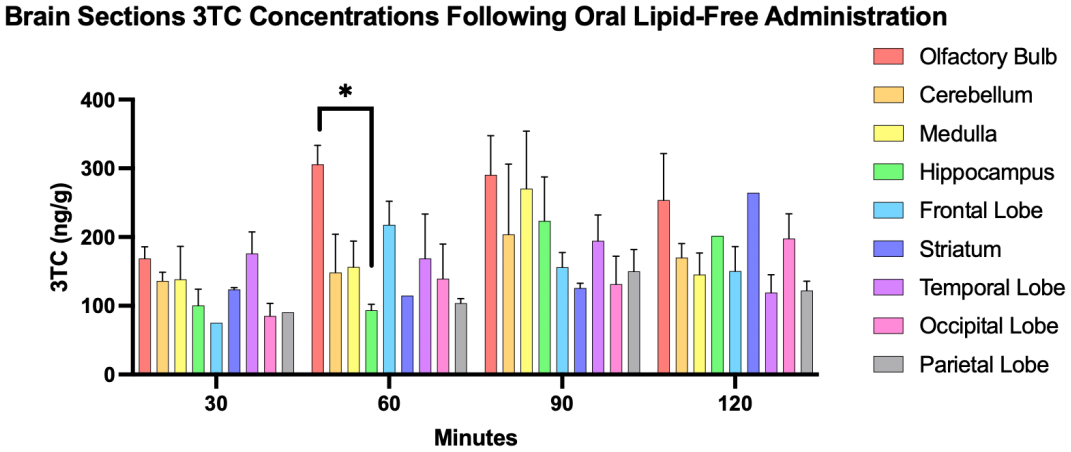

Figure 4-16 *Distribution of 3TC into different sections of the brain following 30 mg/kg lipid-free oral administration of 3TC (mean ± SEM, n = 4). One-way ANOVA followed by Tukey's test was used for statistical analysis. *p < 0.05.*

In the SC-administration biodistribution studies, the olfactory bulb was significantly higher in concentration of 3TC compared to all other sections at 15 minutes except for the cerebellum and medulla. Additionally, at 15 minutes, the cerebellum was significantly higher than the hippocampus, frontal lobe and occipital lobe, and the medulla was also significantly higher than hippocampus, frontal lobe, striatum, temporal and parietal lobes. There were no longer any significant differences between each brain section at 30 and 60 minutes (**Figure 4-16**).

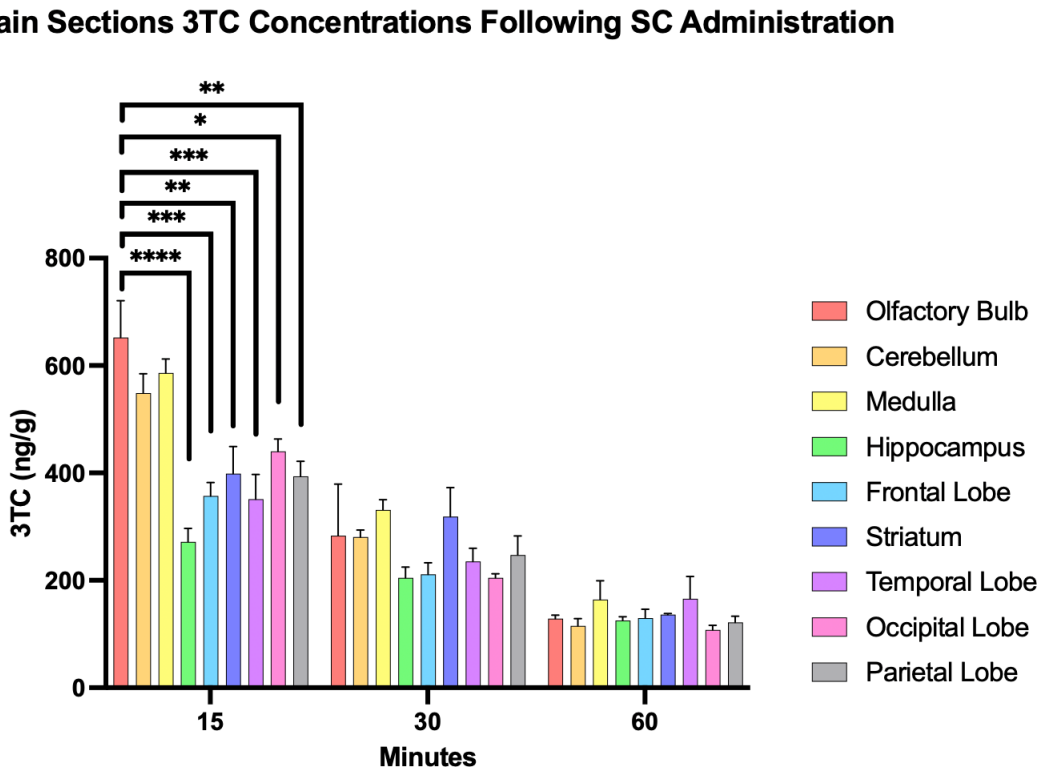

Figure 4-17 *Distribution of 3TC into different sections of the brain following 10 mg/kg SC 3TC administration (mean ± SEM, n = 4). The concentrations found in the olfactory bulbs at 15 minutes are significantly higher than all other sections except for cerebellum and medulla. In addition, at 15 minutes, the cerebellum was significantly higher than the hippocampus, frontal lobe and occipital lobe (unpictured). At 15 minutes, the medulla was also significantly higher than hippocampus, frontal lobe, striatum, temporal and parietal lobes (unpictured). There was no significant difference between any brain section tissues at the 30- and 60-minute time points. One-way ANOVA followed by Tukey's test was used for statistical analysis. *p < 0.05, **p < 0.01, ***p < 0.001, ****p < 0.0001. 3TC, lamivudine; SC, subcutaneous.*

In IV-administration biodistribution studies, the olfactory bulb had a significantly higher concentration than most other brain sections at 15 and 30 minutes as outlined in **Figure 4-17**. The medulla had significantly higher concentrations compared to the hippocampus, frontal lobe, striatum and parietal lobe at 15 minutes but was no longer significantly different at 30 minutes. Notably, the concentration found in the hippocampus at 15 minutes was low, and it were found to be significantly lower than those found in the temporal lobe and occipital lobes at this time point. There were

no significant differences in the concentrations between any of the different brain sections at 60 minutes post-IV dose.

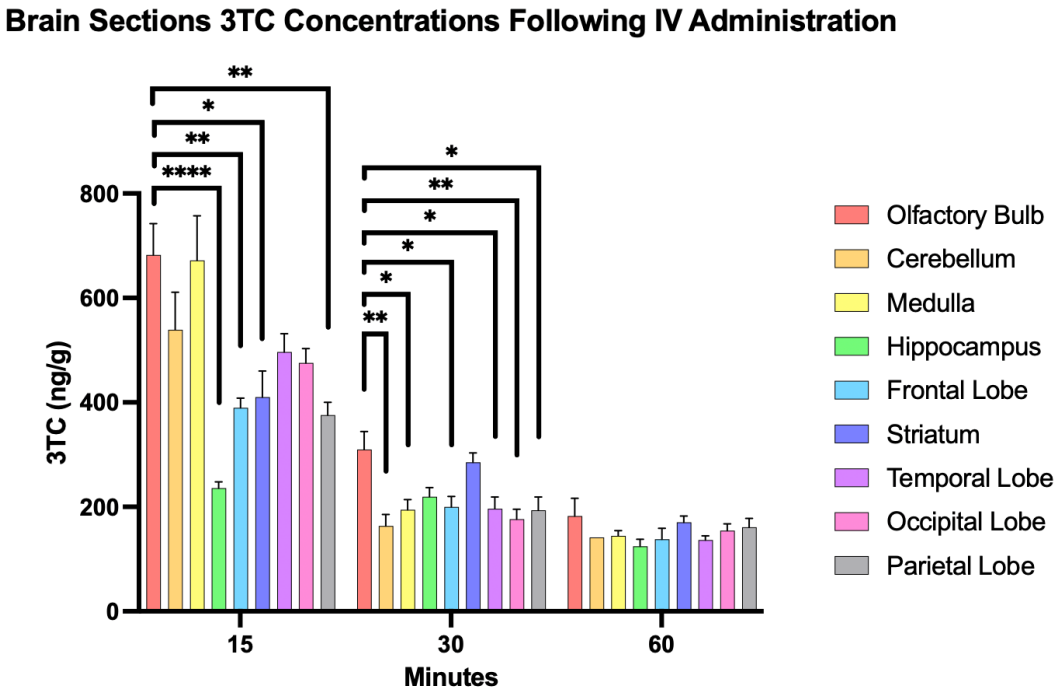

Figure 4-18 *Distribution of 3TC into different sections of the brain following 10 mg/kg IV administration of 3TC (mean ± SEM, n = 4). In addition to the pictured difference in concentrations found in the olfactory bulb compared to other tissues, the concentrations of 3TC found in the cerebellum were also significantly higher compared to the hippocampus at 15 minutes but lower than the striatum at 30 minutes. The medulla had significantly higher concentrations compared to the hippocampus, frontal lobe, striatum and parietal lobe at 15 minutes but lost significance at 30 minutes. The concentrations found in the hippocampus was significantly lower than those found in the temporal and occipital lobes at 15 minutes. One-way ANOVA followed by Tukey's test was used for statistical analysis. *p < 0.05, **p < 0.01, ***p < 0.001, ****p < 0.0001. 3TC, lamivudine; IV, intravenous.*

In all types of administration in which brains were sectioned, not all sections had detectable levels of drug in the chromatography. This may have been due to inter-individual variation. Another contributing factor is that the olfactory bulb, hippocampus and striatum were sometimes too low in mass to obtain the minimum volume needed to prepare samples with the 1:3

(w/v) addition of water. As a result, some samples needed addition of extra water, further decreasing our LOQ. **Table 4-4**, **Table 4-5**, and **Table 4-6** outline the brain sections with corresponding n-numbers and LOQ. Since we used 4 animals per time point for oral lipid-free and SC administration groups, any brain section listed with an n of less than 4 had at least one individual sample with undetectable amounts of 3TC. For IV administration studies, we used 5 animals per time point, so this is true for any brain section listed with an n of less than 5.

Table 4-4 The LOQ and number of samples above LOQ for rats given an oral lipid-free formulation.

Time Point	Olfactory Bulb	Cerebellum	Medulla	Hippocampus	Frontal Lobe	Striatum	Temporal Lobe	Occipital Lobe	Parietal Lobe
30 min	n = 4	n = 3 LOQ: 60 ng/mL	n = 3 LOQ: 60 ng/mL	n = 3 LOQ:	n = 1	n = 2 LOQ: 120 ng/mL	n = 2 LOQ: 60 ng/mL	n = 2 LOQ: 60 ng/mL	n = 1 LOQ: 60 ng/mL
60 min	n = 4	n = 4	n = 4	n = 4	n = 4	n = 1 LOQ: 180 ng/mL	n = 4	n = 4	n = 3 LOQ: 60 ng/mL
90 min	n = 3 LOQ: 75 ng/mL	n = 3 LOQ: 60 ng/mL	n = 3 LOQ: 60 ng/mL	n = 2 LOQ: 60 ng/mL	n = 2 LOQ: 60 ng/mL	n = 3 LOQ: 105 ng/mL	n = 3 LOQ: 60 ng/mL	n = 3 LOQ: 60 ng/mL	n = 3 LOQ: 60 ng/mL
120 min	n = 3 LOQ: 120 ng/mL	n = 4	n = 4	n = 1 LOQ: 60 ng/mL	n = 4	n = 1 LOQ: 180 ng/mL	n = 4	n = 4	n = 4

Table 4-5 The LOQ and number of samples above LOQ for rats given a subcutaneous injection.

Time Point	Olfactory Bulb	Cerebellum	Medulla	Hippocampus	Frontal Lobe	Striatum	Temporal Lobe	Occipital Lobe	Parietal Lobe
15 min	n = 4	n = 4	n = 4	n = 4	n = 4	n = 4	n = 4	n = 4	n = 4
30 min	n = 4	n = 4	n = 4	n = 4	n = 4	n = 4	n = 4	n = 4	n = 4
60 min	n = 3 LOQ: 75 ng/mL	n = 3 LOQ: 60 ng/mL	n = 4	n = 2 LOQ: 90 ng/mL	n = 4	n = 3 LOQ: 90 ng/mL	n = 4	n = 2 LOQ: 60 ng/mL	n = 4

Table 4-6 The LOQ and number of samples above LOQ for rats given an intravenous injection.

Time Point	Olfactory Bulb	Cerebellum	Medulla	Hippocampus	Frontal Lobe	Striatum	Temporal Lobe	Occipital Lobe	Parietal Lobe
15 min	n = 5	n = 5	n = 5	n = 5	n = 5	n = 5	n = 5	n = 5	n = 5
30 min	n = 5	n = 4 LOQ: 60 ng/mL	n = 5	n = 5	n = 5	n = 5	n = 5	n = 5	n = 5
60 min	n = 3 LOQ: 60 ng/mL	n = 1 LOQ: 60 ng/mL	n = 5	n = 4 LOQ: 60 ng/mL	n = 4 LOQ: 60 ng/mL	n = 2 LOQ: 120 ng/mL	n = 5	n = 4 LOQ: 60 ng/mL	n = 4 LOQ: 60 ng/mL

3TC's distribution in the brain was most heterogenous when closest to the t_0 or t_{max} as the only significant difference was detected in the oral-60-minute group (the t_{max} for orally administered 3TC), and the SC and IV groups' differences were not observable by 60 minutes. Although most compartmental models assume homogenous brain tissue distribution[252], we have found that this is not necessarily the case, especially during the distribution phase. Heterogenous drug distribution in the brain has been documented using mass spectrometry imaging[253], and there can be notable differences in distribution patterns between different types of drugs. In a study by Ntshangase *et al*., an NRTI tenofovir alafenamide (TAF) used mass spectrometry imaging and showed similar patterns to those in our study. Ntshangase *et al*. found TAF brain distribution was most heterogenous around t_{max}, with concentrations in different brain regions becoming more similar with passing time, although ultimately drug concentrations did not vary greatly between brain regions.[254] Similarly, in a different study by Ntshangase *et al*., another NRTI, FTC, which is structurally very similar to 3TC, exhibited heterogenous distribution, especially during the t_{max}.[255]

There is some evidence that the BBB in the olfactory bulbs may be more permissible to albumin penetration.[256,257] This could provide some mechanism for 3TC to be transported into the olfactory bulb at higher concentrations compared to other parts of the brain. While it may not be high, 3TC is up to 36% bound to protein.[258] As albumin hitchhiking can aid in drug penetration into lymphatics[259], it is possible that drugs can also utilize

this mechanism to improve penetration into other tissues, such as the olfactory bulb. In addition, Ueno *et al*. show that the increased albumin penetration in the olfactory bulbs may be because of a slightly larger vasculature with some interruption in the endothelial lining, which could result in a more permissible section of the BBB in the olfactory bulbs.[257]

As drug can passively diffuse further into brain tissue from ventricular cerebral spinal fluid[260], it may be helpful to increase dosing frequency of ART to maximize diffusion. This may also be helpful with 3TC because even though 3TC has a short elimination half-life, its active intracellular metabolite, 3TC-triphosphate (3TC-TP), has a long half-life of 15 to 16 hours.[261] More frequent dosing could result in 3TC-TP accumulation inside cells in the brain that are infected with HIV.

4.3.5 Biodistribution of 3TC following oral, IV and SC administrations into the testes, lungs and spleen

In addition, the concentrations of 3TC in other tissues implicated in the HIV reservoir were analysed: testes, spleen and lung. The concentration-time profile of 3TC in these tissues followed the pattern found in plasma pharmacokinetic studies. In animals that were given an oral dose, maximum 3TC concentrations in testes, lung, and spleen were found at 60 to 90 minutes. Similarly, the rats that were given an IV or SC dose had maximal 3TC tissue concentrations at 15 minutes, and these concentrations declined over the following 45 minutes similar to the plasma pharmacokinetic studies.

Post-absorption phase tissue:serum ratios are comparable across different routes of administrations with testes around 0.3, spleen around 0.6 and lungs around 0.7 (**Figure 4-18**). The testes and spleen show ratios steadily increasing throughout the distribution phase, after which the ratios seemed stable post-distribution in the case of the oral studies. This is consistent with drug being redistributed from a central (blood) compartment and reaching an equilibrium. In contrast, the lungs reached and maintained the maximum tissue:serum ratios quickly compared to the other tissues. This is most likely due to the lungs being a highly blood-perfused organ, which is necessary to facilitate oxygen exchange. This is reflected by the high blood flow (5000 mL/min) and perfusion (10.0 mL/min/mL of tissue) rates of the lungs.[262] To contrast, the liver and kidneys, which are also highly blood perfused tissues, only experience a blood flow of 1350 and 1100 mL/min, respectively, and a tissue perfusion rate of 0.8 and 4.0 mL/min/mL of tissue, respectively.[262] Interestingly, despite this, none of the other tissues analysed, including the lungs, reached as high 3TC concentrations as the lymph nodes, suggesting that the finding regarding high lymph node 3TC concentrations is quite unique in relation to other tissues.

One possible reason for relatively low drug concentrations in the testes is likely due to the blood-testis barrier (BTB). Similar to the BBB, the BTB restricts paracellular entry of small molecules into the seminiferous tubules.[263] Whilst this may still allow for drugs to penetrate the interstitium of the testes (which is where CD4+ cells tend to be distributed[264]) it can be

difficult for drugs to reach the seminiferous tubules. This could be problematic because HIV is also capable of crossing the BTB into seminiferous tubules.[265] In contrast with our findings, one other study found relevant transporters on both the testicular endothelium and seminiferous epithelium, which correlated with high concentrations of 3TC in testicle homogenate.[226] However, this study was performed in humans, and interspecies differences may account for the gap between the data from our study and Huang *et al*.

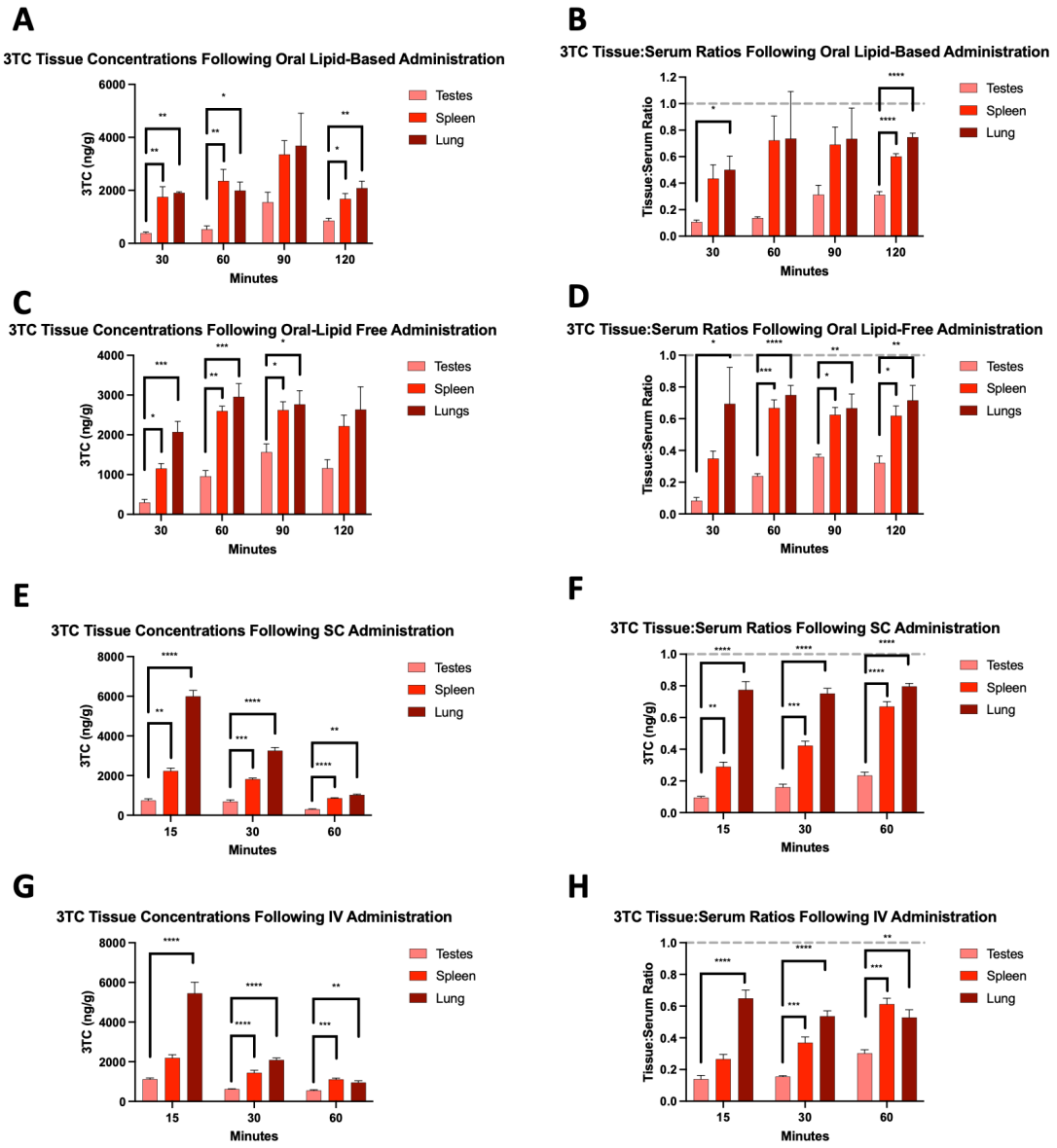

Figure 4-19 *The distribution of 3TC in testes, spleen and lung in 30 mg/kg oral lipid-based animals (A and B), 30 mg/kg oral lipid-free (C and D), 10 mg/kg SC (E and F) and 10mg/kg IV (G and H) administrations (mean ± SEM, n = 4 for all groups except oral lipid-based 90 minutes in which n = 6). One-way ANOVA followed by Tukey's test was used for statistical analysis. Asterisks denote significance against MLNs. *p<0.05, **p<0.01, ***p<0.001, ****p<0.0001. 3TC, lamivudine; SC, subcutaneous; IV, intravenous.*

Chapter 6 Fabrication and *In Vitro* Analysis of 3TC Loaded Microneedles

6.1 Introduction

The data from subcutaneous (SC)-administration biodistribution studies show that following a SC injection of a simple formulation of 3TC dissolved in sterile water, the drug can experience enough lymphatic drainage to achieve concentrations up to 3.2 times higher in draining lymph nodes compared to serum. This could be a simple way for antiretroviral drugs (ARVs) to be delivered to lymph nodes throughout the body to target tissues that harbour latent reservoirs.

Unfortunately, however, daily SC injections can be an unacceptable route of administration for some patients, which may decrease adherence to therapy. This can be due to a variety of reasons including but not limited to a fear of needles, injection site pain, need for special sharps disposal or limited dexterity necessary for self-injection.[266–268] In addition, in order to target peripheral lymph nodes throughout the body, multiple SC injections on various locations would be necessary, which would be unrealistic for patients. In order to ensure the greatest chance of success in therapy, it is important to decrease possible barriers for the patient.

Traditionally, transdermal drug administration methods involve patches.[269] Transdermal patches on the market include those loaded with nicotine, scopolamine, fentanyl, as well as other drugs. Unfortunately, the stratum corneum, composed of dead skin, is a major barrier to drug entry.[270] There are several ways to overcome this barrier, such as needleless jet injectors, iontophoresis, electroporation, sonophoresis, and microneedles (MNs).[269] This study will focus on dissolvable MNs, which have a decreased

risk for sharps-related accidents and are relatively pain free.[271] This is because compared to SC injections in which drug is injected through the dermis into subcutaneous fat, MNs are much shorter and only reach the skin's epidermis (**Figure 5-1**). As pain receptors are located in the dermis, MNs are short enough to be painless whist still providing the mechanical means to bypass the stratum corneum.[272]

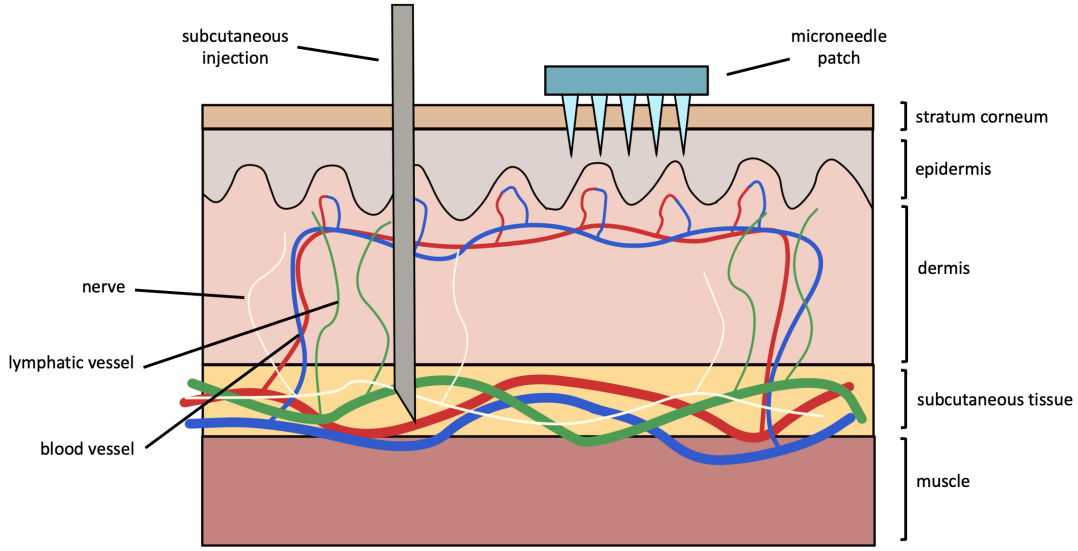

Figure 6-1 *SC injections pass through the dermis, in which many nerve endings are located. Microneedle patches do not reach the dermis and are therefore less painful compared to SC injections.*

Dissolving MNs can be made from a variety of water soluble polymers. Some common polymers used for dissolvable MNs are polyethylene glycol (PEG), polyvinyl alcohol (PVA), PVP (polyvinylpyrrolidone), polylactic acid (PLA), and polylactic-co-glycolic acid (PLGA)[273]. In this study, a previously described method was used to fabricate polyvinylpyrrolidone/vinyl acetate (PVAVA) dissolvable MNs.[157] This method was chosen due to the ease of fabrication process and use of nontoxic materials, which would be an important consideration should these MN

patches proceed to *in vivo* experiments. In addition, it was predicted that this fabrication method could achieve a high loading mass of 3TC as it is a highly water-soluble drug.

Although it could be possible to assemble 3TC-oleate nanocrystals that could selectively target peripheral lymphatics due to size-based preferential uptake, the results of previously performed SC-administration biodistribution studies show that this may not be necessary. Instead, we have hypothesized that a previously described method[274] could be modified to achieve loading of 3TC, a highly water-soluble drug, into dissolving MN patches. These patches could be administered at various places on the body to increase drug delivery to peripheral lymph nodes.

After *in vitro* tests to verify the rigidity and insertion properties of the MN patches, Franz cell diffusion studies were performed using porcine skin to determine whether our patches could successfully deliver 3TC transdermally. Full thickness porcine skin was chosen as the membrane because of the similarities between pig and human skin.[275] Successful delivery of 3TC into the receptor fluid of the Franz cell would suggest that MN delivery of 3TC could be a way to deliver drug into peripheral lymphatic capillaries.

6.2 Experimental Design

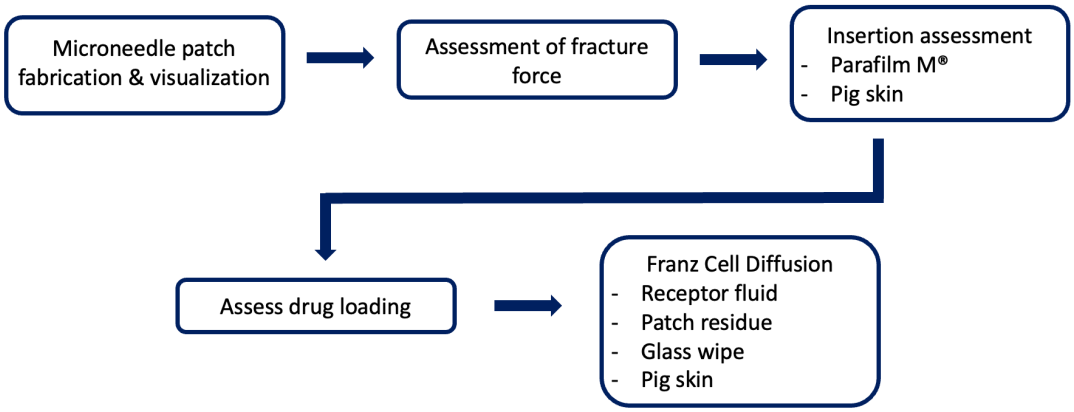

Figure 6-2 *Schematic outlining fabrication and* in vitro *assessments of 3TC-loaded MN patches.*

Fabrication of MN patches is outlined in section 2.17.

Visualization of patches is outlined in section 2.18.

The fracture force was tested using methods outlined in section 2.19.

Parafilm M® and pig skin insertion tests are outlined in section 2.20.

Drug loading and Franz cell diffusion studies are outlined in sections 2.21 and 2.22, respectively.

6.3 Results and Discussion

MN patches were fabricated with solutions of 30 or 60 mg/mL of 3TC in water using a previously described method developed by Sabri *et al*. to fabricate MN patches loaded with imiquimod [157]. The substitution of 3TC instead of imiquimod did not appear to have a negative impact on the force needed to fracture the needles, although there does appear to be a trend of increasing fracture force with increased drug loading (**Figure 5-3**). The force required to fracture the MN fabricated using 60 mg/mL 3TC solution was significantly greater than blank MNs. This pattern can be seen in other

studies[276,277], although the converse is also possible.[278] This could possibly due to hydrogen bonds formed between the drug and polymer, that may enhance the rigidity of the microneedle.

As the fracture force needed to penetrate skin is 0.098 N/needle[279,280], both MNs fabricated using 30 or 60 mg/mL 3TC solution would be acceptable. The MNs fabricated using 60 mg/mL of 3TC solution was chosen due to presumably higher drug loading as well as improved fracture force. As 3TC was difficult to solubilize in water in concentrations higher than 60 mg/mL, the decision was made to proceed with the patches made from this concentration of solution.

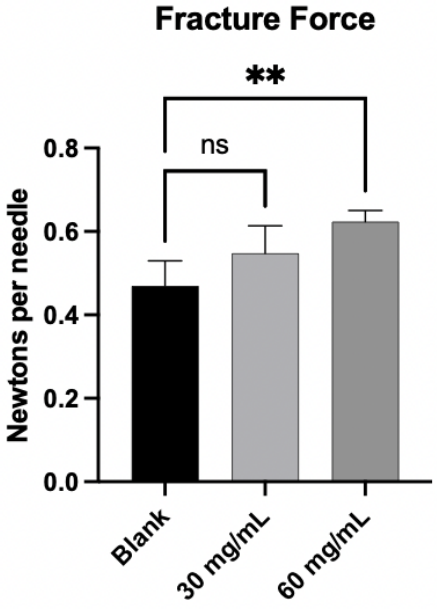

Figure 6-3 *The force needed to fracture blank and two different concentrations of drug-loaded PVAVA MN patches (mean ± STD, n = 4). The MNs made using 60 mg/mL 3TC solution are significantly more rigid compared to blank MNs. One-way ANOVA followed by Dunnett's test was used for statistical analysis. *p < 0.05, **p < 0.01, ***p < 0.001, ****p < 0.0001.*

The patches were visualized under an environmental scanning electron microscope (ESEM), which confirmed the needles' obelisk shape (**Figure 5-4**). The height of the measured MNs ranged from 839.5 to 871.9 µm. The ESEM showed some bubbling on the needle tips and along the edges of the obelisk. This bubbling was suspected to be due to insufficient drying time in the desiccator. Initially, patches were placed in an oven vacuum at 40 °C to assist drying. However, it was found that leaving patches with fresh solution to dry in the oven resulted in overly brittle needles and a broken, flaking backing layer, and so the desiccator was used instead.

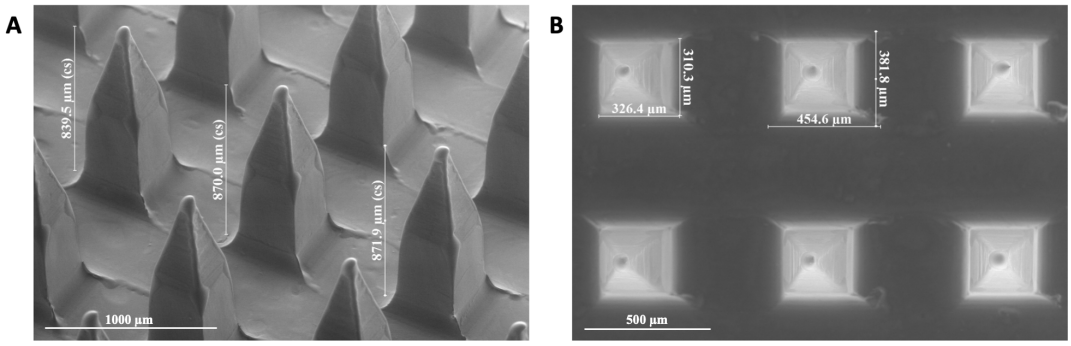

Figure 6-4 *The PVPVA patches loaded with 3TC using 60 mg/mL solution under an ESEM show obelisk shaped MNs. A) The measured MNs range from 839.5 to 871.9 µm in height. B) The bases of the MNs are square shaped and are approximately 300x300 µm.*

Results of the Parafilm M® insertion tests were comparable to the previous study from which this MN fabrication method was derived.[157] The thickness of human stratum corneum varies depending on the site measured, but it ranges from 6.2 µm at its thinnest to 40 µm at its thickest.[281] The patches show promise for delivery of drug into the epidermis as 98 to 100% of needles pierced the first layer of Parafilm M®, which is 127 µm thick per sheet (**Figure 5-5**).

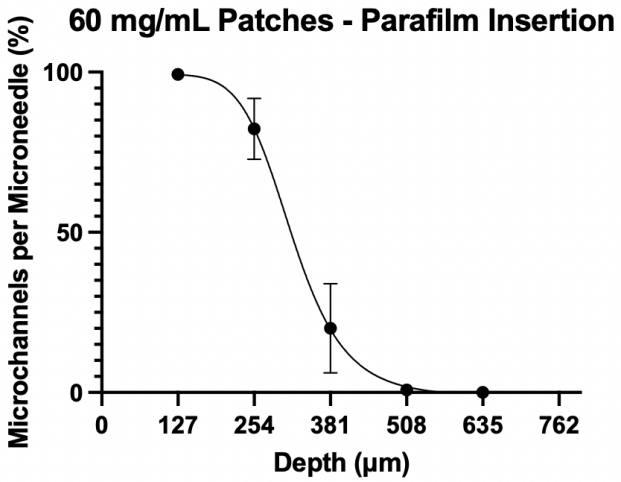

Figure 6-5 *The number of microchannels created when inserting patches into Parafilm M® per MN, expressed as a percentage (mean ± STD, n = 4). Each layer of Parafilm M® is 127 µm thick.*

Next, we tested the MN patch's insertion properties into pig skin. Following insertion and dye staining, MN channels could clearly be observed with the naked eye, although not all MNs had a corresponding dyed channel (**Figure 5-6**). The skin was then sectioned and observed under the profilometer. Visibly stained microchannels were measured, with lengths ranging from 65.2 to 128.4 µm (**Figure 5-7**). This channels may have been much shorter than the needle length due to the uneven surface of the skin. In addition, the needles may not have been inserted perfectly perpendicularly. In this study, the pig skin was not pulled taut when the MN patches were inserted. It has been found that uniaxial or equibiaxial stretching of the skin can improve the depth of MN insertion.[282]

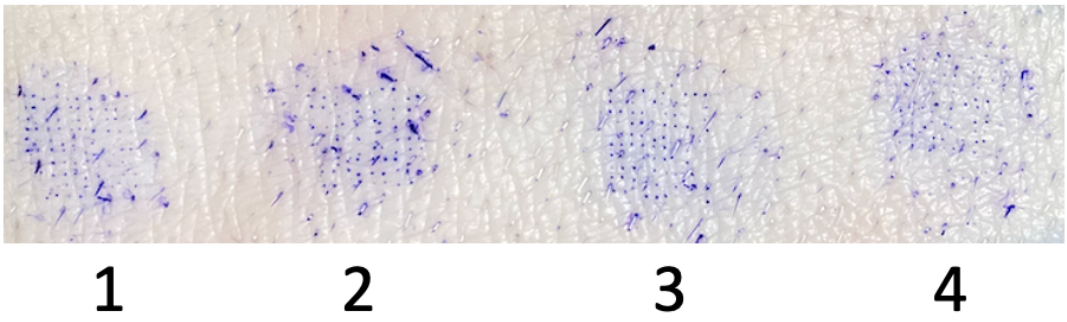

Figure 6-6 *Porcine skin insertion experiments show visible accumulation of methylene blue dye in the microchannels created by each of the four MN patches upon insertion (n=4).*

The drug loading for the MN patches using the 60 mg/mL 3TC in water solution was tested in five patches and found to be 1.39 ± 0.29 mg (mean ± STD) of 3TC per patch. The extent of 3TC drug loading was high compared to the study by Sabri *et al*. using the same method in which 300 μg of imiquimod was loaded.[157] This difference in drug loading is likely due to the high water solubility of 3TC compared to imiquimod. As the drug-solution used to fabricate the patches was highly concentrated, more drug was loaded into each patch. This is reflected in another study in which MN patches designed by He *et al.* had an average of 1.26 mg of propranolol per patch when fabricated into a 12 x 12 array of 300 x 300 x 1200 μm (length x width x height) obelisks.[283] The drug-to-polymer ratio is similar between the study by He *et al.* (4) and the ratio used in our study (3.3). Although this study utilized matrix with a propranolol concentration of 60 mg/mL and our study utilized a final concentration of 58.8 mg/mL of 3TC in matrix, the drug loading of propranolol in this study is comparable to the drug loading found in our study.

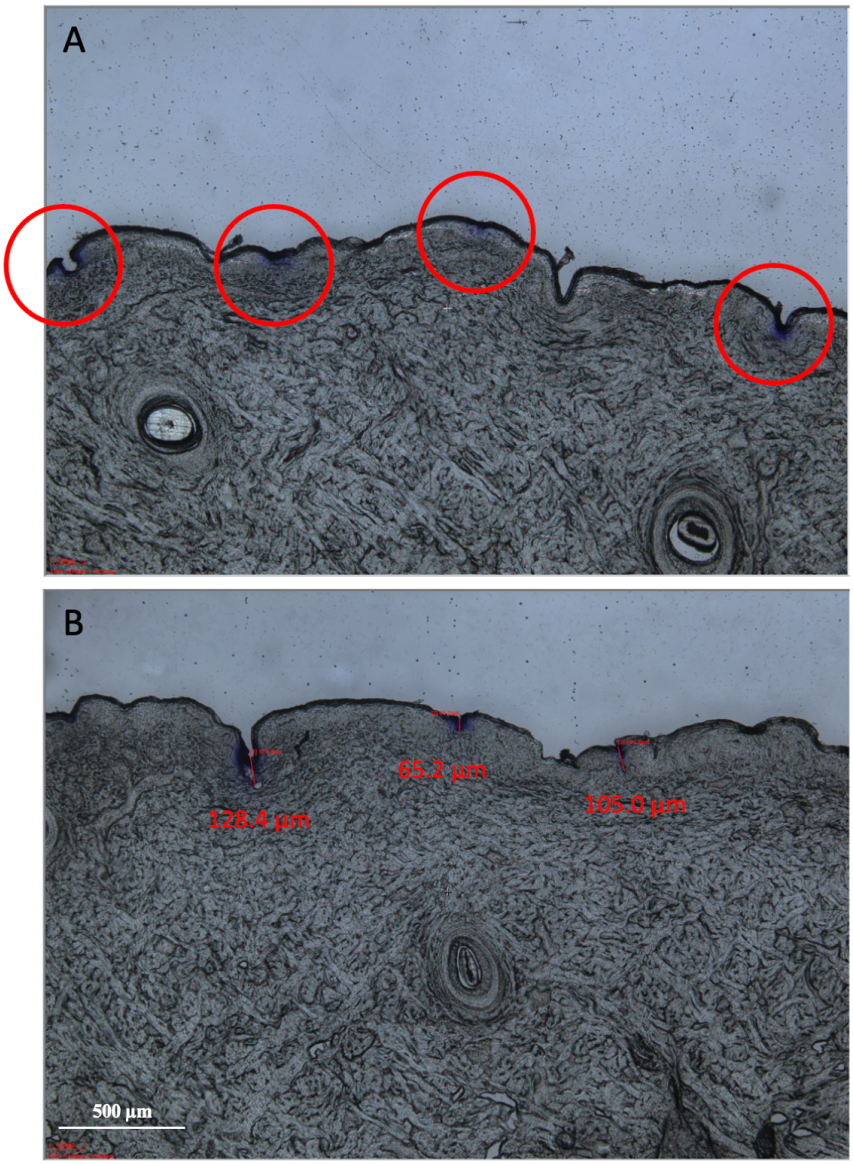

Figure 6-7 *An example of a dye-stained microchannels found in sections of pig skin as viewed under a profilometer after insertion of PVPVA MN patches loaded with 3TC using 60 mg/mL solution. Dye depositing was observable for each of the four MN patches tested (A), with dyed channels ranging from 65.2 µm to 128.4 µm (B).*

Lastly, Franz diffusion cell experiments were performed to observe the permeability of 3TC across pig skin when administered via dissolving MN patches (**Figure 5-8**). Pig skin was found to be difficult to homogenize. Previous tissues analysed such as lung, spleen and testes were homogenized with a tissue:water ratio of 1:3 (w/v) in biodistribution studies performed in section 5.3.4. When this approach was attempted with pig skin, it was found

that the high collagen content resulted in a gel-like homogenate, which stuck onto the inside of the homogenizer probe and was difficult to pipette. It was found that a tissue:water ratio of 1:5 (w/v) produced a homogenate that was pipette-able. Homogenization with a tissue:acetic acid ratio of 1:3 (w/v) also resulted in a pipette-able mixture as collagen is soluble in acetic acid.[284] As the concentrations of 3TC were found to be high in pig skin, we chose to keep our homogenization method in water as 3TC is more stable in neutral compared to acidic conditions.[177]

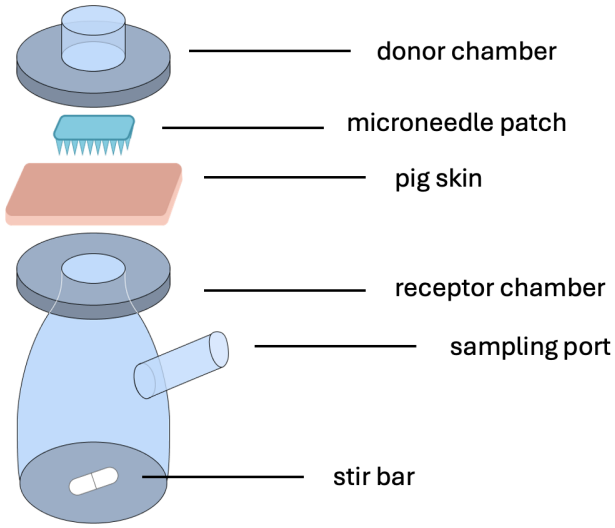

Figure 6-8 *The setup of a Franz diffusion cell. The receptor chamber was filled with PBS.*

Franz cell diffusion experiments showed that 3TC delivered via dissolvable MN patch was able to cross the skin membrane into the receptor fluid, but the amount that was found in the receptor fluid made up a small fraction of the total amount of drug applied (**Figure 5-9**). The majority of 3TC was found undissolved in the patch residue with another smaller portion of drug found as residue on the glass where the Franz cell was pressed against the patch. The receptor fluid recovery of 3TC was 188 ± 69 µg (mean ± STD).

Using the mean patch drug loading of 1.39 mg, this means only 14.5 ± 6% (mean ± STD) of total drug was able to diffuse through the pig skin into the receptor fluid after 24 hours. This percentage of drug recovery in the receptor fluid is comparable to the previously described imiquimod-loaded patches, which utilized the same fabrication process.[157,274] This pattern was also seen in other studies[285], although the extent to which drug can be found in receptor fluid can be quite variable and may depend on the drug being used.[286] Other dissolvable patches with different methods of fabrication using different drug found higher receptor fluid recovery[287] and still others had as low as 1 to 3% mass recovery in the receptor fluid at 24 hours.[288]

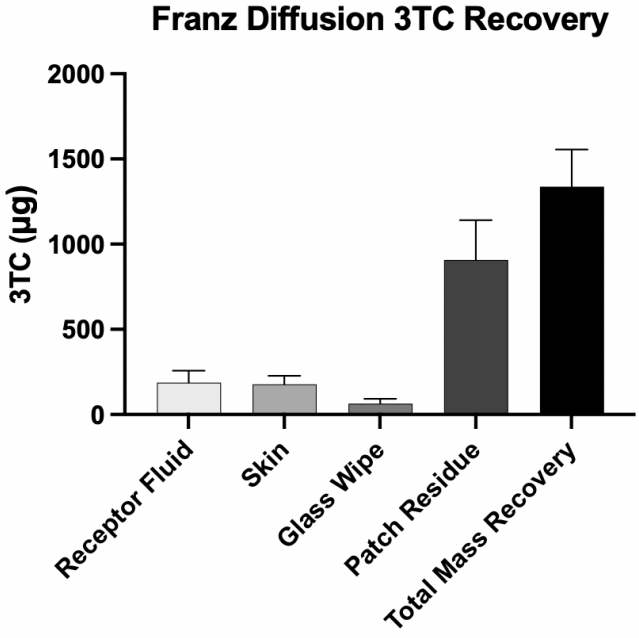

Figure 6-9 *The recovery of 3TC in Franz cell diffusion experiments (mean ± STD, n = 4). Experiments were performed using PVPVA MN patches loaded with 3TC using 60 mg/mL solution. 3TC, lamivudine.*

While some studies show higher percentages of receptor-fluid recovery, it should be noted that these studies have been performed with full-thickness neonatal porcine skin.[289] This is important to note as the neonatal epidermis and dermis has been shown to be thinner than adult skin[290], and thus may present less of a barrier for drug to cross into the receptor fluid. One other study using hydrophilic molecules theophylline and methylene blue achieved high permeation across porcine skin; however, it is important to note that the skin used in this study was neonatal skin trimmed to a thickness of 350 μm[291] whereas full-thickness adult porcine skin was used in our study. This is notable as the dermis alone of pig skin is approximately 3 mm.[292] It has previously been shown that the use of different thickness of membranes can have an influence on the amount of drug found in the receptor fluid.[289] As such, although high recovery of drug in receptor fluids have been found for both highly hydrophilic[293] and less hydrophilic[294] drugs, it is difficult to compare results due to the use of trimmed skin as the Franz cell membrane. Another study using full-thickness porcine skin and a hydrophilic nucleoside analogue achieved similar recovery percentages as we did with 3TC.[295]

A similar amount of drug was recovered in the pig skin, with a mean of 177 μg of 3TC, or 13% of the total dose, found after 24 hours (**Figure 5-9**). Together with the receptor fluid, a mean of 28% of mass recovery was found in these areas. Other studies utilizing dissolvable MN patches also show similar skin-plus-receptor-fluid recovery percentages.[274,288] Additionally,

studies show that the range of recovery in the receptor fluid and skin can be quite variable based on the matrix of the needles.[296,297]

Most of the drug in the patch did not penetrate the skin, however. An average of 72% mass recovery was found in the patch residue and on the glass of the Franz cell (**Figure 5-9**). When the backing layer of the patch was removed, upon visual inspection, not all the needles were completely dissolved. This is consistent with the pig skin insertion experiments in which dyed microchannels were found to be less than 150 µm deep, whereas the ESEM showed needle lengths of approximately 850 µm. In addition, not every MN that was attempted to be inserted resulted in a corresponding dyed channel (**Figure 5-6**). This could explain the large amount of 3TC recovered in the patch residue. Moreover, it is possible that during the patch fabrication process, some of the drug could have leached into the backing layer. During fabrication, the needles are first dried. Then, the backing layer solution is added on top of the needles in the mould before it is further dried in the desiccator. As the backing layer solution is water-based, it is possible that some of the 3TC in the needles dissolved and leached into the backing layer solution before it dried. This concept of drug leaching into the backing layer is acknowledged in literature[298–300], and there is some experimental evidence that this may occur.[288,296] This can possibly be combated with drug-loaded backing layers, which may help to decrease leaching and additionally may provide a drug reservoir for sustained release.[301]

Of course, further optimization of 3TC-loaded MN patches is possible. In this study, we only tested one formulation for the needle matrix, and it is possible that use of a different polymer could increase the percentage of drug delivered into the receptor fluid. In addition, use of a more hydrophilic polymer (such as PVA without the vinyl acetate copolymer) could increase dissolution of the needles in the skin, further increasing drug delivery.

Chapter 7 General Discussion

The primary aim of this PhD project was to deliver 3TC to multiple lymph nodes throughout the body that can harbour HIV reservoirs. The purpose of this would be to possibly decrease HIV replication and formation of the viral reservoir during the acute infection phase, minimize the small amounts of replication that happen during chronic infection, and possibly to be used in conjunction with curative strategies.

In this project, it was found that lipophilic prodrugs were not necessary to achieve concentrations of 3TC in lymph nodes higher than in blood. Through oral administration, 3TC could be delivered to mesenteric lymph nodes (MLNs) to achieve high drug concentrations. Through subcutaneous or possibly transdermal administration on all patient extremities, 3TC could be delivered to various draining lymph nodes in concentrations higher than in blood. When used in conjunction, combining oral and subcutaneous or transdermal deliveries could be useful to target a multitude of lymph nodes throughout the body.

In this project, the following was achieved: 1) a sensitive high performance liquid chromatography with UV detection (HPLC-UV) method was developed for the determination of 3TC-containing biological samples 2) 3TC and its synthesized fatty acid ester prodrugs were analysed for their lymphatic targeting potential 3) 3TC's pharmacokinetic properties and biodistribution profiles in lymph nodes, brain, spleen, lungs, and testes were observed and 4) dissolving microneedle (MN) patches were fabricated and tested *in vitro*.

In chapter 3 of this thesis, a sensitive, accurate, and precise HPLC-UV method was developed for the analysis of 3TC in biological rat matrices and would be simply modifiable for the analysis of highly lipophilic ester prodrugs of 3TC. Although some HPLC-UV methods were able to detect 3TC using mobile phase compositions with 30 to 85% organic solvent[160,162], the method developed in this project utilized a much higher aqueous phase composition at 88%. This was most likely due to a difference of biological matrix as the HPLC-UV methods utilizing high organic solvent mobile phase composition were developed for rabbit or human plasma whereas our method was designed for rat plasma. As a result, a higher aqueous component was necessary to achieve separation of 3TC peaks from endogenous rat plasma peaks.

The limit of quantification (LOQ) of this method was 15 ng/mL for 3TC, which allowed for the quantification of drug in tissue samples with low mass as well as with small quantities of lymph fluid sample. In addition, quantification of low concentrations of 3TC in rat plasma is important for accurately determining the elimination phase in pharmacokinetic studies. This LOQ was much lower than other previously developed HPLC-UV methods for the detection of 3TC in rat plasma[164,175], and was even lower than a method that utilized liquid chromatography and mass spectrometry (LC-MS)[167]. This was likely due to the extraction methods used[164], as well as differences in sample injection volume.[175]

As our method utilized HPLC-UV [as opposed to ultra-performance liquid chromatograph (UPLC) or liquid chromatography-mass spectrometry

(LCMS)] as well as liquid-based extraction techniques (as opposed to SPE[175]), this method is a low-cost way to quantify low concentrations of 3TC in rat biological matrix. This is important as HIV disproportionately affects low- and middle- income countries where research and development costs may be a significant barrier.

Because 3TC does not exhibit lipophilic physicochemical properties, it was not expected to be transported into intestinal lymphatics following oral administration[115]. As described in chapter 4, 3TC was found to have negligible association with chylomicrons and solubility in sesame oil, which was used to represent solubility in triglycerides. This was expected as 3TC is a highly hydrophilic molecule with a cLog P of -0.71 (ACD/I-Lab). Because the extent of association with chylomicrons and triglyceride solubility are predictors of direct lymphatic uptake following oral administration, the transport of 3TC into intestinal lymphatics was expected to be low.

In order to increase 3TC association with chylomicrons, highly lipophilic ester prodrugs were designed. This approach has been used previously to successfully improve the intestinal lymphatic targeting of various drugs[121,124,125]. 3TC-stearate and 3TC-oleate were predicted to have moderate association with chylomicrons and were chosen to be synthesized. While the addition of one double bond in 3TC-oleate compared to 3TC-stearate decreased its cLog P and Log $D_{7.4}$, which in turn decreased the percentage association of prodrug to Intralipid®, both prodrugs exhibited high association with artificial chylomicrons. The Intralipid® association was found to be much higher than the *in silico* model prediction with 3TC-

stearate and 3TC-oleate exhibiting 86% and 61% association with artificial chylomicrons, respectively. The large difference in *in silico* predicted association and *in vitro* experimental association was suspected to be due to the structures of the molecules used to develop the *in silico* model. 3TC prodrugs were highly lipophilic (the cLog Ps for 3TC-stearate and 3TC-oleate were 8.04 and 7.53, respectively) and had amphiphilic structures, whereas the only amphiphilic molecule used to validate the *in silico* model was amphotericin B, which has a relatively low cLog P (1.16).

Because the solubility of drugs in triglycerides can help to predict the direct uptake of drugs into intestinal lymphatics[115], the prodrugs' solubility in sesame oil was tested. 3TC-oleate exhibited higher sesame oil solubility compared to 3TC-stearate, which was a pattern seen in another study utilising fatty acid ester prodrugs[123]. Compared to the stearate moiety, use of an oleic acid moiety likely increased prodrug solubility in sesame oil because oleic acid contributes a much higher percentage of sesame oil fatty acid composition compared to stearic acid.[202]

The stabilities of these prodrugs in rat plasma and FaSSIF and solubilities in sesame oil were also assessed. This is because prodrugs would ideally be stable in the stomach and intestines, yet release the parent drug, 3TC, quickly once it is transported into lymphatics. The introduction of a double bond in 3TC-oleate compared to 3TC-stearate decreased the half-life of the prodrug in both plasma and FaSSIF. This is most likely because unsaturated fatty acids with double bonds at the 6, 9, or 11 position increase lipase activity compared to saturated fatty acids.[201] Using an

unsaturated fatty acid moiety also increased the prodrug's solubility in sesame oil compared to a prodrug with a saturated fatty acid moiety. This was concluded to be due to the fatty acid makeup of sesame oil, which features up to six times more oleic acid than stearic acid.[202]

Despite improved association with chylomicrons for both prodrugs compared to 3TC, 3TC-stearate and 3TC-oleate were not determined to be suitable for progression into *in vivo* studies. This was due to sesame oil solubilities for both prodrugs well under the 50 mg/mL triglyceride solubility that is indicative of intestinal lymphatic uptake, as well as the prodrug solubilities being too low for realistic *in vivo* dosing volumes. In addition, 3TC-oleate was too unstable in FaSSIF, which suggested that it would be converted too quickly in the intestinal lumen.

Previous *in vivo* studies showed relatively high concentrations of hydrophilic drugs in intestinal lymphatics following oral administration[222,223,225]. Additionally, a previous *in vivo* study showed high concentrations of nucleoside analogues tenofovir alafenamide and tenofovir disoproxil in various lymph nodes following a subcutaneous injection[224]. To determine if this could be reproducible with 3TC, in Chapter 4, pharmacokinetic and biodistribution studies were performed on male Sprague-Dawley rats following allometrically-scaled doses of oral lipid based, oral lipid-free, IV, and SC administrations. In order to track the patterns of lymphatic drainage, multiple types of lymph nodes were sampled from various parts of the body.

Biodistribution studies following oral lipid-based and oral lipid-free administrations with 3TC showed concentrations of 3TC in MLNs two to three times as high compared to serum for both treatment groups. This was unexpected due to low predicted and experimental association of 3TC with chylomicrons. To gain a better understanding of how 3TC is being transported into the intestinal lymphatics, we analysed different lymph fluid "compartments." There were low-to-undetectable amounts of 3TC in cells and associated with chylomicrons. Most of the drug was found in the cell-free, chylomicron-free lymph fluid, suggesting that the mechanism by which 3TC enters intestinal lymph is neither through association with chylomicrons nor intracellularly through cell migration.

Next, biodistribution studies following SC administration were performed. Concentrations of 3TC in right-side (administration-side) draining lymph nodes were found to be significantly higher than the corresponding left-side lymph nodes. At the t_{max}, the concentration in these right-side draining lymph nodes were about three times as high compared to serum. This was also unexpected as transport into peripheral lymphatics is size-based in which particles smaller than 10 nm are expected to be transported directly into blood, and the 3TC formulation injected was a simple dissolution of drug in water and was not nano-formulated.

To confirm that the high concentrations of 3TC in MLNs following oral administration and right-side draining lymph nodes following SC administration were not due to redistribution of drug from blood, biodistribution studies with IV administration were performed. In these

studies, we found similar or only slightly higher concentrations of 3TC in all lymph nodes compared to serum. This suggests that the unexpected findings in our oral- and SC-administration biodistribution studies were not due to redistribution of drug from blood.

It is unlikely that transporters are responsible for the uptake of 3TC in LECs due to previous evidence showing low concentrations of another cytidine analogue, FTC, structurally very similar to 3TC, inside of LECs.[241] However, previous studies have shown the presence of OCT3 transporters (for which 3TC is a substrate) on lymph nodes, suggesting that there may be active transport of 3TC in HEVs.[225] This may explain why tissue:serum ratios for lymph nodes following an intravenous administration were around or slightly higher than 1. This ratio is notable as 3TC does not appear to distribute into other highly vascular tissues such as the spleen or lungs (tissue:serum ratios around 0.6 to 0.7, respectively) to the same extent as it does into the lymph nodes.

HIV persistence in lymph nodes despite high distribution of 3TC into these tissues may be due to several reasons. Firstly, intracellular concentrations of 3TC in the lymph has been shown to be lower compared to PBMCs. Secondly, distribution of drug throughout the lymph nodes is not homogenous. Lastly, clonal expansion has recently been shown to contribute to the majority of the lymph node HIV reservoir[246], and 3TC does not address this mechanism of reservoir growth.

Because of its hydrophilicity, 3TC is a Biopharmaceutics Classification System (BCS) Class III drug. As opposed to BCS Class II drugs that exhibit low

concentrations of drug in MLNs compared to blood following oral administration[123–125,221], 3TC has concentrations in MLNs higher than in blood. This pattern is found in other hydrophilic BCS Class III drugs such as TAF and TDF[222,225]. Our hypothesis as to why this occurs is that because highly hydrophilic drugs exhibit poor permeation compared to BCS Class II drugs, these drugs may enter the blood stream more slowly, causing a build-up of drug in the lamina propria in the gut or extracellular matrix peripherally. Therefore, more drug is available to be passively absorbed into lymphatic capillaries, resulting in higher concentrations in lymph fluid and lymph nodes compared to blood.

In the brain, 3TC concentrations were found to be low, especially compared to blood for all routes of administration. This is due to the presence of the BBB and 3TC's hydrophilicity. Despite low amounts of 3TC found in the brain (C_{max} of 222 ng/g in oral lipid-based administration whole brains), the concentrations found overlap the very low end of 3TC's IC50 range (0.7 to 3,450 ng/mL). Such concentrations may be able to inhibit clades of HIV-1 that are very susceptible to 3TC.

The distribution of 3TC in the brain was also found to be heterogenous. Concentrations of 3TC in the olfactory bulb of the brain were found to be significantly higher than many other portions of the brain. Our hypothesis for this occurrence is due to higher permissibility of albumin penetration in the olfactory bulb.[256,257,259] Although 3TC is not highly protein bound, it is still up to 36% bound to protein. Since albumin hitchhiking can contribute to increased concentration into lymphatics[259], this mechanism

may also account for the higher concentrations of 3TC observed in the olfactory bulb.

In the testes, after all drug administration types, 3TC concentrations were found to be low compared to blood with a tissue:serum ratio around 0.3. This could be due to the presence of the BTB, which restricts entry of small molecules into the seminiferous tubules.[263]

Concentrations of 3TC found in the spleen and lungs were relatively higher with tissue:serum ratios around 0.6 and 0.7, respectively. This is likely because the spleen and lungs are highly vascularized tissues[262]. Even so, 3TC tissue:serum ratios of these tissues were not as high as those found in lymph nodes, which shows that the extent of penetration of 3TC into lymph nodes is unique.

The use of 3TC-loaded dissolvable MN patches could improve delivery of drug to draining peripheral lymph nodes where latent reservoir might be hiding. The fabrication of 3TC-loaded MN patches was based off previously described protocols involving imiquimod-loaded MN patches.[157] Although we had attempted to speed up the drying of the MN patches by placing them in a 40 °C vacuum oven, this method resulted in brittle needles and flaking backing layer. As a result, drying of the MN patches was done in a desiccator.

The substitution of 3TC instead of imiquimod did not negatively impact the rigidity and insertion properties of the MNs as the fracture force and insertion into Parafilm M® and pig skin were shown to be similar between the MNs of the two drugs. Because of its high water solubility,

much more 3TC was loaded into these MNs (1.39 mg) compared to imiquimod (300 μg). Indeed, other studies in which fabrication of MNs using solutions in which the drug is highly soluble resulted in higher drug loading as well.[283] Franz cell diffusion experiments showed that the MN patches successfully delivered 3TC into the receptor fluid, with an average of 188 μg of 3TC found in this compartment after 24 hours. A further average of 177 μg was found deposited into the pig skin. When compared to other studies utilizing dissolvable MNs, the percentage of the drug found in the receptor fluid was found to be similar.[157,285,295] However, many studies used full-thickness or even trimmed neonatal porcine skin, which is much thinner than the full-thickness adult porcine skin used in this study.[289,293,294] As a result, it was difficult to draw comparisons as the thickness of the Franz cell membrane can dramatically impact the amount of drug found in the receptor fluid.[289]

However, 72% of the loaded drug was still found on the glass or undissolved in the patch residue. This was likely due to incomplete dissolution of the MNs, which was reflected in the pig skin insertion experiment. In addition, leaching of 3TC into the backing layer of the patch may contribute to the high amount of undelivered drug. Leaching of drug into the backing layer has been shown to happen in previously published studies.[288,296] Because 3TC is an inexpensive drug, this leaching could possibly be addressed by adding 3TC into the backing layer.

These experiments, in conjunction with our subcutaneous administration biodistribution studies, serve as a proof-of-concept that 3TC

might be able to be delivered to lymph nodes with transdermal administration using MN patches. In practice, when used in conjunction with an oral dose of 3TC to target intestinal lymphatics, a transdermal administration of 3TC could be used to effectively deliver drug into draining lymph nodes throughout the body.

Chapter 8 Future Work

Future studies could investigate the ratio of 3TC dose uptake into lymphatics versus into blood. This could be achieved through oral administration biodistribution studies in which blood is taken from the hepatic portal vein and concentrations of 3TC are compared to those in mesenteric lymph fluid. This could alternatively be achieved through mesenteric duct cannulation. This study could be conducted in a variety of drugs in order to create a model that can predict what percentage of dose will be absorbed into lymphatics versus blood.

More studies will need to occur to further understand the mechanism by which 3TC (and possibly other drugs) enters lymphatics following oral and SC dosing. Mechanisms for the transport of drug will need to be examined in relation to: 1) redistribution from blood into lymph nodes via HEVs 2) transport into lacteals from the lamina propria and 3) transport into lymph capillaries from the epidermis. It may be pertinent to examine lymph node HEVs for common transporter proteins for which 3TC is known to be a substrate. In addition, it would be important to know to what extent each possible mechanism (redistribution via HEVs versus transport through lacteals or lymph capillaries) contributes to 3TC's high concentrations in lymph nodes.

In the future, there could be further optimization of the MN patches to increase the percentage of loaded drug that can penetrate across pig skin into the receptor fluid of Franz cell diffusion experiments. Franz cell diffusion experiments could also be performed in order to further understand the drug release mechanisms of the 3TC-loaded MNs. In

addition, *in vivo* pharmacokinetic studies could be performed, and *in vivo* release kinetics could be examined. This could provide further understanding of this dosage form of 3TC. Biodistribution experiments in rats could then be performed whereby MN patches are applied to various parts of the body to verify drug transport to different draining lymph nodes. If successful in rats, these studies could be repeated for higher animals such as in beagles or non-human primates.

An additional *in vivo* study in rats with a combination of oral and MN patch drug administrations would be beneficial to show that 3TC could be simultaneously delivered in high concentrations to all lymph nodes. If successful, humanized mice infected with HIV could also be used to observe the efficacy of this approach against an active infection.[302] This could range from studies in acute infection to examine if lymph node-targeting decreases the size of the viral reservoir to studies in chronic infection to examine if lymph node-targeting could decrease viral replication in these tissues.[303] If successful, these studies could progress to higher animal models such as primates and effectiveness against simian immunodeficiency virus (SIV) could be observed.[304]

References

1. UNAIDS. Global HIV & AIDS statistics — Fact sheet. https://www.unaids.org/sites/default/files/media_asset/UNAIDS_FactSheet_en.pdf (2023).
2. HIV.gov. How is HIV Transmitted? *https://www.hiv.gov/hiv-basics/overview/about-hiv-and-aids/how-is-hiv-transmitted* (2019).
3. Kourtis, A. P., Lee, F. K., Abrams, E. J., Jamieson, D. J. & Bulterys, M. Mother-to-child transmission of HIV-1: timing and implications for prevention. *Lancet Infect Dis* **6**, 726–732 (2006).
4. UNAIDS. IN DANGER: UNAIDS Global AIDS Update 2022. https://www.unaids.org/sites/default/files/media_asset/2022-global-aids-update_en.pdf (2022).
5. Shao, Y. & Williamson, C. The HIV-1 Epidemic: Low- to Middle-Income Countries. *Cold Spring Harb Perspect Med* **2**, a007187–a007187 (2012).
6. Pellowski, J. A., Kalichman, S. C., Matthews, K. A. & Adler, N. A pandemic of the poor: Social disadvantage and the U.S. HIV epidemic. *American Psychologist* **68**, 197–209 (2013).
7. Lerner, A. M., Eisinger, R. W. & Fauci, A. S. Comorbidities in Persons With HIV. *JAMA* **323**, 19 (2020).
8. Lv, T., Cao, W. & Li, T. HIV-Related Immune Activation and Inflammation: Current Understanding and Strategies. *J Immunol Res* **2021**, 1–13 (2021).
9. Nyamweya, S. *et al.* Comparing HIV-1 and HIV-2 infection: Lessons for viral immunopathogenesis. *Rev Med Virol* **23**, 221–240 (2013).

10. Motomura, K., Chen, J. & Hu, W.-S. Genetic Recombination between Human Immunodeficiency Virus Type 1 (HIV-1) and HIV-2, Two Distinct Human Lentiviruses. *J Virol* **82**, 1923–1933 (2008).

11. Peruski, A. H. *et al.* Trends in HIV-2 Diagnoses and Use of the HIV-1/HIV-2 Differentiation Test — United States, 2010–2017. *MMWR Morb Mortal Wkly Rep* **69**, 63–66 (2020).

12. Azevedo-Pereira, J. M. & Santos-Costa, Q. HIV Interaction With Human Host: HIV-2 As a Model of a Less Virulent Infection. *AIDS Rev* **18**, 44–53 (2016).

13. Nyamweya, S. *et al.* Comparing HIV-1 and HIV-2 infection: Lessons for viral immunopathogenesis. *Rev Med Virol* **23**, 221–240 (2013).

14. Panel on Antiretroviral Guidelines for Adults and Adolescents. Guidelines for the Use of Antiretroviral Agents in Adults and Adolescents with HIV. *https://clinicalinfo.hiv.gov/sites/default/files/guidelines/documents/guidelines-adult-adolescent-arv.pdf* (2022).

15. Berry, N. *et al.* Low peripheral blood viral HIV-2 RNA in individuals with high CD4 percentage differentiates HIV-2 from HIV-1 infection. *J Hum Virol* **1**, 457–68 (1998).

16. Damond, F. *et al.* An International Collaboration To Standardize HIV-2 Viral Load Assays: Results from the 2009 ACHIEV2E Quality Control Study. *J Clin Microbiol* **49**, 3491–3497 (2011).

17. Wilen, C. B., Tilton, J. C. & Doms, R. W. HIV: Cell Binding and Entry. *Cold Spring Harb Perspect Med* **2**, a006866–a006866 (2012).

18. Wilen, C. B., Tilton, J. C. & Doms, R. W. HIV: Cell Binding and Entry. *Cold Spring Harb Perspect Med* **2**, a006866–a006866 (2012).

19. Ni, J., Wang, D. & Wang, S. The CCR5-Delta32 genetic polymorphism and HIV-1 infection susceptibility: a meta-analysis. *Open Medicine* **13**, 467–474 (2018).

20. Gonzalo-Gil, E. *et al.* Transcriptional down-regulation of ccr5 in a subset of HIV+ controllers and their family members. *Elife* **8**, (2019).

21. Meijerink, H. *et al.* The number of CCR5 expressing CD4+ T lymphocytes is lower in HIV-infected long-term non-progressors with viral control compared to normal progressors: a cross-sectional study. *BMC Infect Dis* **14**, 683 (2014).

22. O'Brien, T. R. *et al.* HIV-1 infection in a man homozygous for CCR5 ▵ 32. *The Lancet* **349**, 1219 (1997).

23. Hütter, G. *et al.* Long-Term Control of HIV by *CCR5* Delta32/Delta32 Stem-Cell Transplantation. *New England Journal of Medicine* **360**, 692–698 (2009).

24. Mosier, D. E. How HIV changes its tropism: evolution and adaptation? *Curr Opin HIV AIDS* 1 (2008) doi:10.1097/COH.0b013e3283223d61.

25. Kordelas, L., Verheyen, J. & Esser, S. Shift of HIV Tropism in Stem-Cell Transplantation with *CCR5* Delta32 Mutation. *New England Journal of Medicine* **371**, 880–882 (2014).

26. National Institute of Allergy and Infectious Diseases. HIV Replication Cycle. *https://www.niaid.nih.gov/diseases-conditions/hiv-replication-cycle* (2018).

27. NIH. The HIV Life Cycle. https://hivinfo.nih.gov/understanding-hiv/fact-sheets/hiv-life-cycle (2021).

28. Geneva: World Health Organization. Consolidated guidelines on HIV prevention, testing, treatment, service delivery and monitoring: recommendations for a public health approach. (2021).

29. Waters, L. *et al.* BHIVA guidelines on antiretroviral treatment for adults living with HIV-1 2022 (2023 interim update). *HIV Med* **23 Suppl 5**, (2022).

30. Cahn, P. *et al.* Dolutegravir plus lamivudine versus dolutegravir plus tenofovir disoproxil fumarate and emtricitabine in antiretroviral-naive adults with HIV-1 infection (GEMINI-1 and GEMINI-2): week 48 results from two multicentre, double-blind, randomised, non-inferiority, phase 3 trials. *The Lancet* **393**, 143–155 (2019).

31. van Wyk, J. *et al.* Efficacy and Safety of Switching to Dolutegravir/Lamivudine Fixed-Dose 2-Drug Regimen vs Continuing a Tenofovir Alafenamide–Based 3- or 4-Drug Regimen for Maintenance of Virologic Suppression in Adults Living With Human Immunodeficiency Virus Type 1: Phase 3, Randomized, Noninferiority TANGO Study. *Clinical Infectious Diseases* (2020) doi:10.1093/cid/ciz1243.

32. UNAIDS. The path that ends AIDS: UNAIDS Global AIDS Update 2023. https://www.unaids.org/sites/default/files/media_asset/2023-unaids-global-aids-update-summary_en.pdf (2023).

33. LeMessurier, J. *et al.* Risk of sexual transmission of human immunodeficiency virus with antiretroviral therapy, suppressed viral load and condom use: a systematic review. *Can Med Assoc J* **190**, E1350–E1360 (2018).

34. Marcus, J. L. *et al.* Comparison of Overall and Comorbidity-Free Life Expectancy Between Insured Adults With and Without HIV Infection, 2000-2016. *JAMA Netw Open* **3**, e207954 (2020).

35. Lu, M. T. *et al.* Effects of Pitavastatin on Coronary Artery Disease and Inflammatory Biomarkers in HIV. *JAMA Cardiol* **9**, 323 (2024).

36. Sauls, R. S., McCausland, C. & Taylor, B. N. Histology, T-Cell Lymphocyte. *StatPearls* https://www.ncbi.nlm.nih.gov/books/NBK535433 (2023).

37. Caucheteux, S. M., Torabi-Parizi, P. & Paul, W. E. Analysis of naïve lung CD4 T cells provides evidence of functional lung to lymph node migration. *Proceedings of the National Academy of Sciences* **110**, 1821–1826 (2013).

38. Bonomo, A. *et al.* A T Cell View of the Bone Marrow. *Front Immunol* **7**, (2016).

39. Polonsky, M., Chain, B. & Friedman, N. Clonal expansion under the microscope: studying lymphocyte activation and differentiation using live-cell imaging. *Immunol Cell Biol* **94**, 242–249 (2016).

40. Michalek, R. D. & Rathmell, J. C. The metabolic life and times of a T-cell. *Immunol Rev* **236**, 190–202 (2010).

41. Alberts, B. *et al.* Helper T Cells and Lymphocyte Activation. *Garland Science* https://www.ncbi.nlm.nih.gov/books/NBK26827/ (2002).

42. Chun, T.-W. *et al.* Early establishment of a pool of latently infected, resting CD4+ T cells during primary HIV-1 infection. *Proceedings of the National Academy of Sciences* **95**, 8869–8873 (1998).

43. Shelton, E. M., Reeves, D. B. & Bender Ignacio, R. A. Initiation of Antiretroviral Therapy during Primary HIV Infection: Effects on the Latent HIV Reservoir, Including on Analytic Treatment Interruptions. *AIDS Rev* **23**, (2021).

44. Chun, T. *et al.* Persistence of HIV in Gut-Associated Lymphoid Tissue despite Long-Term Antiretroviral Therapy. *J Infect Dis* **197**, 714–720 (2008).

45. Donaldson, D. S., Else, K. J. & Mabbott, N. A. The Gut-Associated Lymphoid Tissues in the Small Intestine, Not the Large Intestine, Play a Major Role in Oral Prion Disease Pathogenesis. *J Virol* **89**, 9532–9547 (2015).

46. Thompson, C. G., Gay, C. L. & Kashuba, A. D. M. HIV Persistence in Gut-Associated Lymphoid Tissues: Pharmacological Challenges and Opportunities. *AIDS Res Hum Retroviruses* **33**, 513–523 (2017).

47. Estes, J. D. *et al.* Defining total-body AIDS-virus burden with implications for curative strategies. *Nat Med* **23**, (2017).

48. Wallet, C. *et al.* Microglial Cells: The Main HIV-1 Reservoir in the Brain. *Front Cell Infect Microbiol* **9**, (2019).

49. Santangelo, P. J. *et al.* Whole-body immunoPET reveals active SIV dynamics in viremic and antiretroviral therapy–treated macaques. *Nat Methods* **12**, 427–432 (2015).

50. Yukl, S. A. *et al.* Differences in HIV Burden and Immune Activation within the Gut of HIV-Positive Patients Receiving Suppressive Antiretroviral Therapy. *J Infect Dis* **202**, 1553–1561 (2010).

51. Liu, R., Simonetti, F. R. & Ho, Y.-C. The forces driving clonal expansion of the HIV-1 latent reservoir. *Virol J* **17**, 4 (2020).

52. Keele, B. F. *et al.* Characterization of the Follicular Dendritic Cell Reservoir of Human Immunodeficiency Virus Type 1. *J Virol* **82**, 5548–5561 (2008).

53. Igarashi, T. Macrophage are the principal reservoir and sustain high virus loads in rhesus macaques after the depletion of CD4+ T cells by a highly pathogenic simian immunodeficiency virus/HIV type 1 chimera (SHIV): Implications for HIV-1 infections of humans. *Proceedings of the National Academy of Sciences* **98**, 658–663 (2001).

54. Whitney, J. B. *et al.* Rapid seeding of the viral reservoir prior to SIV viraemia in rhesus monkeys. *Nature* **512**, 74–77 (2014).

55. Vanhamel, J., Bruggemans, A. & Debyser, Z. Establishment of latent HIV-1 reservoirs: what do we really know? *J Virus Erad* **5**, 3–9 (2019).

56. Chun, T.-W. *et al.* Rebound of plasma viremia following cessation of antiretroviral therapy despite profoundly low levels of HIV reservoir: implications for eradication. *AIDS* **24**, 2803–2808 (2010).

57. Martínez-Bonet, M. *et al.* Establishment and Replenishment of the Viral Reservoir in Perinatally HIV-1-infected Children Initiating Very Early Antiretroviral Therapy. *Clinical Infectious Diseases* **61**, 1169–1178 (2015).

58. Shelton, E. M., Reeves, D. B. & Bender Ignacio, R. A. Initiation of Antiretroviral Therapy during Primary HIV Infection: Effects on the Latent HIV Reservoir, Including on Analytic Treatment Interruptions. *AIDS Rev* **23**, (2021).

59. McManus, W. R. *et al.* HIV-1 in lymph nodes is maintained by cellular proliferation during antiretroviral therapy. *Journal of Clinical Investigation* **129**, 4629–4642 (2019).

60. Li, J. Z. *et al.* The size of the expressed HIV reservoir predicts timing of viral rebound after treatment interruption. *AIDS* 1 (2015) doi:10.1097/QAD.0000000000000953.

61. Luzuriaga, K. *et al.* Viremic Relapse after HIV-1 Remission in a Perinatally Infected Child. *New England Journal of Medicine* **372**, 786–788 (2015).

62. Shan, L. *et al.* Transcriptional Reprogramming during Effector-to-Memory Transition Renders CD4+ T Cells Permissive for Latent HIV-1 Infection. *Immunity* **47**, 766-775.e3 (2017).

63. Chen, J. *et al.* The reservoir of latent HIV. *Front Cell Infect Microbiol* **12**, (2022).

64. Lassen, K. G., Bailey, J. R. & Siliciano, R. F. Analysis of Human Immunodeficiency Virus Type 1 Transcriptional Elongation in Resting CD4 $^{+}$ T Cells In Vivo. *J Virol* **78**, 9105–9114 (2004).

65. Eisele, E. & Siliciano, R. F. Redefining the Viral Reservoirs that Prevent HIV-1 Eradication. *Immunity* **37**, 377–388 (2012).

66. Shan, L. & Siliciano, R. F. From reactivation of latent HIV-1 to elimination of the latent reservoir: The presence of multiple barriers to viral eradication. *BioEssays* **35**, 544–552 (2013).

67. Zhou, Y., Zhang, H., Siliciano, J. D. & Siliciano, R. F. Kinetics of Human Immunodeficiency Virus Type 1 Decay following Entry into Resting CD4 $^{+}$ T Cells. *J Virol* **79**, 2199–2210 (2005).

68. Wei, X. *et al.* Viral dynamics in human immunodeficiency virus type 1 infection. *Nature* **373**, 117–122 (1995).

69. Crooks, A. M. *et al.* Precise Quantitation of the Latent HIV-1 Reservoir: Implications for Eradication Strategies. *Journal of Infectious Diseases* **212**, 1361–1365 (2015).

70. Siliciano, J. D. *et al.* Long-term follow-up studies confirm the stability of the latent reservoir for HIV-1 in resting CD4+ T cells. *Nat Med* **9**, 727–728 (2003).

71. Sedaghat, A. R., Siliciano, R. F. & Wilke, C. O. Low-level HIV-1 replication and the dynamics of the resting CD4+T cell reservoir for HIV-1 in the setting of HAART. *BMC Infect Dis* **8**, 2 (2008).

72. Crotty, S. T Follicular Helper Cell Differentiation, Function, and Roles in Disease. *Immunity* **41**, 529–542 (2014).

73. Kohler, S. L. *et al.* Germinal Center T Follicular Helper Cells Are Highly Permissive to HIV-1 and Alter Their Phenotype during Virus Replication. *The Journal of Immunology* **196**, 2711–2722 (2016).

74. Fukazawa, Y. *et al.* B cell follicle sanctuary permits persistent productive simian immunodeficiency virus infection in elite controllers. *Nat Med* **21**, 132–139 (2015).

75. Hey-Nguyen, W. J. *et al.* Quantification of Residual Germinal Center Activity and HIV-1 DNA and RNA Levels Using Fine Needle Biopsies of Lymph Nodes During Antiretroviral Therapy. *AIDS Res Hum Retroviruses* **33**, 648–657 (2017).

76. Banga, R. *et al.* PD-1+ and follicular helper T cells are responsible for persistent HIV-1 transcription in treated aviremic individuals. *Nat Med* **22**, 754–761 (2016).

77. Wallet, C. *et al.* Microglial Cells: The Main HIV-1 Reservoir in the Brain. *Front Cell Infect Microbiol* **9**, (2019).

78. Williams, D. W., Eugenin, E. A., Calderon, T. M. & Berman, J. W. Monocyte maturation, HIV susceptibility, and transmigration across the blood brain barrier are critical in HIV neuropathogenesis. *J Leukoc Biol* **91**, 401–415 (2012).

79. Bai, R. *et al.* Role of microglia in HIV-1 infection. *AIDS Res Ther* **20**, 16 (2023).

80. Saylor, D. *et al.* HIV-associated neurocognitive disorder — pathogenesis and prospects for treatment. *Nat Rev Neurol* **12**, 234–248 (2016).

81. Réu, P. *et al.* The Lifespan and Turnover of Microglia in the Human Brain. *Cell Rep* **20**, 779–784 (2017).

82. Illes, P., Rubini, P., Ulrich, H., Zhao, Y. & Tang, Y. Regulation of Microglial Functions by Purinergic Mechanisms in the Healthy and Diseased CNS. *Cells* **9**, 1108 (2020).

83. Dos Santos, S. E. *et al.* Similar Microglial Cell Densities across Brain Structures and Mammalian Species: Implications for Brain Tissue Function. *The Journal of Neuroscience* **40**, 4622–4643 (2020).

84. Kongsui, R., Beynon, S. B., Johnson, S. J. & Walker, F. R. Quantitative assessment of microglial morphology and density reveals remarkable consistency in the distribution and morphology of cells within the healthy prefrontal cortex of the rat. *J Neuroinflammation* **11**, 182 (2014).

85. Wake, H., Moorhouse, A. J., Jinno, S., Kohsaka, S. & Nabekura, J. Resting Microglia Directly Monitor the Functional State of Synapses In Vivo and Determine the Fate of Ischemic Terminals. *The Journal of Neuroscience* **29**, 3974–3980 (2009).

86. Wahl, A. & Al-Harthi, L. HIV infection of non-classical cells in the brain. *Retrovirology* **20**, 1 (2023).

87. Lutgen, V. *et al.* HIV infects astrocytes in vivo and egresses from the brain to the periphery. *PLoS Pathog* **16**, e1008381 (2020).

88. Chauhan, A., Mehla, R., Vijayakumar, T. S. & Handy, I. Endocytosis-mediated HIV-1 entry and its significance in the elusive behavior of the virus in astrocytes. *Virology* **456–457**, 1–19 (2014).

89. Sofroniew, M. V. & Vinters, H. V. Astrocytes: biology and pathology. *Acta Neuropathol* **119**, 7–35 (2010).

90. Osborne, O., Peyravian, N., Nair, M., Daunert, S. & Toborek, M. The Paradox of HIV Blood–Brain Barrier Penetrance and Antiretroviral Drug Delivery Deficiencies. *Trends Neurosci* **43**, 695–708 (2020).

91. Kalidasan, V. & Theva Das, K. Lessons Learned From Failures and Success Stories of HIV Breakthroughs: Are We Getting Closer to an HIV Cure? *Front Microbiol* **11**, (2020).

92. Ongadi, B. A., Obiero, G., Lihana, R. W. & Kiiru, J. N. Distribution of Genetic Polymorphism in the CCR5 among Caucasians, Asians and Africans: A Systematic Review and Meta-Analysis. *Open J Genet* **08**, 54–66 (2018).

93. Hsu, J. *et al.* HIV-1 remission and possible cure in a woman after haplo-cord blood transplant. *Cell* **186**, 1115-1126.e8 (2023).

94. Ruggeri, A. Optimizing cord blood selection. *Hematology* **2019**, 522–531 (2019).

95. Bhatia, S. Long-term health impacts of hematopoietic stem cell transplantation inform recommendations for follow-up. *Expert Rev Hematol* **4**, 437–454 (2011).

96. Sanz, J., Veys, P. & Rocha, V. Umbilical Cord Blood Transplantation in Children and Adults. in *The EBMT Handbook* 473–478 (Springer International Publishing, Cham, 2019). doi:10.1007/978-3-030-02278-5_64.

97. Styczyński, J. *et al.* Death after hematopoietic stem cell transplantation: changes over calendar year time, infections and associated factors. *Bone Marrow Transplant* **55**, 126–136 (2020).

98. Rothenberger, M. K. *et al.* Large number of rebounding/founder HIV variants emerge from multifocal infection in lymphatic tissues after treatment interruption. *Proceedings of the National Academy of Sciences* **112**, (2015).

99. Fletcher, C. V. *et al.* Persistent HIV-1 replication is associated with lower antiretroviral drug concentrations in lymphatic tissues. *Proceedings of the National Academy of Sciences* **111**, 2307–2312 (2014).

100. Licht, A. & Alter, G. A Drug-Free Zone—Lymph Nodes as a Safe Haven for HIV. *Cell Host Microbe* **19**, 275–276 (2016).

101. Deeks, S. G. Shock and kill. *Nature* **487**, 439–440 (2012).

102. Lichterfeld, M. Reactivation of latent HIV moves shock-and-kill treatments forward. *Nature* **578**, 42–43 (2020).

103. Moranguinho, I. & Valente, S. T. Block-And-Lock: New Horizons for a Cure for HIV-1. *Viruses* **12**, 1443 (2020).

104. Shelton, E. M., Reeves, D. B. & Bender Ignacio, R. A. Initiation of Antiretroviral Therapy during Primary HIV Infection: Effects on the Latent HIV Reservoir, Including on Analytic Treatment Interruptions. *AIDS Rev* **23**, (2021).

105. Null, M. & Agarwal, M. *Anatomy, Lymphatic System*. (StatPearls Publishing, 2022).

106. Feingold, K. Introduction to Lipids and Lipoproteins. in *Endotext* (MDText, South Dartmouth, 2015).

107. Carey, M. C., Small, D. M. & Bliss, C. M. Lipid Digestion and Absorption. *Annu Rev Physiol* **45**, 651–677 (1983).

108. McClements, D. J. The biophysics of digestion: lipids. *Curr Opin Food Sci* **21**, 1–6 (2018).

109. Jackson, A. D. & McLaughlin, J. Digestion and absorption. *Surgery (Oxford)* **27**, 231–236 (2009).

110. Shi, Y. & Cheng, D. Beyond triglyceride synthesis: the dynamic functional roles of MGAT and DGAT enzymes in energy metabolism. *American Journal of Physiology-Endocrinology and Metabolism* **297**, E10–E18 (2009).

111. Xiao, C., Stahel, P. & Lewis, G. F. Regulation of Chylomicron Secretion: Focus on Post-Assembly Mechanisms. *Cell Mol Gastroenterol Hepatol* **7**, 487–501 (2019).

112. Polomska, A. K. & Proulx, S. T. Imaging technology of the lymphatic system. *Adv Drug Deliv Rev* **170**, 294–311 (2021).

113. Zhang, F., Zarkada, G., Yi, S. & Eichmann, A. Lymphatic Endothelial Cell Junctions: Molecular Regulation in Physiology and Diseases. *Front Physiol* **11**, (2020).

114. German, J. B., Smilowitz, J. T. & Zivkovic, A. M. Lipoproteins: When size really matters. *Curr Opin Colloid Interface Sci* **11**, 171–183 (2006).

115. Charman, W. N. A. & Stella, V. J. Estimating the maximal potential for intestinal lymphatic transport of lipophilic drug molecules. *Int J Pharm* **34**, 175–178 (1986).

116. Gershkovich, P. *et al.* The role of molecular physicochemical properties and apolipoproteins in association of drugs with triglyceride-rich lipoproteins: in-silico prediction of uptake by chylomicrons. *Journal of Pharmacy and Pharmacology* **61**, 31–39 (2009).

117. Feng, W. *et al.* Vegetable oils composition affects the intestinal lymphatic transport and systemic bioavailability of co-administered lipophilic drug cannabidiol. *Int J Pharm* **624**, 121947 (2022).

118. Kim, K. S., Suzuki, K., Cho, H., Youn, Y. S. & Bae, Y. H. Oral Nanoparticles Exhibit Specific High-Efficiency Intestinal Uptake and Lymphatic Transport. *ACS Nano* **12**, 8893–8900 (2018).

119. Ye, J. *et al.* Oral SMEDDS promotes lymphatic transport and mesenteric lymph nodes target of chlorogenic acid for effective T-cell antitumor immunity. *J Immunother Cancer* **9**, e002753 (2021).

120. Han, S. *et al.* Lymphatic Transport and Lymphocyte Targeting of a Triglyceride Mimetic Prodrug Is Enhanced in a Large Animal Model: Studies in Greyhound Dogs. *Mol Pharm* **13**, 3351–3361 (2016).

121. Kochappan, R. *et al.* Targeted delivery of mycophenolic acid to the mesenteric lymph node using a triglyceride mimetic prodrug approach enhances gut-specific immunomodulation in mice. *Journal of Controlled Release* **332**, 636–651 (2021).

122. Bibby, D. C., Charman, W. N., Charman, S. A., Iskander, M. N. & Porter, C. J. H. Synthesis and evaluation of 5’ alkyl ester prodrugs of zidovudine for directed lymphatic delivery. *Int J Pharm* **144**, 61–70 (1996).

123. Chu, Y. *et al.* Development of lipophilic ester prodrugs of dolutegravir for intestinal lymphatic transport. *European Journal of Pharmaceutics and Biopharmaceutics* **191**, 90–102 (2023).

124. Qin, C. *et al.* Targeted delivery of lopinavir to HIV reservoirs in the mesenteric lymphatic system by lipophilic ester prodrug approach. *Journal of Controlled Release* **329**, (2021).

125. Lee, J. B. *et al.* Lipophilic activated ester prodrug approach for drug delivery to the intestinal lymphatic system. *Journal of Controlled Release* **286**, 10–19 (2018).

126. Yang, Q. & Forrest, L. Drug Delivery to the Lymphatic System. in *Drug Delivery* 503–548 (2016). doi:10.1002/9781118833322.ch21.

127. Permana, A. D., Nainu, F., Moffatt, K., Larrañeta, E. & Donnelly, R. F. Recent advances in combination of microneedles and nanomedicines for lymphatic targeted drug delivery. *WIREs Nanomedicine and Nanobiotechnology* **13**, (2021).

128. Oussoren, C., Zuidema, J., Crommelin, D. J. A. & Storm, G. Lymphatic uptake and biodistribution of liposomes after subcutaneous injection. *Biochimica et Biophysica Acta (BBA) - Biomembranes* **1328**, 261–272 (1997).

129. Moghimi, S. Subcutaneous and intravenous delivery of diagnostic agents to the lymphatic system: applications in lymphoscintigraphy and indirect lymphography. *Adv Drug Deliv Rev* **37**, 295–312 (1999).

130. Singh, Y. *et al.* Subcutaneously Administered Ultrafine PLGA Nanoparticles Containing Doxycycline Hydrochloride Target Lymphatic Filarial Parasites. *Mol Pharm* **13**, (2016).

131. Permana, A. D. *et al.* Solid lipid nanoparticle-based dissolving microneedles: A promising intradermal lymph targeting drug delivery system with potential

for enhanced treatment of lymphatic filariasis. *Journal of Controlled Release* **316**, 34–52 (2019).

132. Oussoren, C. Liposomes to target the lymphatics by subcutaneous administration. *Adv Drug Deliv Rev* **50**, 143–156 (2001).

133. Mao, Y., Liu, J., Shi, T., Chen, G. & Wang, S. A Novel Self-Assembly Nanocrystal as Lymph Node-Targeting Delivery System: Higher Activity of Lymph Node Targeting and Longer Efficacy Against Lymphatic Metastasis. *AAPS PharmSciTech* **20**, 292 (2019).

134. Izumi, W., Komatsu, H., Ishimitsu, S. & Okada, S. [Pyridoxine hydrochloride reference standard (Control 911) of the National Institute of Hygienic Sciences]. *Eisei Shikenjo Hokoku* 107–9 (1992).

135. Girouard, M. P. *et al.* The Cost-effectiveness and Budget Impact of 2-Drug Dolutegravir-Lamivudine Regimens for the Treatment of HIV Infection in the United States. *Clinical Infectious Diseases* **62**, 784–791 (2016).

136. Deng, P., Chen, M. & Si, L. Temporal trends in inequalities of the burden of HIV/AIDS across 186 countries and territories. *BMC Public Health* **23**, 981 (2023).

137. Roberts, J. D., Bebenek, K. & Kunkel, T. A. The Accuracy of Reverse Transcriptase from HIV-1. *Science (1979)* **242**, 1171–1173 (1988).

138. Bębenek, A. & Ziuzia-Graczyk, I. Fidelity of DNA replication—a matter of proofreading. *Curr Genet* **64**, 985–996 (2018).

139. Götte, M., Arion, D., Parniak, M. A. & Wainberg, M. A. The M184V Mutation in the Reverse Transcriptase of Human Immunodeficiency Virus Type 1

Impairs Rescue of Chain-Terminated DNA Synthesis. *J Virol* **74**, 3579–3585 (2000).

140. Quercia, R. *et al.* Twenty-Five Years of Lamivudine: Current and Future Use for the Treatment of HIV-1 Infection. *JAIDS Journal of Acquired Immune Deficiency Syndromes* **78**, 125–135 (2018).

141. Quan, Y., Brenner, B. G., Oliveira, M. & Wainberg, M. A. Lamivudine Can Exert a Modest Antiviral Effect against Human Immunodeficiency Virus Type 1 Containing the M184V Mutation. *Antimicrob Agents Chemother* **47**, 747–754 (2003).

142. Götte, M., Arion, D., Parniak, M. A. & Wainberg, M. A. The M184V Mutation in the Reverse Transcriptase of Human Immunodeficiency Virus Type 1 Impairs Rescue of Chain-Terminated DNA Synthesis. *J Virol* **74**, 3579–3585 (2000).

143. Diallo, K., Götte, M. & Wainberg, M. A. Molecular Impact of the M184V Mutation in Human Immunodeficiency Virus Type 1 Reverse Transcriptase. *Antimicrob Agents Chemother* **47**, 3377–3383 (2003).

144. Tilney, N. L. Patterns of lymphatic drainage in the adult laboratory rat. *J Anat* **109**, 369–83 (1971).

145. Components of the Immune System. in *Primer to the Immune Response* 21–54 (Elsevier, 2014). doi:10.1016/B978-0-12-385245-8.00002-9.

146. Food and Drug Administration. Bioanalytical Method Validation Guidance for Industry. *https://www.fda.gov/files/drugs/published/Bioanalytical-Method-Validation-Guidance-for-Industry.pdf* (2018).

147. Jebrane, M., Terziev, N. & Heinmaa, I. Biobased and Sustainable Alternative Route to Long-Chain Cellulose Esters. *Biomacromolecules* **18**, 498–504 (2017).

148. Skilling, K. J. *et al.* Nucleoside-Based Self-Assembling Drugs for Localized Drug Delivery. *ChemMedChem* **13**, 1098–1101 (2018).

149. Gottlieb, H. E., Kotlyar, V. & Nudelman, A. NMR Chemical Shifts of Common Laboratory Solvents as Trace Impurities. *J Org Chem* **62**, 7512–7515 (1997).

150. Beckman Instruments. *Ultracentrifuge Methods for Lipoprotein Research*. (1989).

151. Marques, M. Dissolution Media Simulating Fasted and Fed States. *Dissolut Technol* **11**, 16–16 (2004).

152. Zgair, A. *et al.* Strawberry Decreases Intraluminal and Intestinal Wall Hydrolysis of Testosterone Undecanoate. *Molecules* **26**, 233 (2021).

153. Stappaerts, J. *et al.* Rapid conversion of the ester prodrug abiraterone acetate results in intestinal supersaturation and enhanced absorption of abiraterone: In vitro, rat in situ and human in vivo studies. *European Journal of Pharmaceutics and Biopharmaceutics* **90**, 1–7 (2015).

154. Zgair, A. *et al.* Oral administration of cannabis with lipids leads to high levels of cannabinoids in the intestinal lymphatic system and prominent immunomodulation. *Sci Rep* **7**, 14542 (2017).

155. Walpole, S. C. *et al.* The weight of nations: an estimation of adult human biomass. *BMC Public Health* **12**, 439 (2012).

156. Jewell, A. *et al.* Distribution of a highly lipophilic drug cannabidiol into different lymph nodes following oral administration in lipidic vehicle. *European Journal of Pharmaceutics and Biopharmaceutics* **174**, 29–34 (2022).

157. Sabri, A. Application of microneedles for the treatment of nodular basal cell carcinoma. (University of Nottingham, Nottingham, 2020).

158. Donnelly, R. F. *et al.* Design, Optimization and Characterisation of Polymeric Microneedle Arrays Prepared by a Novel Laser-Based Micromoulding Technique. *Pharm Res* **28**, 41–57 (2011).

159. Larrañeta, E. *et al.* A proposed model membrane and test method for microneedle insertion studies. *Int J Pharm* **472**, 65–73 (2014).

160. Vikram Singh, A., Nath, L. K. & Pani, N. R. Development and validation of analytical method for the estimation of lamivudine in rabbit plasma. *J Pharm Anal* **1**, 251–257 (2011).

161. Kano, E. K., Serra, C. H. dos R., Koono, E. E. M., Andrade, S. S. & Porta, V. Determination of lamivudine in human plasma by HPLC and its use in bioequivalence studies. *Int J Pharm* **297**, 73–79 (2005).

162. Jayaseelan, S., Suresh, S., Sathishkumar, G., Sekar, V. & Perumal, P. Bioanalytical method development and validation of lamivudine by RP-HPLC method. *Int J Chemtech Res* **2**, 163–167 (2010).

163. Alebouyeh, M. & Amini, H. Rapid determination of lamivudine in human plasma by high-performance liquid chromatography. *Journal of Chromatography B* **975**, 40–44 (2015).

164. Chimalakonda, K. C., Agarwal, H. K., Kumar, A., Parang, K. & Mehvar, R. Synthesis, Analysis, in Vitro Characterization, and in Vivo Disposition of a

Lamivudine–Dextran Conjugate for Selective Antiviral Delivery to the Liver. *Bioconjug Chem* **18**, 2097–2108 (2007).

165. Alnouti, Y., White, C. A. & Bartlett, M. G. Simultaneous determination of zidovudine and lamivudine from rat plasma, amniotic ?uid and tissues by HPLC. *Biomedical Chromatography* **18**, 641–647 (2004).

166. Li, C.-L., Hsieh, C.-H. & Tsai, T.-H. Preclinical Pharmacokinetics of Lamivudine and Its Interaction with *Schisandra chinensis* Extract in Rats. *ACS Omega* **5**, 1997–2004 (2020).

167. Alnouti, Y., Lewis, S. R., White, C. A. & Bartlett, M. G. Simultaneous determination of zidovudine and lamivudine from rat tissues by liquid chromatography/tandem mass spectrometry. *Rapid Communications in Mass Spectrometry* **19**, 503–508 (2005).

168. Matta, M. K., Burugula, L., Pilli, N. R., Inamadugu, J. K. & JVLN, S. R. A novel LC-MS/MS method for simultaneous quantification of tenofovir and lamivudine in human plasma and its application to a pharmacokinetic study. *Biomedical Chromatography* **26**, 1202–1209 (2012).

169. National Centre for the Replacement Refinement and Reduction of Animals in Research. Blood sampling: General principles. https://www.nc3rs.org.uk/3rs-resources/blood-sampling/blood-sampling-general-principles (2021).

170. Diehl, K.-H. *et al.* A good practice guide to the administration of substances and removal of blood, including routes and volumes. *Journal of Applied Toxicology* **21**, 15–23 (2001).

171. Nirogi, R. *et al.* Exploring dried blood spot sampling technique for simultaneous quantification of antiretrovirals: lamivudine, stavudine and nevirapine in a rodent pharmacokinetic study. *Biomedical Chromatography* **26**, 1472–1481 (2012).

172. Jiang, Q. *et al.* Simultaneous determination of entecavir and lamivudine in rat plasma by UPLC-MS/MS and its application to a pharmacokinetic study. *RSC Adv* **6**, 70990–70998 (2016).

173. TAKUBO, T. *et al.* Studies on the Metabolic Fate of Lamivudine (I): Absorption, Metabolism and Excretion of Lamivudine in Rats. *Drug Metab Pharmacokinet* **12**, 85–91 (1997).

174. Kumar, P., Lakshmi, Y. S. & Kondapi, A. K. Triple Drug Combination of Zidovudine, Efavirenz and Lamivudine Loaded Lactoferrin Nanoparticles: an Effective Nano First-Line Regimen for HIV Therapy. *Pharm Res* **34**, 257–268 (2017).

175. Alnouti, Y., White, C. A. & Bartlett, M. G. Simultaneous determination of zidovudine and lamivudine from rat plasma, amniotic ?uid and tissues by HPLC. *Biomedical Chromatography* **18**, 641–647 (2004).

176. Walter, T., Iraneta, P. & Capparella, M. Observations on the wetting of reversed-phase HPLC packings. in *21st International Symposium on High Performance Liquid Phase Separations and Related Techniques* (Birmingham, 1997).

177. Bedse, G., Kumar, V. & Singh, S. Study of forced decomposition behavior of lamivudine using LC, LC–MS/TOF and MSn. *J Pharm Biomed Anal* **49**, 55–63 (2009).

178. White, K. L. *et al.* Lymphatic Transport of Methylnortestosterone Undecanoate (MU) and the Bioavailability of Methylnortestosterone Are Highly Sensitive to the Mass of Coadministered Lipid after Oral Administration of MU. *Journal of Pharmacology and Experimental Therapeutics* **331**, 700–709 (2009).

179. Fessi, H., Puisieux, F., Devissaguet, J. Ph., Ammoury, N. & Benita, S. Nanocapsule formation by interfacial polymer deposition following solvent displacement. *Int J Pharm* **55**, R1–R4 (1989).

180. Epivir Package Insert. *ViiV Healthcare* Preprint at (2017).

181. de Chasteigner, S., Fessi, H., Devissaguet, J.-P. & Puisieux, F. Comparative study of the association of itraconazole with colloidal drug carriers. *Drug Dev Res* **38**, 125–133 (1996).

182. Barichello, J. M., Morishita, M., Takayama, K. & Nagai, T. Encapsulation of Hydrophilic and Lipophilic Drugs in PLGA Nanoparticles by the Nanoprecipitation Method. *Drug Dev Ind Pharm* **25**, 471–476 (1999).

183. Cochrane, C. R. *et al.* Intact HIV Proviruses Persist in the Brain Despite Viral Suppression with ART. *Ann Neurol* **92**, 532–544 (2022).

184. Brown, L. S. *et al.* Pericytes and Neurovascular Function in the Healthy and Diseased Brain. *Front Cell Neurosci* **13**, (2019).

185. Asahchop, E. L. *et al.* Reduced antiretroviral drug efficacy and concentration in HIV-infected microglia contributes to viral persistence in brain. *Retrovirology* **14**, 47 (2017).

186. Ståhle, L., Martin, C., Svensson, J.-O. & Sönnerborg, A. Indinavir in cerebrospinal fluid of HIV-1-infected patients. *The Lancet* **350**, 1823 (1997).

187. Russell, J. W., Whiterock, V. J., Marrero, D. & Klunk, L. J. Pharmacokinetics of A New Anti-HIV Ageht: 2',3'-Dideoxy-2',3'-Didehydrothymidine (d4T). *Nucleosides Nucleotides Nucleic Acids* **8**, 845–848 (1989).

188. Enting, R. H. *et al.* Antiretroviral drugs and the central nervous system. *AIDS* **12**, 1941–1955 (1998).

189. Jenabian, M.-A. *et al.* Immune tolerance properties of the testicular tissue as a viral sanctuary site in ART-treated HIV-infected adults. *AIDS* **30**, 2777–2786 (2016).

190. Mzingwane, M. L. & Tiemessen, C. T. Mechanisms of HIV persistence in HIV reservoirs. *Rev Med Virol* **27**, e1924 (2017).

191. Costiniuk, C. T. & Jenabian, M.-A. The lungs as anatomical reservoirs of HIV infection. *Rev Med Virol* **24**, 35–54 (2014).

192. Wong, J. K. & Yukl, S. A. Tissue reservoirs of HIV. *Curr Opin HIV AIDS* **11**, 362–370 (2016).

193. Chu, Y. *et al.* Oral administration of tipranavir with long-chain triglyceride results in moderate intestinal lymph targeting but no efficient delivery to HIV-1 reservoir in mesenteric lymph nodes. *Int J Pharm* **602**, 120621 (2021).

194. Gershkovich, P. & Hoffman, A. Uptake of lipophilic drugs by plasma derived isolated chylomicrons: Linear correlation with intestinal lymphatic bioavailability. *European Journal of Pharmaceutical Sciences* **26**, 394–404 (2005).

195. Skilling, K. J. *et al.* Gelation properties of self-assembling N-acyl modified cytidine derivatives. *J. Mater. Chem. B* **2**, 8412–8417 (2014).

196. Wang, T., Ménard-Moyon, C. & Bianco, A. Self-assembly of amphiphilic amino acid derivatives for biomedical applications. *Chem Soc Rev* **51**, 3535–3560 (2022).

197. Jung, J. H., Shinkai, S. & Shimizu, T. Spectral Characterization of Self-Assemblies of Aldopyranoside Amphiphilic Gelators: What is the Essential Structural Difference Between Simple Amphiphiles and Bolaamphiphiles? *Chemistry - A European Journal* **8**, 2684 (2002).

198. Fenwick, N., Griffin, G. & Gauthier, C. The welfare of animals used in science: how the 'Three Rs' ethic guides improvements. *Can Vet J* **50**, 523–30 (2009).

199. Li, Q. *et al.* Synthesis of Lamivudine stearate and antiviral activity of stearic acid-g-chitosan oligosaccharide polymeric micelles delivery system. *European Journal of Pharmaceutical Sciences* **41**, 498–507 (2010).

200. Augustinsson, K. Electrophoresis Studies on Blood Plasma Esterases. *Acta Chem Scand* **13**, 571–592 (1959).

201. van Kuiken, B. A. & Behnke, W. D. The activation of porcine pancreatic lipase by cis-unsaturated fatty acids. *Biochimica et Biophysica Acta (BBA) - Lipids and Lipid Metabolism* **1214**, 148–160 (1994).

202. Hwang, L. S. Sesame Oil. in *Bailey's Industrial Oil and Fat Products, Sixth Edition* 537–576 (John Wiley & Sons, Inc., 2005).

203. Jumaah, M. A., Yusoff, M. F. M., Salimon, J. & Bahadi, M. Separation of Saturated and Unsaturated Fatty Acids of Palm Fatty Acid Distilled via Low-temperature Methanol Crystallization. *Malaysian Journal of Chemistry* **21**, 8–16 (2019).

204. McConnell, E. L., Basit, A. W. & Murdan, S. Measurements of rat and mouse gastrointestinal pH, fluid and lymphoid tissue, and implications for in-vivo experiments. *Journal of Pharmacy and Pharmacology* **60**, 63–70 (2010).

205. Morton, D. B. *et al.* Refining procedures for the administration of substances. *Lab Anim* **35**, 1–41 (2001).

206. Macias, E., Waltmann, T. & Travesset, A. Assembly of nanocrystal clusters by solvent evaporation: icosahedral order and the breakdown of the Maxwell regime. *Soft Matter* **16**, 7350–7358 (2020).

207. Nirogi, R. *et al.* Exploring dried blood spot sampling technique for simultaneous quantification of antiretrovirals: lamivudine, stavudine and nevirapine in a rodent pharmacokinetic study. *Biomedical Chromatography* **26**, 1472–1481 (2012).

208. Lu, C.-M., Hou, M.-L., Lin, L.-C. & Tsai, T.-H. Development of a microdialysis system to monitor lamivudine in blood and liver for the pharmacokinetic application in herbal drug interaction and the gene expression in rats. *J Pharm Biomed Anal* **96**, 231–240 (2014).

209. Bourry, O. *et al.* Prevention of vaginal simian immunodeficiency virus transmission in macaques by postexposure prophylaxis with zidovudine, lamivudine and indinavir. *AIDS* **23**, 447–454 (2009).

210. Marcucci, G., Silverman, L., Eller, M., Lintz, L. & Beach, C. L. Bioavailability of Azacitidine Subcutaneous Versus Intravenous in Patients With the Myelodysplastic Syndromes. *The Journal of Clinical Pharmacology* **45**, 597–602 (2005).

211. Crook, K. I. *et al.* The pharmacokinetics of cytarabine in dogs when administered via subcutaneous and continuous intravenous infusion routes. *J Vet Pharmacol Ther* **36**, 408–411 (2013).

212. Du, X. *et al.* Efficacy, safety and pharmacokinetics of subcutaneous azacitidine in Chinese patients with higher risk myelodysplastic syndromes: Results from a multicenter, single-arm, open-label phase 2 study. *Asia Pac J Clin Oncol* **14**, 270–278 (2018).

213. Grabowski, T. *et al.* Ustekinumab pharmacokinetics after subcutaneous administration in swine model. *J Vet Sci* **22**, (2021).

214. Linde, B. Dissociation of Insulin Absorption and Blood Flow During Massage of a Subcutaneous Injection Site. *Diabetes Care* **9**, 570–574 (1986).

215. Strober, W. Trypan Blue Exclusion Test of Cell Viability. *Curr Protoc Immunol* **21**, (1997).

216. Hunter, M. C., Teijeira, A. & Halin, C. T Cell Trafficking through Lymphatic Vessels. *Front Immunol* **7**, (2016).

217. Bourry, O. *et al.* Effect of a short-term HAART on SIV load in macaque tissues is dependent on time of initiation and antiviral diffusion. *Retrovirology* **7**, 78 (2010).

218. Dumond, J. B. *et al.* Differential Extracellular and Intracellular Concentrations of Zidovudine and Lamivudine in Semen and Plasma of HIV-1-Infected Men. *JAIDS Journal of Acquired Immune Deficiency Syndromes* **48**, 156–162 (2008).

219. Harrell, M. I., Iritani, B. M. & Ruddell, A. Lymph node mapping in the mouse. *J Immunol Methods* **332**, 170–174 (2008).

220. Thomas, S. N., Rohner, N. A. & Edwards, E. E. Implications of Lymphatic Transport to Lymph Nodes in Immunity and Immunotherapy. *Annu Rev Biomed Eng* **18**, 207–233 (2016).

221. Han, S. *et al.* Targeted delivery of a model immunomodulator to the lymphatic system: Comparison of alkyl ester versus triglyceride mimetic lipid prodrug strategies. *Journal of Controlled Release* **177**, 1–10 (2014).

222. Labarthe, L. *et al.* Pharmacokinetics and tissue distribution of tenofovir, emtricitabine and dolutegravir in mice. *Journal of Antimicrobial Chemotherapy* **77**, 1094–1101 (2022).

223. Garzon-Aburbeh, A., Poupaert, J. H., Claesen, M. & Dumont, P. A lymphotropic prodrug of L-dopa: synthesis, pharmacological properties and pharmacokinetic behavior of 1,3-dihexadecanoyl-2-[(S)-2-amino-3-(3,4-dihydroxyphenyl)propanoyl]propane-1,2,3-triol. *J Med Chem* **29**, 687–691 (1986).

224. Dyavar, S. R. *et al.* Intramuscular and subcutaneous administration of antiretroviral drugs, compared with oral, enhances delivery to lymphoid tissues in BALB/c mice. *Journal of Antimicrobial Chemotherapy* **76**, 2651–2658 (2021).

225. Burgunder, E. *et al.* Antiretroviral Drug Concentrations in Lymph Nodes: A Cross-Species Comparison of the Effect of Drug Transporter Expression, Viral Infection, and Sex in Humanized Mice, Nonhuman Primates, and Humans. *Journal of Pharmacology and Experimental Therapeutics* **370**, 360–368 (2019).

226. Huang, Y. *et al.* Antiretroviral drug transporters and metabolic enzymes in human testicular tissue: potential contribution to HIV-1 sanctuary site. *Journal of Antimicrobial Chemotherapy* **71**, 1954–1965 (2016).

227. Guo, Y. *et al.* How is mRNA expression predictive for protein expression? A correlation study on human circulating monocytes. *Acta Biochim Biophys Sin (Shanghai)* **40**, 426–436 (2008).

228. Camargo, S. M. R. *et al.* The Molecular Mechanism of Intestinal Levodopa Absorption and Its Possible Implications for the Treatment of Parkinson's Disease. *Journal of Pharmacology and Experimental Therapeutics* **351**, 114–123 (2014).

229. Anderson, P. L. *et al.* Pharmacological considerations for tenofovir and emtricitabine to prevent HIV infection. *Journal of Antimicrobial Chemotherapy* **66**, 240–250 (2011).

230. Shugarts, S. & Benet, L. Z. The Role of Transporters in the Pharmacokinetics of Orally Administered Drugs. *Pharm Res* **26**, 2039–2054 (2009).

231. Savla, R., Browne, J., Plassat, V., Wasan, K. M. & Wasan, E. K. Review and analysis of FDA approved drugs using lipid-based formulations. *Drug Dev Ind Pharm* **43**, 1743–1758 (2017).

232. Chaudhary, S. *et al.* Enhanced Solubility and Bioavailability of Dolutegravir by Solid Dispersion Method: In Vitro and In Vivo Evaluation—a Potential Approach for HIV Therapy. *AAPS PharmSciTech* **22**, 127 (2021).

233. Reese, M. J. *et al.* In Vitro Investigations into the Roles of Drug Transporters and Metabolizing Enzymes in the Disposition and Drug Interactions of

Dolutegravir, a HIV Integrase Inhibitor. *Drug Metabolism and Disposition* **41**, 353–361 (2013).

234. Hu, M., Patel, S. K., Zhou, T. & Rohan, L. C. Drug transporters in tissues and cells relevant to sexual transmission of HIV: Implications for drug delivery. *Journal of Controlled Release* **219**, 681–696 (2015).

235. Mansoor, A. & Mahabadi, N. Volume of Distribution. *StatPearls* https://www.ncbi.nlm.nih.gov/books/NBK545280/ (2022).

236. Johnson, M. A., Moore, K. H. P., Yuen, G. J., Bye, A. & Pakes, G. E. Clinical Pharmacokinetics of Lamivudine. *Clin Pharmacokinet* **36**, 41–66 (1999).

237. Hu, M., Patel, S. K., Zhou, T. & Rohan, L. C. Drug transporters in tissues and cells relevant to sexual transmission of HIV: Implications for drug delivery. *Journal of Controlled Release* **219**, 681–696 (2015).

238. Mallayasamy, S. & Penzak, S. R. Pharmacogenomic Considerations in the Treatment of HIV Infection. in *Pharmacogenomics* 227–245 (Elsevier, 2019). doi:10.1016/B978-0-12-812626-4.00008-5.

239. Anderson, P. L., Lamba, J., Aquilante, C. L., Schuetz, E. & Fletcher, C. V. Pharmacogenetic Characteristics of Indinavir, Zidovudine, and Lamivudine Therapy in HIV-Infected Adults. *JAIDS Journal of Acquired Immune Deficiency Syndromes* **42**, 441–449 (2006).

240. Arimany-Nardi, C. *et al.* Role of Human Organic Cation Transporter 1 (hOCT1) Polymorphisms in Lamivudine (3TC) Uptake and Drug-Drug Interactions. *Front Pharmacol* **7**, (2016).

241. Dyavar, S. R. *et al.* Assessing the lymphoid tissue bioavailability of antiretrovirals in human primary lymphoid endothelial cells and in mice. *Journal of Antimicrobial Chemotherapy* **74**, 2974–2978 (2019).

242. Fletcher, C. V. *et al.* Persistent HIV transcription and variable antiretroviral drug penetration in lymph nodes during plasma viral suppression. *AIDS* **36**, 985–990 (2022).

243. Rosen, E. P. *et al.* Antiretroviral drug exposure in lymph nodes is heterogeneous and drug dependent. *J Int AIDS Soc* **25**, (2022).

244. Boritz, E. A. & Douek, D. C. Perspectives on Human Immunodeficiency Virus (HIV) Cure: HIV Persistence in Tissue. *J Infect Dis* **215**, S128–S133 (2017).

245. McManus, W. R. *et al.* HIV-1 in lymph nodes is maintained by cellular proliferation during antiretroviral therapy. *Journal of Clinical Investigation* **129**, 4629–4642 (2019).

246. Yeh, Y.-H. J., Yang, K., Razmi, A. & Ho, Y.-C. The Clonal Expansion Dynamics of the HIV-1 Reservoir: Mechanisms of Integration Site-Dependent Proliferation and HIV-1 Persistence. *Viruses* **13**, 1858 (2021).

247. Stranford, S. & Ruddle, N. H. Follicular dendritic cells, conduits, lymphatic vessels, and high endothelial venules in tertiary lymphoid organs: Parallels with lymph node stroma. *Front Immunol* **3**, (2012).

248. Roozendaal, R., Mebius, R. E. & Kraal, G. The conduit system of the lymph node. *Int Immunol* **20**, 1483–1487 (2008).

249. Pardridge, W. M. Drug Transport across the Blood–Brain Barrier. *Journal of Cerebral Blood Flow & Metabolism* **32**, 1959–1972 (2012).

250. Varatharajan, L. & Thomas, S. A. The transport of anti-HIV drugs across blood–CNS interfaces: Summary of current knowledge and recommendations for further research. *Antiviral Res* **82**, A99–A109 (2009).

251. Tachibana, K. *et al.* Tight Junction Modulating Bioprobes for Drug Delivery System to the Brain: A Review. *Pharmaceutics* **12**, 1236 (2020).

252. Vendel, E., Rottschäfer, V. & de Lange, E. C. M. The need for mathematical modelling of spatial drug distribution within the brain. *Fluids Barriers CNS* **16**, 12 (2019).

253. Guo, S., Li, K., Chen, Y. & Li, B. Unraveling the drug distribution in brain enabled by MALDI MS imaging with laser-assisted chemical transfer. *Acta Pharm Sin B* **12**, 2120–2126 (2022).

254. Ntshangase, S. *et al.* Spatial distribution of elvitegravir and tenofovir in rat brain tissue: Application of matrix-assisted laser desorption/ionization mass spectrometry imaging and liquid chromatography/tandem mass spectrometry. *Rapid Communications in Mass Spectrometry* **33**, 1643–1651 (2019).

255. Ntshangase, S. *et al.* Mass Spectrometry Imaging Demonstrates the Regional Brain Distribution Patterns of Three First-Line Antiretroviral Drugs. *ACS Omega* **4**, 21169–21177 (2019).

256. Ueno, M. *et al.* The persistence of high uptake of serum albumin in the olfactory bulbs of mice throughout their adult lives. *Arch Gerontol Geriatr* **13**, 201–209 (1991).

257. Ueno, M., Dobrogowska, D. H. & Vorbrodt, A. W. Immunocytochemical evaluation of the blood-brain barrier to endogenous albumin in the olfactory

bulb and pons of senescence-accelerated mice (SAM). *Histochem Cell Biol* **105**, 203–212 (1996).

258. Eckhardt, B. J. & Gulick, R. M. Drugs for HIV Infection. in *Infectious Diseases* 1293-1308.e2 (Elsevier, 2017). doi:10.1016/B978-0-7020-6285-8.00152-0.

259. Abdallah, M. *et al.* Lymphatic targeting by albumin-hitchhiking: Applications and optimisation. *Journal of Controlled Release* **327**, 117–128 (2020).

260. Pardridge, W. M. Drug Transport across the Blood–Brain Barrier. *Journal of Cerebral Blood Flow & Metabolism* **32**, 1959–1972 (2012).

261. Moore, K. H. P. *et al.* The pharmacokinetics of lamivudine phosphorylation in peripheral blood mononuclear cells from patients infected with HIV-1. *AIDS* **13**, 2239–2250 (1999).

262. Derendorf, H. & Schmidt, S. *Clincal Pharmacokinetics and Pharmacodynamics*. (Wolters Kluwer, Philadelphia, 2020).

263. Cheng, C. Y. & Mruk, D. D. The Blood-Testis Barrier and Its Implications for Male Contraception. *Pharmacol Rev* **64**, 16–64 (2012).

264. Pérez, C. V. *et al.* Dual role of immune cells in the testis. *Spermatogenesis* **3**, e23870 (2013).

265. Shehu-Xhilaga, M., de Kretser, D., Dejucq-Rainsford, N. & Hedger, M. Standing in the Way of Eradication: HIV-1 Infection and Treatment in the Male Genital Tract. *Curr HIV Res* **3**, 345–359 (2005).

266. Leback, C. *et al.* Barriers and Facilitators to Injection Safety in Ambulatory Care Settings. *Infect Control Hosp Epidemiol* **39**, 841–848 (2018).

267. Keininger, D. & Coteur, G. Assessment of self-injection experience in patients with rheumatoid arthritis: psychometric validation of the Self-Injection Assessment Questionnaire (SIAQ). *Health Qual Life Outcomes* **9**, 2 (2011).

268. Brod, M., Alolga, S. L. & Meneghini, L. Barriers to Initiating Insulin in Type 2 Diabetes Patients: Development of a New Patient Education Tool to Address Myths, Misconceptions and Clinical Realities. *The Patient - Patient-Centered Outcomes Research* **7**, 437–450 (2014).

269. Tanner, T. & Marks, R. Delivering drugs by the transdermal route: review and comment. *Skin Research and Technology* **14**, 249–260 (2008).

270. Alkilani, A., McCrudden, M. T. & Donnelly, R. Transdermal Drug Delivery: Innovative Pharmaceutical Developments Based on Disruption of the Barrier Properties of the Stratum Corneum. *Pharmaceutics* **7**, 438–470 (2015).

271. Waghule, T. *et al.* Microneedles: A smart approach and increasing potential for transdermal drug delivery system. *Biomedicine & Pharmacotherapy* **109**, 1249–1258 (2019).

272. Waghule, T. *et al.* Microneedles: A smart approach and increasing potential for transdermal drug delivery system. *Biomedicine & Pharmacotherapy* **109**, 1249–1258 (2019).

273. Ali, M., Namjoshi, S., Benson, H. A. E., Mohammed, Y. & Kumeria, T. Dissolvable polymer microneedles for drug delivery and diagnostics. *Journal of Controlled Release* **347**, 561–589 (2022).

274. Sabri, A. H. *et al.* Intradermal delivery of imiquimod using polymeric microneedles for basal cell carcinoma. *Int J Pharm* **589**, 119808 (2020).

275. Swindle, M. M., Makin, A., Herron, A. J., Clubb, F. J. & Frazier, K. S. Swine as Models in Biomedical Research and Toxicology Testing. *Vet Pathol* **49**, 344–356 (2012).

276. Muresan, P. *et al.* Development of nanoparticle loaded microneedles for drug delivery to a brain tumour resection site. *European Journal of Pharmaceutics and Biopharmaceutics* **182**, 53–61 (2023).

277. Bhatnagar, S. *et al.* Corneal delivery of besifloxacin using rapidly dissolving polymeric microneedles. *Drug Deliv Transl Res* **8**, 473–483 (2018).

278. Zhu, D. D., Zhang, X. P., Shen, C. B., Cui, Y. & Guo, X. D. The maximum possible amount of drug in rapidly separating microneedles. *Drug Deliv Transl Res* **9**, 1133–1142 (2019).

279. Lee, J., Park, S. H., Seo, I. H., Lee, K. J. & Ryu, W. Rapid and repeatable fabrication of high A/R silk fibroin microneedles using thermally-drawn micromolds. *European Journal of Pharmaceutics and Biopharmaceutics* **94**, 11–19 (2015).

280. Yu, W. *et al.* Polymer microneedles fabricated from alginate and hyaluronate for transdermal delivery of insulin. *Mater Sci Eng C Mater Biol Appl* **80**, 187–196 (2017).

281. Holbrook, K. A. & Odland, G. F. Regional Differences in the Thickness (Cell Layers) of the Human Stratum Corneum: An Ultrastructural Analysis. *Journal of Investigative Dermatology* **62**, 415–422 (1974).

282. Kim, J. *et al.* Bioinspired microneedle insertion for deep and precise skin penetration with low force: Why the application of mechanophysical stimuli should be considered. *J Mech Behav Biomed Mater* **78**, 480–490 (2018).

283. He, J. *et al.* Design and Evaluation of Dissolving Microneedles for Enhanced Dermal Delivery of Propranolol Hydrochloride. *Pharmaceutics* **13**, 579 (2021).

284. Lewandowska, K., Szulc, M. & Sionkowska, A. Effect of Solvent on the Hydrodynamic Properties of Collagen. *Polymers (Basel)* **13**, 3626 (2021).

285. Peng, K. *et al.* Dissolving microneedle patches loaded with amphotericin B microparticles for localised and sustained intradermal delivery: Potential for enhanced treatment of cutaneous fungal infections. *Journal of Controlled Release* **339**, 361–380 (2021).

286. Quinn, H. L., Bonham, L., Hughes, C. M. & Donnelly, R. F. Design of a Dissolving Microneedle Platform for Transdermal Delivery of a Fixed-Dose Combination of Cardiovascular Drugs. *J Pharm Sci* **104**, 3490–3500 (2015).

287. González-Vázquez, P. *et al.* Transdermal delivery of gentamicin using dissolving microneedle arrays for potential treatment of neonatal sepsis. *Journal of Controlled Release* **265**, 30–40 (2017).

288. Paredes, A. J. *et al.* Novel tip-loaded dissolving and implantable microneedle array patches for sustained release of finasteride. *Int J Pharm* **606**, 120885 (2021).

289. Garland, M. J. *et al.* Influence of skin model on in vitro performance of drug-loaded soluble microneedle arrays. *Int J Pharm* **434**, 80–89 (2012).

290. Vreman, S. *et al.* Early immune responses in skin and lymph node after skin delivery of Toll-like receptor agonists in neonatal and adult pigs. *Vaccine* **39**, 1857–1869 (2021).

291. Garland, M. J., Caffarel–Salvador, E., Migalska, K., Woolfson, A. D. & Donnelly, R. F. Dissolving polymeric microneedle arrays for electrically

assisted transdermal drug delivery. *Journal of Controlled Release* **159**, 52–59 (2012).

292. Fujita, A. K. L. *et al.* Correlation between Porcine and Human Skin Models by Optical Methods. in *Human Skin Cancers - Pathways, Mechanisms, Targets and Treatments* (InTech, 2018). doi:10.5772/intechopen.75788.

293. González-Vázquez, P. *et al.* Transdermal delivery of gentamicin using dissolving microneedle arrays for potential treatment of neonatal sepsis. *Journal of Controlled Release* **265**, 30–40 (2017).

294. McCrudden, M. T. C. *et al.* Design and physicochemical characterisation of novel dissolving polymeric microneedle arrays for transdermal delivery of high dose, low molecular weight drugs. *Journal of Controlled Release* **180**, 71–80 (2014).

295. Pamornpathomkul, B. *et al.* Dissolving polymeric microneedle arrays for enhanced site-specific acyclovir delivery. *European Journal of Pharmaceutical Sciences* **121**, 200–209 (2018).

296. Paredes, A. J. *et al.* Systemic delivery of tenofovir alafenamide using dissolving and implantable microneedle patches. *Mater Today Bio* **13**, 100217 (2022).

297. Ronnander, P., Simon, L., Spilgies, H., Koch, A. & Scherr, S. Dissolving polyvinylpyrrolidone-based microneedle systems for in-vitro delivery of sumatriptan succinate. *European Journal of Pharmaceutical Sciences* **114**, 84–92 (2018).

298. Dinesh, B., Patil, U., Desai, B., Raghu, K. & Sadashivaiah, R. Design and evaluation of haloperidol lactate transdermal patches containing ethyl cellulose-povidone as film formers. *Asian J Pharm* **2**, 43 (2008).

299. Pahal, S. *et al.* Microneedles for Extended Transdermal Therapeutics: A Route to Advanced Healthcare. *European Journal of Pharmaceutics and Biopharmaceutics* **159**, 151–169 (2021).

300. Alexander, A. *et al.* Approaches for breaking the barriers of drug permeation through transdermal drug delivery. *Journal of Controlled Release* **164**, 26–40 (2012).

301. Lee, J. W., Park, J.-H. & Prausnitz, M. R. Dissolving microneedles for transdermal drug delivery. *Biomaterials* **29**, 2113–2124 (2008).

302. Marsden, M. D. Benefits and limitations of humanized mice in HIV persistence studies. *Retrovirology* **17**, 7 (2020).

303. Li, Y. *et al.* A human immune system mouse model with robust lymph node development. *Nat Methods* **15**, 623–630 (2018).

304. Zhou, Y., Bao, R., Haigwood, N. L., Persidsky, Y. & Ho, W. SIV infection of rhesus macaques of Chinese origin: a suitable model for HIV infection in humans. *Retrovirology* **10**, 89 (2013).